RADIATION-INDUCED POLYMERIZATION MONITORED WITH FLUOROGENIC MOLECULAR PROBES

Mark Stephen FRAHN

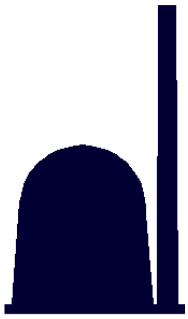

The research described in this thesis was performed at the Radiation Chemistry department of the Interfaculty Reactor Institute (IRI), Delft University of Technology, Mekelweg15, 2629 JB Delft, The Netherlands.

RADIATION-INDUCED POLYMERIZATION MONITORED WITH FLUOROGENIC MOLECULAR PROBES

Proefschrift

Ter verkrijging van de graad van doctor
aan de Technische Universiteit Delft,
op gezag van de Rector Magnificus prof. dr. ir. J. T. Fokkema,
voorzitter van het College voor Promoties,
in het openbaar te verdedigen op dinsdag 25 november 2003 om 10:30 uur

door

Mark Stephen FRAHN

bachelor of science in de scheikunde
geboren te Dunedin, Florida, de Verenigde Staten

Dit proefschrift is goedgekeurd door de promotor:
Prof. dr. L. D. A. Siebbeles

Toegevoegd promotor: dr. J. M. Warman

Samenstelling promotiecommissie:

Rector Magnificus,	voorzitter
Prof. dr. L. D. A. Siebbeles,	Technische Universiteit Delft, promotor
Dr. J. M. Warman,	Technische Universiteit Delft, toegevoegd promotor
Prof. dr. S. J. Picken,	Technische Universiteit Delft
Prof. dr. A. M. van Herk,	Technische Universiteit Eindhoven
Prof. dr. J. W. Verhoeven,	Universiteit van Amsterdam
Prof. dr. L. Wojnarovits,	Hungarian Academy of Sciences, Budapest
Dr. L. H. Luthjens,	Technische Universiteit Delft

Published and distributed by: DUP Science

DUP Science is an imprint of
Delft University Press
P.O. Box 98
2600 MG Delft
The Netherlands
Telephone: +31 15 2785678
Telefax: +31 15 2785706
E-mail: info@library.tudelft.nl

ISBN 90-407-2450-X

Keywords: fluorescence, molecular probe, methyl methacrylate

Printed in The Netherlands

Contents

Chapter One

An Introduction to Radiation-Induced Polymerization

1.1. Introduction

Polymers are large molecules formed by the linking together of many small molecular units known as monomers. Examples of such macromolecules can be found in nature; cellulose and amylose (polysaccharides constituting plant cell walls), hevea rubber or gutta percha (polyisoprenes isolated from trees), and proteins and nucleic acids which are found in all living species. The synthesis of polymers from monomers is given the term polymerization. Generally, polymerization can occur by either a condensation (step) mechanism or an addition (chain) mechanism. In the former a polymer is formed by the elimination of a small molecular byproduct or the polymer

contains functional groups in its main-chain repeat unit. Examples include polyamide or polyurethane polymers as shown in figure 1.1. Addition polymerization on the other hand usually involves synthesis from monomers containing a carbon-carbon double- or triple-bond. Examples of addition polymers are given in figure 1.2. Methods of polymerization include thermal or radiation-induced polymerization as well as catalyst-assisted polymerizations such as Ziegler-Natta and ring-opening metathesis (ROMP) polymerizations. In this thesis only addition polymerization induced by high-energy ionizing radiation will be considered.

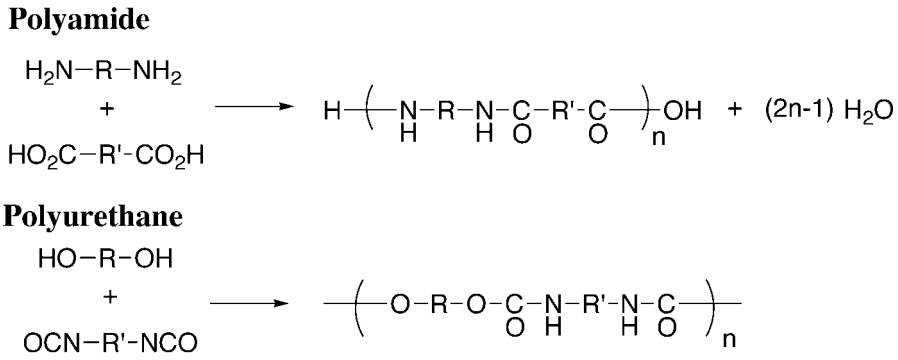

Figure 1.1 Examples of condensation polymerization.

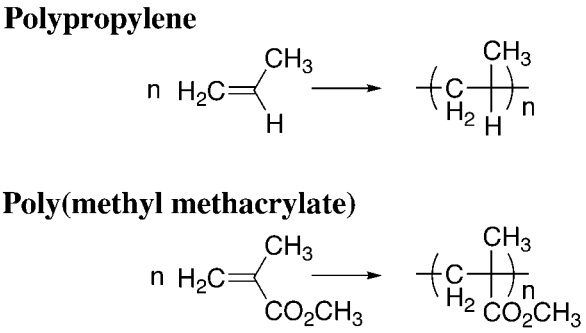

Figure 1.2 Examples of addition polymerization.

Addition polymers can be synthesized by a variety of means depending upon the nature of the reactive species involved in the polymerization reaction. Such reactive species can be either a free radical, an anion or a cation. Radical polymerization is by far the most versatile technique as it is applicable to a very wide variety of monomers. Monomers containing an electron-withdrawing group (*e.g.* acrylates and methacrylates) can be polymerized by both radical and anionic mechanisms, but not by a cationic mechanism. Monomers containing an electron-donating group (*e.g.* vinyl ethers) can be polymerized by either radical or cationic mechanisms, but not by an

anionic mechanism. The experimental conditions required for radical polymerization are less demanding than those required for ionic polymerization, *i.e.* thoroughly dried monomers and extremely pure solvents. Radical polymerization is however very sensitive to the presence of free radical scavengers, in particular oxygen.

The initiation of radical polymerization can be achieved by a variety of means. Chemical initiators are often employed for this purpose. These can be either organic molecules (thermal-initiators and photo-initiators) or inorganic substances (*e.g.* oxidation-reduction pairs). Thermal- and photo-initiators both possess labile covalent bonds which undergo homolytic dissociation once sufficient energy is absorbed by the molecule. Radicals are formed when dissociation occurs and these radicals react with monomer to initiate the chain reaction. Examples of some common initiators are given in figure 1.3. Polymer chemistry based upon such initiator systems is a well established and commercially highly successful field[1,2].

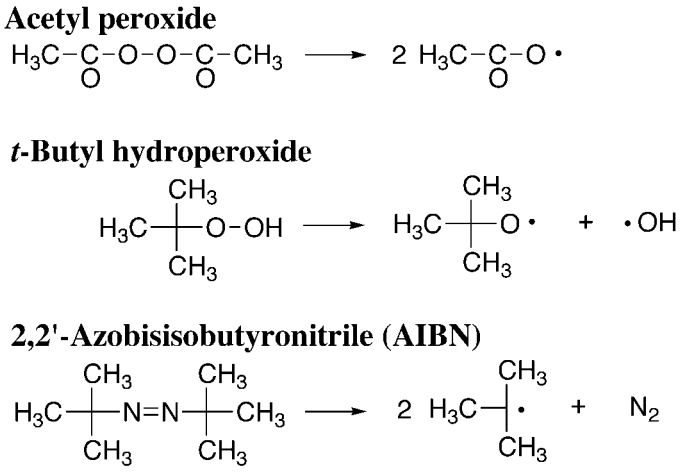

Figure 1.3 Initiators for radical polymerization.

An alternative method of initiating polymerization involves the use of ionizing radiation. There are several advantages to the use of ionizing radiation for the initiation of polymerization. From a commercial point of view, the attractiveness lies in the fact that such reactions can be initiated at ambient temperature with potentially reduced energy costs. Furthermore, products can be made without added initiator resulting in materials of high purity. The only residue present in the final product, provided the reaction is conducted in the bulk monomer, is the monomer itself and a low concentration of side-products produced by ionizing radiation. Residues present in conventional initiator-based systems can result in products with undesirable properties. For example, there is evidence that some initiator-derived end-groups can lead to yellowing and thermal instability[1]. There is also a growing concern about the toxicity of trace amounts of initiator residues

present in polymeric products, especially for products which are used in the food packaging and medical industries. Another important aspect to the use of ionizing radiation is the optical purity which can be obtained. Advanced polymeric products for device applications are required to meet many strict specifications, one of which is the ability to transmit light over a wide range of wavelengths[3,4]. Many thermal- and photo-initiators absorb strongly in the ultraviolet region of the electromagnetic spectrum, a property which excludes their use in the fabrication of certain products such as lenses and fiber-optic cables.

1.2. Ionizing Radiation

Ionization involves the transfer of sufficient energy to a bound electron located in an atomic or molecular orbital of the irradiated material that the electron becomes free. Such ejected electrons eventually loose their excess kinetic energy via electronic, vibrational and rotational excitation of the molecules in the medium. "Ionizing radiation" is a general term which includes several different forms of radiation. This can be ultra-short electromagnetic waves such as X- or γ-rays, or high-energy particle beams of electrons, ions, or neutrons. All of these forms of radiation can be employed for the preparation of polymeric products. However, in this thesis the major focus will be on the use of γ-rays and high-energy electrons.

While high-energy (accelerated) ions or neutrons could in principle also be employed for the production of polymers, the practical application of these types of radiation on an industrial scale is unlikely. However, research is being carried out currently on the use of accelerated ions for the *modification* of polymeric products[5]. For example, ion beams have been used for the preparation of porous polymer membranes which are responsive to changes in temperature or pH[6,7]. Changes in the electrical conductivity of certain polymeric materials on ion bombardment have also been investigated with a view to commercial application[8,9].

1.2.1. High-Energy Electromagnetic Radiation

In order for electromagnetic (EM) radiation to be considered ionizing in character, it must by definition contain sufficient energy to cause ionizations in an irradiated material (*i.e.* the energy of the individual photons must exceed the ionization potential of the constituent molecules which for organic materials is usually several electron volts). According to the 1996 European Guideline of the European Atomic Energy Community (EURATOM), EM radiation with a wavelength of 100 nm or less is considered ionizing in character. This corresponds to a photon energy of 12.4 eV or more. Equation 1.1 shows the relationship between the photon energy, E_λ, in joules and the frequency, ν, in Hertz or the wavelength, λ, in meters.

$$E_\lambda = h\nu = \frac{hc}{\lambda} \tag{1.1}$$

In equation 1.1, h is Planck's constant (6.626 x 10^{-34} J s) and c is the speed of light in vacuum (2.998 x 10^8 m/s).

Figure 1.4 qualitatively depicts the relationship between the photon energies for various forms of EM radiation and their corresponding wavelengths. It should be noted that a sharp division in energy between different forms of EM radiation does not always exist. For example, there is overlap between ultraviolet (UV) radiation, with wavelengths between 4 and 400 nm, and X-rays, with wavelengths typically between 0.01 and 100 nm. Likewise, there is no sharp division between the energies of X-rays and γ-rays. The primary distinguishing feature of the different types of EM radiation is the source of the radiation.

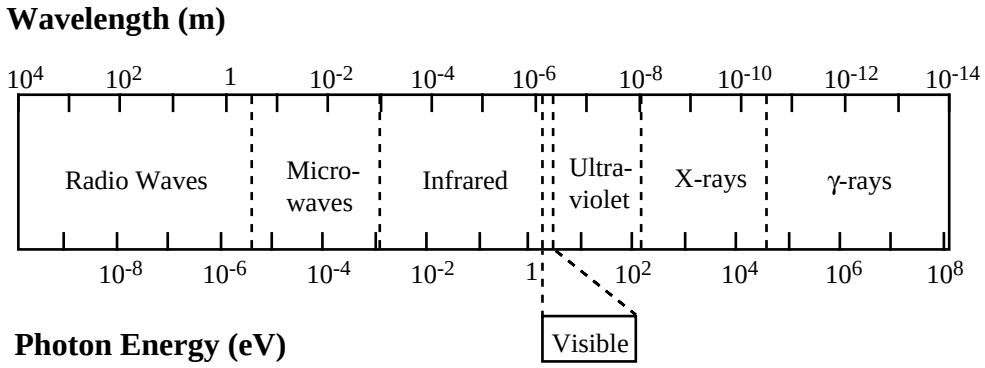

Figure 1.4. The electromagnetic spectrum from the longest wavelength (lowest energy) radio waves to the shortest wavelength (highest energy) γ-rays.

Typical sources for the generation of ionizing UV radiation include rare gas discharge lamps and lasers. In such devices, rare gas ions and excited states are formed by an electrical or radio-frequency discharge. The input energy required for the emission of EM radiation in the vacuum UV region with wavelengths below 100 nm is high and the photon intensities obtained are low. Furthermore, in order to apply ionizing UV radiation for the initiation of polymerization, reactors must be made with a window-less construction and the process must be carried out under vacuum because of the absorption by oxygen in air. For these reasons, the use of ionizing UV radiation for the production of polymers has not been commercially developed.

There are two different origins of X-rays; the slowing down of electrons in a coulombic field (*Bremsstrahlung*) and the filling of inner electron orbital vacancies by electrons from outer orbitals (characteristic X-rays). Both processes occur in the X-ray tubes used for the preparation of X-ray photographs. In such devices, electrons are accelerated between a heated cathode and a metal anode target in which the electrons are stopped and consequently the X-rays are produced. The

photon energy spectrum of the X-rays from such devices consist of a number of peaks superimposed on a broad continuum. X-rays can also be produced by electron accelerators by the interaction of the high-energy electrons with heavy atom targets.

Gamma-rays are produced by the transitions that occur within the nuclei of certain radioactive elements. The emitted photons are mono-energetic and specific to the isotope from which they originate. By far the most commonly employed radioactive isotope for γ-irradiations is cobalt-60 (Co-60), an isotope with a half-life of 5.272 years. Co-60 emits two γ-photons of equal intensity at 1.17 and 1.33 MeV. It is produced in nuclear reactors by a neutron-capture reaction involving Co-59. Due to the long half-life, the high penetrating power and the ease of production, Co-60 γ-irradiators have become the most commonly encountered sources of γ-rays in both industrial and academic research institutions.

Another frequently used γ-ray source is cesium-137, a fission product from nuclear reactors. The energy of the emitted photon is 662 keV and the half-life is 30.17 years.

Nuclear reactors themselves are potential sources of γ-rays. However, the radiation field produced is highly mixed with γ-ray photons of various energies and neutrons. This complicates the interpretation of experimental data from a fundamental research point of view and furthermore can result in activation of the irradiated materials.

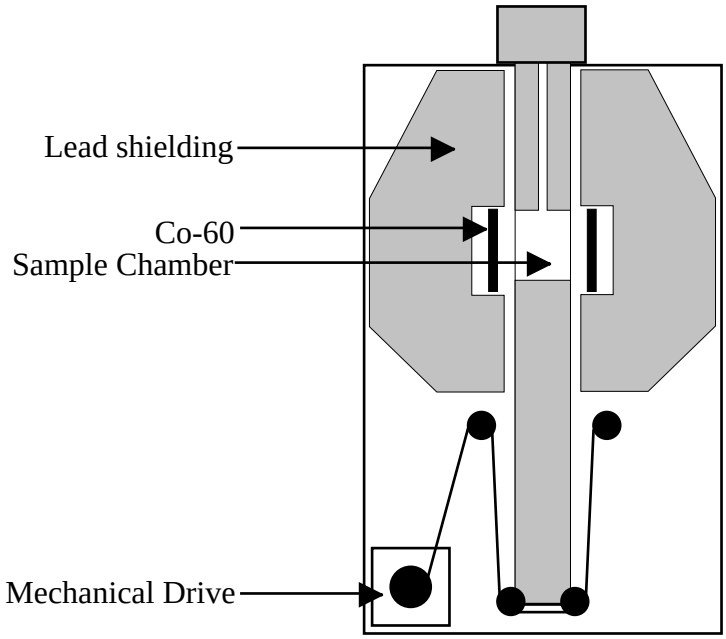

Figure 1.5. A schematic representation of a Cobalt-60 γ-ray irradiator.

A convenient apparatus employed for γ-irradiation is a cylindrical cavity with the source in the form of Co-60 "pencils" fixed concentrically around the cavity. The source is enclosed in lead shielding and samples are lowered into the irradiation field by a mechanical drive mechanism (see figure 1.5 for a schematic representation). The radiation field within the cavity is close to homogeneous, thus permitting the uniform irradiation of samples of a limited size. Because of the sample size constraint, the use of this type of radiation source is usually limited to academic research institutions. All of the γ-irradiation experiments described in this thesis involve the use of this type of irradiator. For the irradiation of large or multiple samples, open, retractable source designs are usually employed. Such designs involve an irradiation room in which raising and lowering of the source is controlled from a safe, remote location.

1.2.2. High-Energy Electrons

Electron accelerators are employed as sources of high-energy electrons both in research institutions and in industry. There exist various types of electron accelerators which can produce intense electron beams with energies ranging from tens of kilovolts up to gigavolts. For commercial purposes, electron energies are limited to less than 12 MeV because of the likelihood of forming unstable, radioactive elements in the irradiated materials at higher energies. The type used for experiments described in this thesis is a Van de Graaff electrostatic accelerator (see figure 1.6) which produces pulses of 3 MeV electrons with a variable pulse duration from 0.2 to 250 ns. The maximum beam current during the pulse is *ca* 4 A. The accelerator can also be operated in continuous-current mode with a maximum DC current of 1 mA. For a more detailed description of this Van de Graaff accelerator, the reader is referred to the publications of the IRI accelerator group[10-13].

Another type of accelerator used for the generation of electron (or ion) pulsed beams is the LINAC (Linear Accelerator) which can produce electron energies from a few MeV up to hundreds of GeV. Such accelerators utilize alternating current along a linear array of electrodes which results in synchronous acceleration along the path of the charged particles. These accelerators produce inherently trains of short (picosecond) pulses of electrons.

The Electrocurtain® processor is an accelerator specifically designed for the continuous electron irradiation of large areas. Such an accelerator employs a long, heated cathode for the thermal emission of electrons across a potential (10's to 100's of keV) perpendicular to the irradiated samples typically placed on a conveyor belt. Such a design is particularly suited for the curing of coatings in a continuous process.

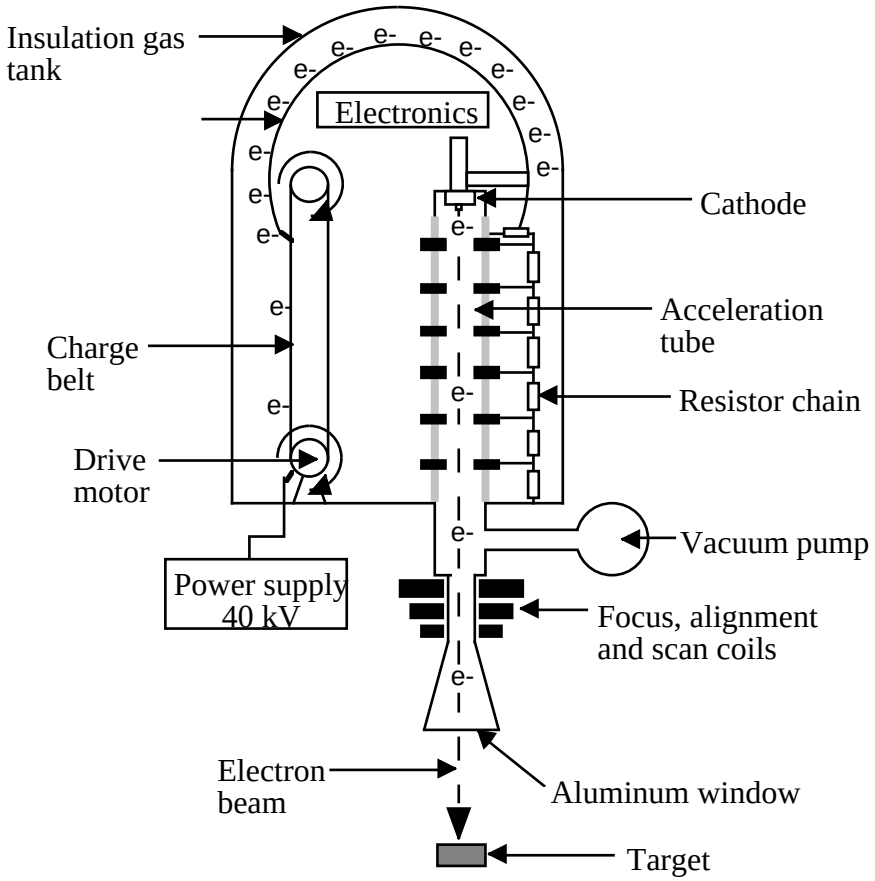

Figure 1.6. A Schematic representation of a Van de Graaff accelerator.

1.3. Interactions of Ionizing Radiation with Matter

The discussion of the interaction of ionizing radiation with matter will be divided into those involving X- or γ-rays and those involving high-energy electrons. These two forms of ionizing radiation produce ultimately very similar radiation-chemical effects since the energy of high-energy photons is converted into kinetic energy of electrons. The main difference is in their penetrating power and dose-depth profiles. The initial physical processes involved in the interaction of ionizing radiation with matter are discussed prior to a discussion of the primary chemical species formed.

1.3.1. X-rays and γ-rays

The initial interactions of high-energy photons with matter are classified under the following types; the photoelectron effect, the Compton effect and electron-positron pair production. Which effect occurs with the highest probability depends upon both the photon energy and the Z-value, or

atomic number, of the irradiated material (see figure 1.7). These processes are discussed separately below.

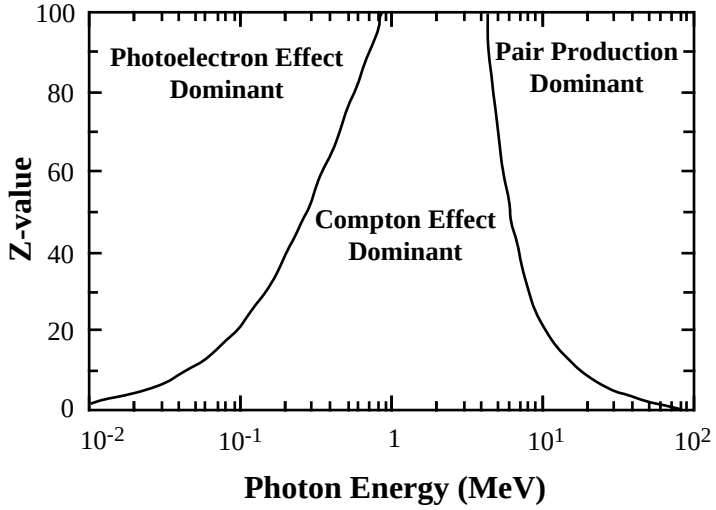

Figure 1.7. Dominant photon interactions as a function of the interacting photon energy and the Z-value (atom number) of the irradiated material.

1.3.1.1. The Photoelectron Effect

The photoelectron effect, or photo-effect, involves the complete transfer of all the energy of a γ-photon to a bound electron of the medium. This electron, termed the photoelectron, obtains a kinetic energy equal to the energy of the incident gamma-photon less the binding energy (E_b) of the electron. As such, E_b is a threshold energy value since the photo-effect cannot take place at lower photon energies. The energy of the photoelectron is subsequently lost by coulombic interactions with other electrons in the material resulting in excitations and ionizations, as described in section 1.4.1.

The probability of the photo-effect occurring is largest when the energy of the photon is close to the binding energy of the interacting electron. This means that for photons with energies of several hundred eV or more, the photo-effect will occur with the electrons located in the innermost atomic orbitals. At lower energies, electrons in outer orbitals will be involved. For low-Z materials, the photoelectron effect is only important for energies of a few hundred eV or less and is therefore relatively unimportant in organic materials for primary Co-60 γ-rays.

Photons of low to moderate energies when irradiating samples with *ca* 1 MeV Co-60 γ-rays can be generated by the secondary electrons produced. One mechanism is by the emission of *Bremsstrahlung*. This can originate when electrons travel close to atomic nuclei and experience a deceleration due to the coulombic interaction. The energy lost by the electron due to this slowing

down is converted into an X-ray photon. The probability of this occurring is quite low for materials with low Z-values. The occurrence of *Bremsstrahlung* in Co-60 γ-irradiators can be explained by the presence of the high-Z lead shielding.

A second source of low-energy photons arises from the ejection of photoelectrons from inner shell orbitals. This leaves a void behind which is rapidly filled by an outer electron. The resulting release of energy can be dissipated by one of two processes; the emission of a characteristic X-ray photon or the expulsion of an Auger-electron. In the former case, the energy of the X-ray photon is equal to the difference between the binding energies of the inner (previously vacant) orbital and the outer (newly created) orbital void. Another source of photons with lower energies than the primary γ-ray is the Compton-effect which is discussed in the following section.

1.3.1.2. The Compton Effect

The Compton effect is the predominant primary interaction between γ-ray photons from Co-60 and low-Z materials. The Compton effect involves a billiard-ball-like collision between a photon and a bound electron. A fraction of the energy from the γ-photon is transferred to the electron which is known as the Compton recoil electron. The remainder of the energy is carried away by the photon which is scattered by the collision. How much energy is transferred during this process is related to the deflection angle of the scattered photon. The maximum energy transfer occurs when the deflection angle is 180º. As for a photoelectron, the energy of the Compton recoil electron is dissipated within the irradiated sample via coulombic interactions with other electrons in the material resulting in excitations and ionizations.

1.3.1.3. Pair Production

Pair production is a process in which a photon in the close vicinity of an atomic nucleus is converted into an electron and a positron. Einstein's equation ($E=mc^2$) requires that the energy of the photon is greater than that corresponding to the rest mass of the two particles, *i.e.* $h\nu > 2m_ec^2 = 1.022$ MeV. Any excess energy is carried away by the particles in the form of kinetic energy. These particles will loose their excess kinetic energy via coulombic interactions with electrons in the material until they become thermalized by inelastic collisions involving vibrational, rotational and kinetic excitation of the molecules of the medium. The positron will ultimately undergo annihilation with an electron in the sample. Annihilation is the opposite of pair production in that the masses of the positron and electron are converted into high-energy photons. These photons can interact further with the electrons in the sample via the photoelectron or the Compton effects.

Pair production becomes a predominant effect only when the energy of the photon involved exceeds *ca* 4 MeV and the Z-value of the irradiated material is high. For this reason, only the

photoelectron and Compton effects will be prevalent in the Co-60 irradiations of the materials discussed in this thesis.

1.3.1.4. Penetration Profiles of X-rays and γ-rays

As mentioned above, ca 1 MeV γ–rays transfer their energy to an irradiated medium mainly via Compton scattering. The decrease in the photon flux as a function of depth, *x*, within a medium is determined by the "linear attenuation coefficient", $\mu_C(E_\lambda)$, which is related to the number density of molecules, *N*, the number of electrons per molecule, *Z*, and the Compton cross section per electron, $\sigma_C(E_\lambda)$.

$$\mu_C\left(E_\lambda\right) = NZ\sigma_C\left(E_\lambda\right) \tag{1.2}$$

The photon intensity, *I*, decreases exponentially with depth according to equation 1.3.

$$I = I_0 \exp\left[-\mu_C(E_\lambda)x\right] \tag{1.3}$$

This exponential decrease in photon flux is illustrated in figure 1.8 for 1 MeV photons in water. For most condensed organic materials $\mu_C(E_\lambda)$ is close to 0.06 cm^{-1} for 1 MeV photons which corresponds to a 1/e penetration depth of 17 cm. For the typical sample dimensions of *ca* 1 cm used in the present work, the intensity would decrease by only *ca* 6% on passing through the material. However, because of the concentric arrangement of the source used, the variation in dose within the sample is in fact negligible.

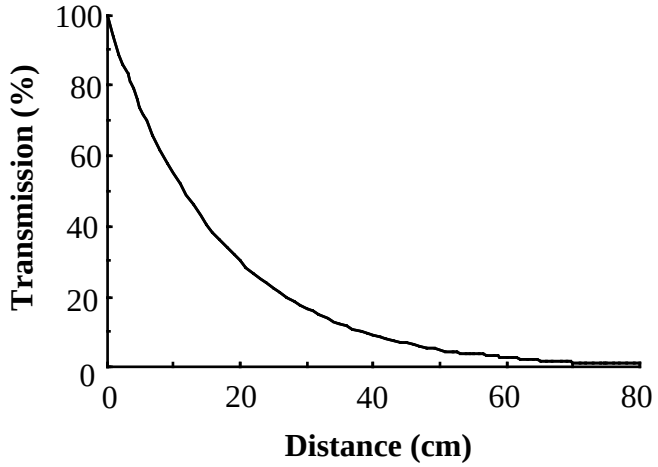

Figure 1.8. Transmission curve of 1 MeV photons through water.

1.3.2. High-Energy Electrons

Fast electrons loose their kinetic energy predominantly by inelastic collisions involving fractional energy losses to bound electrons of an irradiated material. The mechanism of energy transfer involves coulombic interactions which cause discrete excitation and ionization events along the track (*i.e.* path) of an electron. Often, the energy transfer is sufficient to form secondary, high-energy electrons, δ-rays, which in turn loose their kinetic energy via small losses. Fast electrons eventually become thermalized by inelastic collisions involving vibrational, rotational and kinetic excitation of the molecules of the medium. The following sections will discuss in detail energy transfer and the dose-depth profiles for samples irradiated with high-energy electrons.

1.3.2.1. Linear Energy Transfer

The energy dissipated locally along the track of a primary electron is quantitatively described by the so-called linear energy transfer, LET (LET = -*dE/dx*). For relativistic electrons, *i.e.* those with a velocity, v, on the order of the speed of light, c, the LET in joules per meter is given by the Bethe equation[14],

$$-\frac{dE}{dx} = \frac{2\pi e^4}{(4\pi\varepsilon_0)^2 m_e \mathrm{v}^2} N_e \left[\ln\left(\frac{m_e \mathrm{v}^2 E}{2I^2(1-\beta^2)} \right) + F(\beta) \right] \tag{1.4}$$

In equation 1.4, m_e is the rest mass of the electron, N_e is the number density of electrons per cubic meter, $F(\beta)$ is a complex function of β (β = v/c, see equation1.5) and I is an empirical parameter called the *mean excitation energy*.

$$F(\beta) = 1 - \beta^2 + \frac{1}{8}(1 - \sqrt{1-\beta^2})^2 - \ln 2(2\sqrt{1-\beta^2} - 1 + \beta^2) \tag{1.5}$$

For 3 MeV electrons β equals 0.9894 and equation 1.4 reduces to equation 1.6.

$$-\frac{dE}{dx} = \frac{2\pi e^4}{(4\pi\varepsilon_0)^2 m_e \mathrm{v}^2} N_e \left[\ln\left(\frac{m_e \mathrm{v}^2 E}{0.042 I^2} \right) - 0.299 \right] \tag{1.6}$$

An important conclusion that can be drawn from the Bethe equation is that the LET of electrons should be only weakly dependent on the electron energy via the logarithmic term in equation 1.6. The LET of 3 MeV electrons in water has been determined to be 1.88 MeV/cm[15] which corresponds to a value of I equal to 99.5 eV.

To a good approximation, electrons have a maximum penetration power (or range, R) in water and hydrocarbon liquids of *ca* 0.5 cm/MeV. Since primary energy loss events involve on average *ca* 40 eV for low-Z molecular materials[16], such events will be separated on average by a

distance of 200 nm. Because most secondary electrons have considerably less energy than the primary electron, they become thermalized within a few nanometers of the primary electron track.

1.3.2.2. Dose-Depth Profile of Electrons

Experimentally, the dose-depth distribution is found to be complex due to scattering effects. The data for 3 MeV electrons in water is shown in figure. 1.9. As is evident in the figure, the dose-depth distribution for electrons is very different from the close to exponential dependence expected for γ-rays (see figure 1.8).

Irradiations performed with the Van de Graaff electron accelerator described in this thesis involve a beam of electrons impinging on the sample from only one side. The energy is initially attenuated in the quartz window of the cell containing the sample as shown in figure 1.9. The variation in the energy imparted within the sample is *ca* ten percent compared to the average. Energy deposition is therefore close to uniform throughout the bulk of the material.

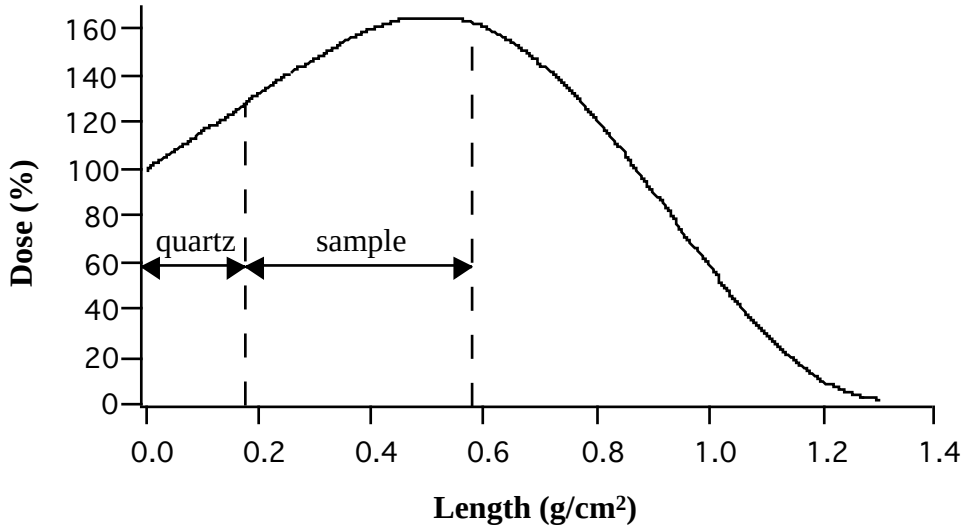

Figure 1.9. The dose-depth dependence for 3 MeV electrons. The position of the sample for experiments in this thesis is shown by the vertical dashed lines.

As is evident in equation 1.4, the dose imparted by high-energy electrons is directly proportional to the electron density of the irradiated material, N_e (1/L), which is given by equation 1.7.

$$N_e = \frac{\rho N_A \sum_x Z_x}{M_W} \tag{1.7}$$

In equation 1.7 ρ is the density in kilograms per liter, N_A is Avogadro's number (6.022 x 10^{23} 1/mole), Z_x is the atomic number of the constituent atoms in the molecule and M_W is the molecular mass of the molecule. A consequence of this is that the dose, D_m, in a material *m* can be determined from that in a standard, D_s, using the ratio of the electron densities as shown in equation 1.8.

$$D_m = D_s \frac{N_{e,m}}{N_{e,s}} \tag{1.8}$$

In practice, the dose imparted by high-energy electrons is usually determined in water by a dosimetry method which is discussed in detail in chapter 2. This results in equation 1.9 for the determination of dose in a material *m*.

$$D_m = 1.80 \times D_{H_2O} \left[\rho \sum_x Z_x \Big/ M_W \right]_m \tag{1.9}$$

1.4. Radiation-Chemical Species

As a result of the primary interactions approximately equal numbers of excitations and ionizations occur in an irradiated material. Subsequently a number of secondary reactions can take place; molecular dissociation, electron capture, charge recombination as well as inter- or intramolecular energy transfer. For many years, the exact nature and fates of the primary species were not known and many reaction mechanisms proposed in the early days of radiation chemistry were highly speculative[17].

Direct evidence for the formation of ions came via early conductivity measurements with gases exposed to α-rays which resulted in the term "ionizing radiation". Much later, mass spectrometry provided information about the precise nature of the primary ionic species formed in gaseous media. Electron spin resonance (ESR) experiments gave further information about the free radical products formed by radiolysis[18-21]. In more recent times, pulse radiolysis experiments using a variety of time-resolved detection techniques have provided extensive information on the nature of the primary species and their reactions[22-24].

In the following sections, the products and processes in an irradiated material will be discussed. Section 1.4.1 deals with excitation and ionization. These two processes lead initially to the formation of energetic species which are often unstable and can decompose into free radicals which are separately discussed in section 1.4.2.

1.4.1. Excitation and Ionization

All molecules possess a number of orbitals which can be occupied by their electrons. Each of these orbitals can contain a maximum of two electrons with opposite spin. The vast majority of molecules in their energetically relaxed ground state contain an even number of electrons with the electron pairs having opposite spin. This results in a net spin of zero and the molecule is said to be in a singlet state which is represented as S_0 in figure 1.10. A notable exception is molecular oxygen, O_2, which has a triplet (T) ground state in which two valence electrons have parallel spins. Excitation involves the promotion of an electron within a molecule to an energetically higher and previously unoccupied orbital. This can occur by the absorption of a photon or the transfer of energy due to coulombic interactions with energetic, charged particles. If the promoted electron maintains its spin the molecule is said to be in an excited singlet state. This is represented by states S_1, S_2 and S_3 in figure 1.10. If however the electron undergoes a change of spin, the net spin of the molecule changes from zero to one and the molecule is said to be in a triplet state (T). The classification of triplet and singlet states is due to the fact that in a magnetic field, molecules with a net spin of one have three discrete energy levels whereas with a net spin of zero there is only one. Triplet states can be formed from singlet states by a process known as intersystem crossing (step *4* in figure 1.10).

With increasing excitation energy, the orbitals become more extended in space until ultimately the ionized state is reached in which the electron is no longer bound to the molecule. This is schematically depicted as step *2* in figure 1.10. The energy required to ionize the molecule is termed the ionization potential. The ionization potentials of the outermost electrons for most molecules lie between 6 and 15 eV.

For much higher excitation energies electronic transitions can also occur with the inner electrons of a molecule, *i.e.* those electrons located in orbitals closer to the atomic nucleus. Typically, the energies required for ionization of these inner electrons are on the order of several hundred eV or more.

A molecule which is in an energetically excited state can relax back to the ground state via one of three processes; fluorescence, phosphorescence or non-radiative decay. Fluorescence is a spin-allowed transition (illustrated by step *3* of figure 1.10) which usually occurs on a time scale of nanoseconds. Phosphorescence (step *5* of figure 1.10) on the other hand is a spin-forbidden process which usually occurs on a time scale of microseconds to minutes.

Figure 1.11 is a potential energy diagram which, while greatly simplified, is useful in describing the excitation process. Although the diagram strictly only applies to a diatomic molecule, it provides at least a qualitative picture of the processes occurring for any two atoms or groups of atoms in a polyatomic molecule. Typically, atomic nuclei vibrate about a nuclear separation which corresponds to the minimum of the potential energy surface (represented by the parabolic curves). The Franck-Condon principle states that because atomic nuclei are much more massive than electrons, an electronic transition will take place faster than the nuclei can respond

resulting in a "vertical" transition as represented by k_1 in figure 1.11. This can lead to the formation of a vibrationally excited state if the equilibrium geometry of the relaxed excited state is different from that of the ground state. Vibrational relaxation (*i.e.* nuclear rearrangement) will follow on a time scale of a few picoseconds. The molecule will eventually return to a vibrationally excited ground state via radiative or radiationless deactivation (represented by k_2). The difference between the energies of the absorptive and emissive transitions leads to the well-known Stokes shift.

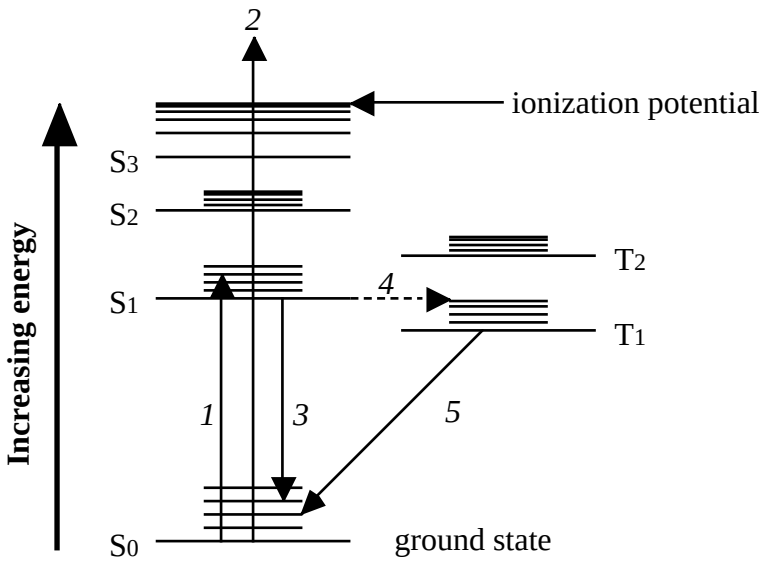

1 *excitation*
2 *ionization*
3 *fluorescence / non-radiative relaxation*
4 *intersystem crossing*
5 *phosphorescence / non-radiative relaxation*

Figure 1.10. Schematic energy level diagram for a molecule.

The dissociation energy, E_D, is also shown in figure 1.11. This is equal to the difference between the lowest vibrational level of the ground state and the plateau region of the potential energy curve, corresponding to a nuclear separation at which the atoms no longer interact.

Also represented in figure 1.11 is a dissociative excited state, S^{**}, which exhibits no minimum in the potential energy surface but approaches the dissociation limit asymptotically . In this case, the potential energy in excess of E_D is converted into kinetic energy of the nuclei which fly apart from each other and molecular dissociation results. If this occurs by homolytic bond fission, two free radicals (*i.e.* molecules with unpaired electrons) will be formed.

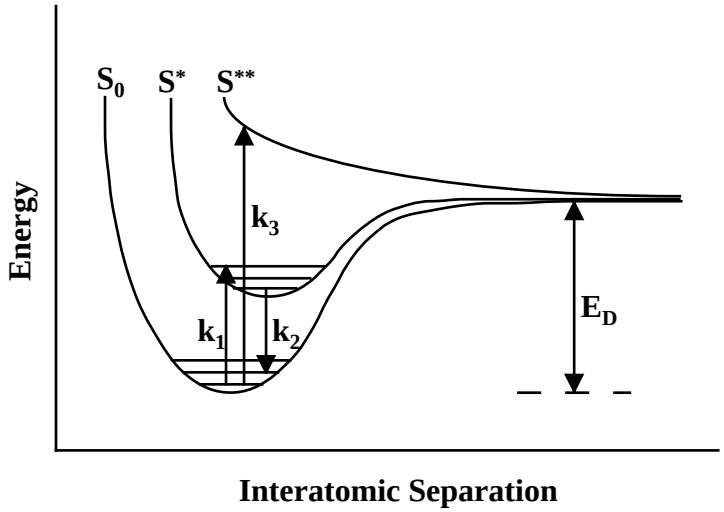

Figure 1.11. Potential energy diagram for a diatomic molecule.

1.4.2. Free Radicals

A frequently occurring dissociative process in organic materials is C-H bond scission which results in the formation of an organic free radical and a hydrogen atom as shown below.

$$RH \rightarrow R\bullet + H\bullet \qquad \text{(A)}$$

The hydrogen atom can undergo a subsequent hydrogen atom abstraction reaction with the formation of a second free radical and H_2 (reaction B).

$$H\bullet + RH \rightarrow R\bullet + H_2 \qquad \text{(B)}$$

Free radicals can also originate from radical cations and anions. When ionization occurs, the interacting molecule is left with both an unpaired electron and a net positive charge. Such a species is known as a radical cation. Reactions of radical cations with neutral molecules are also possible and can result in the formation of neutral free radical species. The classic example of this is the reaction of the radical cation of water with water to form the hydroxyl radical.

$$H_2O^+\bullet + H_2O \rightarrow H_3O^+ + OH\bullet \qquad \text{(C)}$$

Electron capture is a reaction which can occur in the radiolysis of certain materials which have a positive electron affinity. This can lead to dissociation if the molecule contains an atom or group of atoms having an electron affinity higher than the binding energy to the rest of the molecule (*e.g.* halogenated compounds). In this case, molecular dissociation will occur spontaneously

leading to the formation of a negative ion and a free radical. The electron capture reaction of carbon tetrachloride is an example of such a reaction.

$$CCl_4 + e^- \rightarrow CCl_3 \bullet + Cl^- \qquad \text{(D)}$$

Ultimately, positive and negative charges will mutually neutralize by recombination of positive ions with electrons or negative ions. The former reaction can be of importance for radiation-chemical change since the energy gained by the resulting neutral molecule is equal to its ionization potential. Such highly excited molecules have a high probability of undergoing dissociation. Charge neutralization via positive ion-negative ion recombination can also lead to molecular excited states. However, this process is expected to lead to less radiation-chemical change than electron-ion recombination since the energy released is lower than the ionization potential. Furthermore, this energy can be distributed between the two molecular and/or atomic products of the reaction.

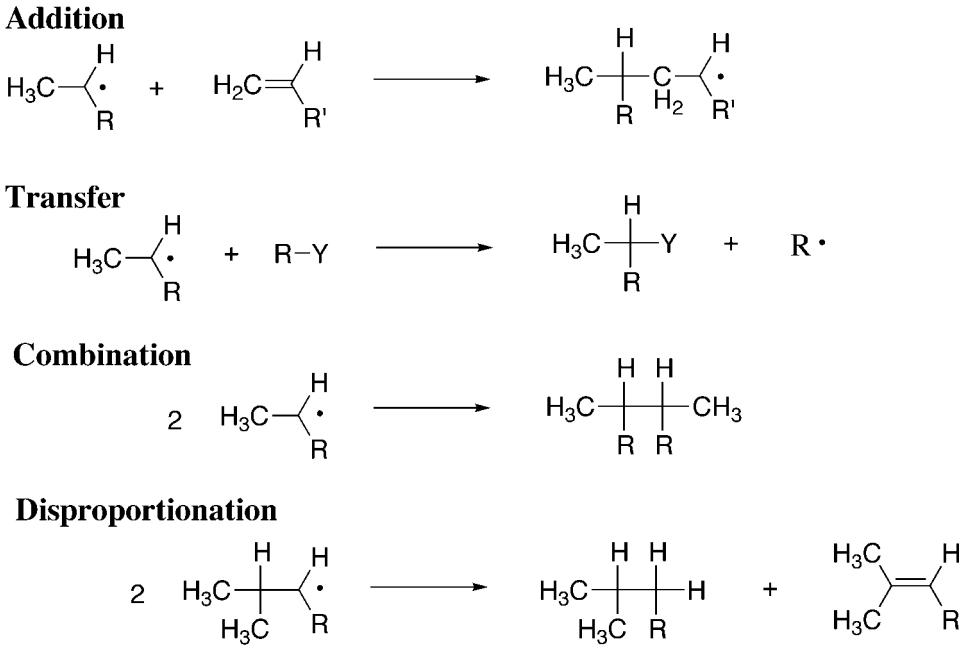

Figure 1.12. Reactions of free radicals.

As can be seen from the above, neutral free radical species are formed in many of the secondary processes following energy deposition. The reactions of free radicals are of the following types; addition, transfer, combination and disproportionation (see figure 1.12). Addition and transfer involve reactions in which a free radical remains as a product. Combination and

disproportionation on the other hand result in elimination of free radical species. The relevance of these reactions in radiation-induced polymerization will be discussed in more detail in the following sections.

1.5. Radiation-Induced Polymerization

Polymerization initiated by ionizing radiation most often occurs via a free radical mechanism. The radiation-induced cationic polymerization of monomers such as styrene[17], isobutene[25] and vinyl ethers[26] has been observed. The polymerizations investigated in this thesis involve exclusively the free radical mechanism and the discussion which follows is limited accordingly to free radical processes.

The overall process of polymerization can be broken down into four distinguishable steps; free radical formation, initiation, propagation and termination. These reactions are general and can be applied to various types of monomers and initiating mechanisms. Some aspects unique to the special case of radiation-induced polymerization will be mentioned below.

1.5.1. Free Radical Formation

Polymerization requires the formation of free radical species which start the chain reaction.

$$R \xrightarrow{F_R} R\bullet \qquad \text{(E)}$$

The rate of radical formation, F_R (M/s), will be dependant upon the dose rate, D' (Gy/s), in the sample according to equation 1.10.

$$F_R = \frac{\rho D' G(R\bullet)}{100 e N_A} \qquad (1.10)$$

Here ρ is the density (g/cm^3), $G(R\bullet)$ is the number of free radicals formed per 100 eV absorbed, e is the value of the elementary charge (1.602 x 10^{-19} C) and N_A is Avogadro's number. The dose rate is usually determined by a secondary dosimeter such as the aqueous Fricke dosimeter (described in chapter 3)[27,28]. The dose rate in the material of interest is then calculated from its electron density using equation 1.9.

A consequence of the nonselective nature of the primary energy deposition events when using high-energy radiation is that a variety of primary radicals may be produced. Furthermore, as polymerization proceeds, energy can be absorbed by polymeric chains leading to the direct formation of polymeric radicals. These macromolecular radicals may further react by initiating

polymerization resulting in branched polymer chains. The relative importance of this initiation mechanism should increase as the extent of the monomer conversion increases.

1.5.2. Initiation

Initiation is the reaction of the primary radicals with a monomer unit.

$$R\bullet + M \xrightarrow{k_i} RM\bullet \qquad \text{(F)}$$

The rate constants for initiation, k_i, by carbon-centered radicals[1] typically lie within the range of 10^5-10^6 $M^{-1}s^{-1}$. These rates are orders of magnitude lower than expected for diffusion-controlled reactions, *i.e.* 10^9-10^{10} $M^{-1}s^{-1}$ in liquids of viscosity close to 1 cP. In other words, reaction F occurs with an efficiency much less than 1 % per encounter between $R\bullet$ and M.

1.5.3. Propagation

Propagation involves the repeated addition of monomer units to a polymeric free radical resulting in a continuous increase in molecular mass. This is represented by the general reaction

$$RM_n\bullet + M \xrightarrow{k_p} RM_{n+1}\bullet \qquad \text{(G)}$$

The rate constant of propagation, k_p, can vary considerably depending upon the monomer. Many acrylates for example have propagation rate constants of *ca* 10^4 $M^{-1}s^{-1}$ whereas propagation rate constants for styrene monomers at the same temperature are *ca* 10^2 $M^{-1}s^{-1}$ or less. Evidence from pulsed laser polymerization (PLP) experiments[29,30] indicates that the propagation rate constant is independent of the size of the polymeric radical. Propagation will continue until either all of the monomer in the system is consumed or the activity of the free radical is destroyed by a termination reaction.

1.5.4. Termination

Termination is the most complicated and extensively studied process in polymer production. It can occur by bimolecular reaction between two growing polymeric free radicals or by chain transfer or addition reactions of a polymeric free radical with other constituents of the medium. In the case of radical-radical termination (RRT) non-radical products are formed by either combination or disproportionation reactions. Combination results in the formation of a polymeric molecule with a molecular mass equal to the sum of the masses of the two reacting species.

$$RM_m\bullet + R'M_n\bullet \xrightarrow{k_{tc}} RM_{(m+n)}R' \qquad \text{(H)}$$

Disproportionation involves the abstraction of a β-hydrogen atom by one macroradical from another to form a saturated chain end on the former and a double-bond chain end on the latter. For example, in the case of polyethylene polymerization

$$RM_mCH_2CH_2\bullet + R'M_nCH_2CH_2\bullet \xrightarrow{k_{td}} RM_mCH_2CH_3 + R'M_nCH=CH_2 \qquad \text{(I)}$$

When RRT involves a polymeric radical and a primary free radical, the reaction is called primary radical termination (PRT)[31,32]. This specific case of termination becomes important when very high dose rates are employed or in the late stages of polymerization when the monomer concentration is very low.

A three-stage mechanistic picture of RRT has been proposed[33] and this is illustrated in figure 1.13. Stage 1 involves the diffusional motion of the growing polymer chains into the vicinity of each other. This motion is controlled by the bulk viscosity of the medium and the molecular mass. Stage 2 involves the segmental motion of radical chain ends towards each other which is controlled by the microscopic viscosity of the local environment and the flexibility of the chains. Stage 3 involves the chemical reaction between the radical sites.

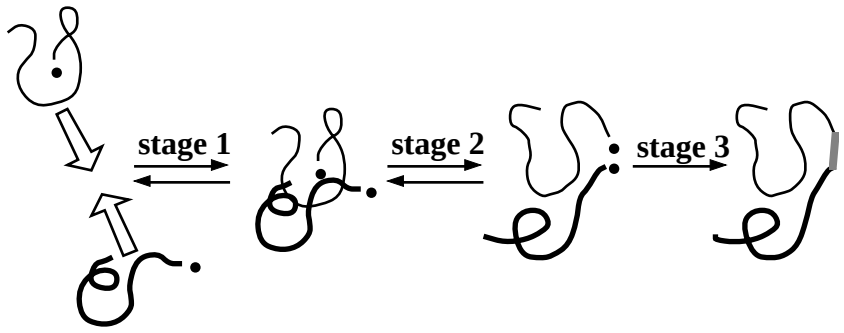

Figure 1.13. Individual stages in bimolecular free radical termination.

The complexity of RRT is due to the highly system-specific diffusional capabilities of polymeric free radicals (*e.g.* chain length, polymer concentration, temperature, *etc.*). This sensitivity is apparent even at low monomer conversion. Consequently, published literature values for the termination rate constant for a given monomer can vary by more than an order of magnitude[34]. The Trommsdorff or "gel" effect[35] is a direct consequence of this *diffusional control*[36-43] of RRT.

Chain transfer (depicted in reaction J), unlike combination or disproportionation, involves the reaction between a radical and a non-radical species.

$$RM_n\bullet \; + \; \mathrm{YX} \xrightarrow{k_{tct}} RM_nX \; + \; Y\bullet \qquad \text{(J)}$$

The free radical product, $Y\bullet$, may or may not initiate the growth of another polymer chain. Effectively, the reactive site is transferred from a growing polymeric molecule to another molecular species. The co-reactant in chain transfer can be either monomer, polymer, solvent or an intentionally added chain transfer agent (*e.g.* thiol or halogenated compounds).

Termination can also occur by reaction of free radicals with molecular oxygen leading to the formation of peroxides and hydrogen peroxides according to the following general reaction schemes.

$$R\bullet + O_2 \rightarrow RO_2\bullet \qquad \text{(K)}$$

$$RO_2\bullet + R'H \rightarrow RO_2H + R'\bullet \qquad \text{(L)}$$

$$RO_2\bullet + M \rightarrow RO_2M\bullet \qquad \text{(M)}$$

The reaction of free radicals with oxygen occurs at the diffusion limit and consequently the production of high molecular mass polymer from typical monomers (*e.g.* styrene and methacrylates) can only occur when the oxygen concentration in a polymerizing system is sub-micromolar.

Control over the termination reaction, and therefore control over the product polymer molecular mass, can be accomplished via a number of means[1] including the use of nitroxides, atom transfer radical polymerization (ATRP), alkyl iodide mediated polymerization or reversible addition-fragmentation chain transfer (RAFT) polymerization. The prerequisites for such control are the following; a small contribution of termination, fast initiation compared to propagation and fast exchange between active and dormant species. For example, nitroxide mediated polymerization involves a reversible deactivation of the free radical species by forming an alkoxyamine (a stable nitroxide) adduct. When the free radicals are active, *i.e.* sufficient thermal energy is absorbed that the nitroxide bond dissociates, polymerization ensues. Effectively, RRT is inhibited.

1.6. Historical Development of Polymerization via Ionizing Radiation

Radiation-induced polymerization has been studied extensively for more than sixty years. Some of the earliest investigations were carried out by Hopwood and Phillips[44] who employed gamma-rays and fast neutrons for the polymerization of methyl methacrylate, styrene and vinyl acetate monomers. Since that time, various sources of ionizing radiation have been investigated for the initiation of polymerization including X-rays[45,46], mixed reactor radiation[47,48], electron beams[49-51], beta-rays[52] and alpha-particles[53]. The historical development of ionizing radiation-induced

polymerization has been thoroughly reviewed by Chapiro[17,54]. Ultimately, the initiative for many research groups to become involved in the radiation chemistry of polymerization was driven by the post World War II rapid growth of nuclear-energy power plants and consequently the ready availability of isotopic sources of high-energy radiation.

In the early stages of research, it was unclear what the underlying mechanism of radiation-induced polymerization was. This uncertainty arose from the realization that both ions and free radicals are formed by the radiolysis of matter. Today it is evident that most radiation-induced polymerizations occur via a free radical chain mechanism, however a contribution from ionic reactions is apparent in some specific systems[17,55]. The evidence for the free radical mechanism came from the following experimental observations; the inhibiting effect of oxygen and benzoquinone (both well-known free radical scavengers), studies in which the chemical composition of radiation-induced polymers were found to be identical to those from known free radical processes, and temperature studies which showed identical activation energies to those found for free radical mechanisms.

1.7. Technological Applications

To date there are several important industrial processes in the polymer field which are based on the application of high-energy radiation. These processes can be classified under one of two types; the synthesis of polymeric materials via radiation-induced polymerization or the modification of preexisting polymeric materials via radiolysis. Examples of the former type include the production of coatings on metals, paper, plastic and wood, the production of hydrogels for medical applications, and radiation-induced graft polymerizations. Examples of the modification of polymeric products are the cross-linking of polyethylene for the production of heat-shrinkable film and tubing and the chain-scission of polymeric products such as poly(tetrafluoroethylene) and natural cellulose in order to assist in processing.

An interesting development in the past decade with considerable commercial potential is in the field of electron-beam lithography. Unlike optical lithography which is intrinsically limited in spatial resolution to micron-sized pattern designs due to the wavelength of the light employed, electron-beam lithography can potentially produce patterns with much higher spatial resolution, down to tens of nanometers[56]. The above technological applications are discussed in more detail in the following sections.

1.7.1. Polymerization Processes

Most existing commercial processes involving ionizing radiation-induced polymerization are based upon electron-beam curing of thin layers. Typically, electrons with energies of 300-500

keV are employed along with curing mixtures composed of preformed polymers and multifunctional monomers. Such systems polymerize at a very fast rate and therefore can be applied to the on-line production of coated materials at fast production speeds. An important advantage of electron-beam curing over commercially-competitive photo-initiated curing is that materials containing large amounts of pigments, such as paints, can be processed.

Hydrogels are two-component materials based upon a cross-linked polymer network and a water phase. These materials often exhibit excellent biocompatibility and are therefore used in contact lenses and wound dressings. Due to their ability to absorb water, ions and certain drugs, hydrogels are excellent materials as dressings on large, open wounds such as those arising from severe burns. The preparation of hydrogels via ionizing radiation has advantages over other methods. For one, the initiation of the reaction occurs in the absence of toxic initiators which must be removed prior to the end use as biomaterials. In addition, radiation-sterilization occurs simultaneously during the processes of gel formation. An excellent review on hydrogels and their preparation by ionizing radiation was written in 1991 by J. M. Rosiak[57].

Graft polymerization involves the polymerization of monomer onto preexisting polymer surfaces. The resultant product has the physical properties of both constituent polymers. Graft polymerization can be accomplished by irradiating the support polymer in the presence of oxygen and subsequently adding monomer, degassing and thermally heating the system. The peroxy species produced in the first step are thermally unstable and upon heating decompose into free radicals which can initiate polymerization of the second component.

An alternative method of inducing graft polymerization is to irradiate a mixture of preformed polymer and monomer. The radical yield from the polymer should be high in comparison to that from the monomer in order to promote the production of graft polymer chains rather than the homopolymerization of monomer. Industrial applications of graft polymerization include the grafting of acrylic acid onto polyethylene (for better adhesion to aluminum metal) and poly(tetrafluoroethylene) (for membranes in batteries).

1.7.2. Cross-Linking and Chain-Scission Processes

Preformed polymers are known to undergo chemical change when exposed to ionizing radiation. The two most important changes in regard to the physical and mechanical properties of the irradiated material are cross-linking and chain-scission. It has been found empirically that polymers containing a main-chain repeat unit with the following structure:

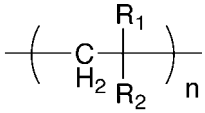

in which R is an alkyl group, chlorine or fluorine atom tend to undergo chain-scission in preference to cross-linking. Examples of this type of polymer are poly(methyl methacrylate) and poly(vinylidene chloride). On the other hand, polymers with the following structure:

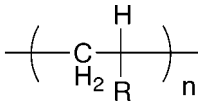

tend to cross-link when exposed to radiation. Examples of this type of polymer include polyethylene and poly(vinyl acetate). It follows that vinyl polymers containing a tetrasubstituted carbon atom along the main chain repeat unit undergo chain-scission, whereas polymers in which each carbon atom in the main chain repeat unit contains at least one hydrogen atom undergo cross-linking[17].

The cross-linking of polyethylene via electron-beam irradiation is an extremely successful industrial process. If after irradiation the polyethylene is deformed by applying a stress at a temperature above the melting point of the crystallites and then allowed to cool, new crystallites form which can impart enough mechanical strength to maintain the shape of the stressed material. The application of heat, and consequent remelting of the crystallites, then leads to a "memory effect" in which the material returns to its original unstressed shape.

Another application with considerable commercial potential is electron-beam lithography. Unlike photolithography which is limited in resolution by the wavelength of the light employed, electron-beam lithography can produce smaller patterns with high resolution. Depending upon the choice of material for the resist (*i.e.* polymer layer), the underlying principle can be either radiation-induced cross-linking or chain-scission. In the former case, the resist material forms an insoluble network. A design can be created by exposure through a patterned mask followed by dissolution of the non-irradiated material. In the latter case the exposed area of the resist becomes soluble leaving the non-exposed areas intact after developing the pattern.

1.8. Thesis Overview

The following three chapters provide additional information pertaining to both radiation-induced polymerization and certain novel techniques employed for monitoring the polymerization process. The latter is of course the reason for preparing this thesis. Chapter 2 describes the experimental methods employed in the investigations discussed in following chapters. This includes detailed descriptions of the ionizing radiation sources and the novel techniques mentioned above. Chapter 3 is describes in detail the specific chemical materials studied in this thesis. Chapter 4 is a detailed discussion relating to the specific polymerization system mentioned in the following chapters, namely that of the methyl methacrylate (MMA) monomer. As the primary

intention of this thesis is to introduce a novel technique by which to monitor the polymerization process, it is imperative to have a detailed understanding of the process itself.

The contents of chapters 5 through 9 have all been either accepted[58-60] or submitted[61,62] for publication by various international journals. Chapter 5 describes the application of a commercial probe molecule for monitoring the radiation-induced polymerization of MMA by steady-state fluorescence techniques. Chapters 6 and 7 introduce two non-commercial probe molecules that also were used for monitoring MMA polymerization by steady-state fluorescence techniques. Chapters 8 and 9 describe the application of time-resolved fluorescence measurements for further investigations. It is shown in chapter 8 that fluorescence decay from two unique probe molecules in solution can be employed for monitoring MMA polymerization. Chapter 9 is essentially a continuation of the investigations described in chapter 8.

References

(1) Moad, G.; Solomon, D. H. *The Chemistry of Free Radical Polymerization*, First ed.; Elsevier Science Ltd.: Kidlington, Oxford, 1995.

(2) Odian, G. *Principles of Polymerization*, Third ed.; John Wiley & Sons, Inc.: New York, 1991.

(3) Kloosterboer, J. G. *Adv. Polym. Sci.* **1988**, *84*, 1.

(4) Kloosterboer, H.; Touwerslager, F. "Chain Crosslinking Photopolymerization of Diacrylates and some Applications in Electronics"; Radtech Asia '93 UV/EB Conference and Exposition: Conference Proceedings, 1993, Tokyo, Japan.

(5) Lee, E. H. *Nucl. Instr. Meth. Phys. Res. B* **1999**, *151*, 29.

(6) Omichi, H. *Nucl. Instr. Meth. Phys. Res. B* **1995**, *105*, 302.

(7) Kaetsu, I.; Uchida, K.; Sutani, K.; Sakata, S. *Radiat. Phys. Chem.* **2000**, *57*, 465.

(8) Bonis, A. D.; Bearzotti, A.; Marletta, G. *Nucl. Instr. Meth. Phys. Res. B* **1999**, *151*, 101.

(9) Davenas, J.; Massardier, V.; Tran, V. H. *Nucl. Instr. Meth. Phys. Res. B* **1996**, *112*, 120.

(10) Luthjens, L. H.; Hom, M. L.; Vermeulen, M. J. W. *Rev. Sci. Instrum.* **1978**, *49*, 230.

(11) Luthjens, L. H.; Hom, M. L.; Vermeulen, M. J. W. *Rev. Sci. Instrum.* **1986**, *57*, 2230.

(12) Luthjens, L. H.; Vermeulen, M. J. W.; Hom, M. L. *Rev. Sci. Instrum.* **1980**, *51*, 1183.

(13) Luthjens, L. H.; Vermeulen, M. J. W.; Hom, M. L. *Rev. Sci. Instrum.* **1982**, *53*, 476.

(14) Bethe, H. A.; Heitler, W. *Proc. Royal Soc. London Ser. A* **1934**, *146*, 83.

(15) *CRC Handbook of Radiation Chemistry*; Tabata, Y., Ed.; CRC Press, Inc.: Boca Raton, 1991.

(16) Hummel, A. Radiation chemistry of alkanes and cycloalkanes. In *The Chemistry of Alkanes and Cycloalkanes*; Patai, S., Rappoport, A., Eds.; John Wiley & Sons: New York, 1992; pp 1-75.

(17) Chapiro, A. *Radiation Chemistry of Polymer Systems*; Interscience Publishers: New York, 1962.

(18) Fessenden, R. W.; Schuler, R. H. *J. Chem. Phys.* **1963**, *39*, 2147.

(19) Bullock, A. T.; Griffiths, W. E.; Sutcliffe, L. H. *Trans. Faraday Soc.* **1967**, *63*, 1846.

(20) Bullock, A. T.; Sutcliffe, L. H. *Trans. Faraday Soc.* **1964**, *60*, 2112.

(21) Zimbrick, J.; Hoecker, F.; Kevan, L. *J. Phys. Chem.* **1968**, *72*, 3277.

(22) Matheson, M. S.; Dorfman, L. M. *J. Chem. Phys.* **1960**, *32*, 1870.

(23) McCarthy, R. L.; MacLachlen, A. *Trans. Faraday Soc.* **1960**, *56*, 1187.

(24) Keene, J. P. *Nature* **1960**, *188*, 843.

(25) Davison, W. H. T.; Pinner, S. H.; Worral, R. *Chem. Ind. London* **1957**, *1957*, 1274.

(26) Hayashi, K. *J. Polym. Sci., Polym. Chem. Ed.* **1980**, *18*, 179.

(27) Fricke, H.; Morse, S. *Am. J. Roentg. Radium Ther. Nucl. Med.* **1927**, *18*, 430.

(28) *Manual on Radiation Dosimetry*; Holm, N. W.; Berry, R. J., Eds.; Marcel Dekker, Inc.: New York, 1970.

(29) Coote, M. L.; Zammit, M. D.; Davis, T. P. *Trends Polym. Sci.* **1996**, *4*, 189.

(30) van Herk, A. M. *J. Macromol. Sci.: Rev. Macromol. Chem. Phys.* **1997**, *C37*, 633.

(31) Dionisio, J.; O'Driscoll, K. *J. Polym. Sci., Polym. Chem. Ed.* **1980**, *18*, 241.

(32) Takács, E.; Wojnárovits, L. *Radiat. Phys. Chem.* **1996**, *47*, 441.

(33) Benson, S. W.; North, A. M. *J. Am. Chem. Soc.* **1959**, *81*, 1339.

(34) de Kock, J. Chain-Length Dependent Bimolecular Termination in Free-Radical Polymerization, Technische Universiteit Eindhoven, 1999.

(35) Trommsdorff, V. E.; Köhle, H.; Lagally, P. *P. Makromol. Chem.* **1947**, *1*, 169.

(36) Norrish, R. G. W.; Smith, R. R. *Nature* **1942**, *150*, 336.

(37) Russell, G. T. *Macromol. Theory Simul.* **1994**, *3*, 439.

(38) Buback, M.; Huckestein, B.; Russell, G. *Macromol. Chem. Phys.* **1994**, *195*, 539.

(39) O'Neil, G. A.; Torkelson, J. M. *Trends Polym. Sci.* **1997**, *5*, 349.

(40) O'Neil, G. A.; Torkelson, J. M. *Macromolecules* **1999**, *32*, 411.

(41) O'Neil, G. A., Wisnudel, M. B.; Torkelson, J. M. *Macromolecules* **1998**, *31*, 4537.

(42) Clay, P.; Gilbert, R. *Macromolecules* **1995**, *28*, 552.

(43) Sack, R.; Schulz, G. V.; Meyerhoff, G. *Macromolecules* **1988**, *21*, 3345.

(44) Hopwood, F. L.; Phillips, J. T. *Nature* **1939**, *143*, 640.

(45) Collinson, E.; Dainton, F. S.; McNaughton, G. S. *Trans. Faraday Soc.* **1957**, *53*, 357.

(46) Prevot, A. *C.R. Seances Acad. Sci.* **1950**, *230*, 288.

(47) Landler, Y.; Magat, M. *Comptes Rendus Hebdomadaires des Séances de L'Academie des Sciences* **1948**, *226*, 1720.

(48) Prevot-Bérnas, A.; Chapiro, A.; Cousin, C.; Landler, Y.; Magat, M. *Disc. Faraday Soc.* **1952**, *12*, 98.

(49) Schmitz, J. V.; Lawton, E. J. *Science* **1951**, *113*, 718.

(50) Brasch, A.; Huber, W. *Science* **1947**, *15*, 297.

(51) Majury, T. G. *J. Polym. Sci.* **1955**, *15*, 297.

(52) Seitzer, W. H.; Tobolsky, A. V. *J. Am. Chem. Soc.* **1955**, *77*, 2687.

(53) Mund, W.; Herman, J. A.; Verfaillie, G. *Bull. Acad. Roy. Belg.* **1949**, *35*, 656.

(54) Chapiro, A. *Historical Outline of the Radiation Chemistry of Polymers*; Royal Society of Chemistry: Cambridge, 1989.

(55) Lawton, E. J.; Grubb, W. T.; Balwit, J. S. *J. Polym. Sci.* **1956**, *19*, 455.

(56) Chang, T. H. P.; Mankos, M.; Lee, K. Y.; Muray, L. P. *Microelectr. Eng.* **2001**, *57*, 117.

(57) Rosiak, J. M. "Hydrogel Dressings"; Radiation Effects on Polymers, ACS Symposium Series; 475, 1990, Washington, D.C., U.S.A.

(58) Frahn, M. S.; Warman, J. M.; Abellon, R. D.; Luthjens, L. H. *Radiat. Phys. Chem.* **2001**, *60*, 433.

(59) Frahn, M. S.; Abellon, R. D.; Jager, W. F.; Luthjens, L. H.; Warman, J. M. *Nucl. Instr. Meth. Phys. Res. B* **2001**, *185*, 241.

(60) Frahn, M. S.; Abellon, R. D.; Luthjens, L. H.; Vermeulen, M. J. W.; Warman, J. M. *Nucl. Instr. Meth. Phys. Res. B* **2003**, *208*, 405.

(61) Frahn, M. S.; Luthjens, L. H.; Warman, J. M. *Polymer* **accepted 2003**.

(62) Frahn, M. S.; Luthjens, L. H.; Warman, J. M. *J. Phys. Chem. B* **submitted 2003**.

Chapter Two

Experimental Techniques

2.1. Introduction

The following sections describe the experimental techniques used in obtaining data presented in this thesis. The sources of ionizing radiation employed for the initiation of polymerization reactions are discussed separately. These include two cobalt-60 (Co-60) γ-ray sources for continuous irradiations and a Van de Graaff electron accelerator for pulsed irradiations. Dosimetry, *i.e.* the method of determining the rate of energy deposition in samples, is discussed separately for both the γ-ray irradiators and the electron accelerator. The set-ups employed for fluorescence experiments are also discussed in this chapter. These include two spectrofluorimeters, one designed for obtaining fluorescence spectra *in situ*, and two fluorescence lifetime set-ups, one

designed for *in situ* lifetime measurements. The remaining sections are devoted to experimental techniques used in determining monomer conversion and polymer molecular mass.

2.2. Continuous γ-Ray Irradiation

Cobalt-60 is the most commonly employed radioactive isotope for γ-ray irradiations. The activity of Co-60 prepared in nuclear reactors can be up to 40 Ci/g (1.5 TBq/g), however sources of 1 to 5 Ci/g are typically encountered. Over 80% of the Co-60 produced world-wide is manufactured by the Canadian company Ontario Hydro and then marketed by another Canadian company, MDS Nordion.

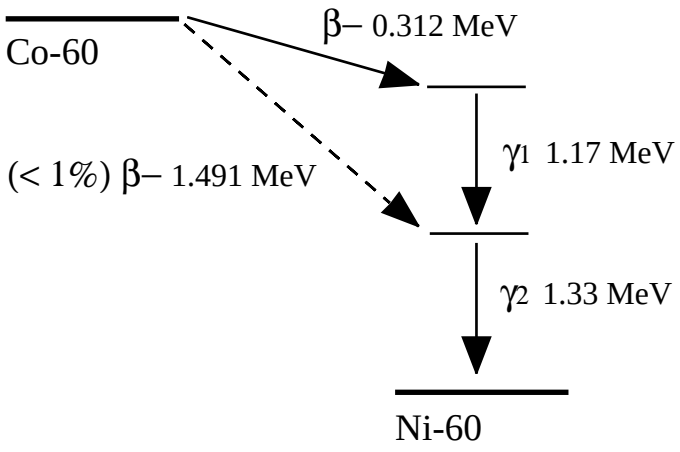

Figure 2.1. Decay scheme of cobalt-60.

Cobalt-60 decays to stable nickel-60 by a nuclear transition (β^--decay) in which a neutron is converted into a proton via the emission of a β^--particle with an energy of 312 keV and two γ-photons, one of 1.17 MeV and another of 1.33 MeV. The half-life of Co-60 is 5.272 years and the decay scheme of this isotope is illustrated in figure 2.1. Gamma-ray irradiations described in this thesis were accomplished with Gammacell irradiators. Such irradiators produce a uniform radiation field by a concentric arrangement of the source around a cylindrical irradiation chamber. The source is encapsulated in stainless steel "pencils". The encapsulation prevents the transmission of the β^--particles and hence the radiation field is composed solely of γ-photons. Irradiations at *ca* 0.7 kGy/hr were carried out with the Gammacell 200 irradiator and those at *ca* 10 kGy/hr were accomplished with the Gammacell 220 irradiator.

2.2.1. The Gammacell 200 Irradiator

The sample irradiation chamber of the Gammacell 200 (Atomic Energy of Canada Ltd.) is cylindrical with a diameter of 8.5 cm and a height of 11 cm. A mechanical drive is used for raising and lowering a central piston which positions the sample in the center of the radiation field (see figure 2.2). The top of the central piston can be opened so that cables, optical fibers, *etc*. can be introduced into the sample chamber. In this way experiments can be conducted *in situ*, *i.e*. during the course of irradiation without the necessity of interruption of the irradiation and removal of the sample for external examination.

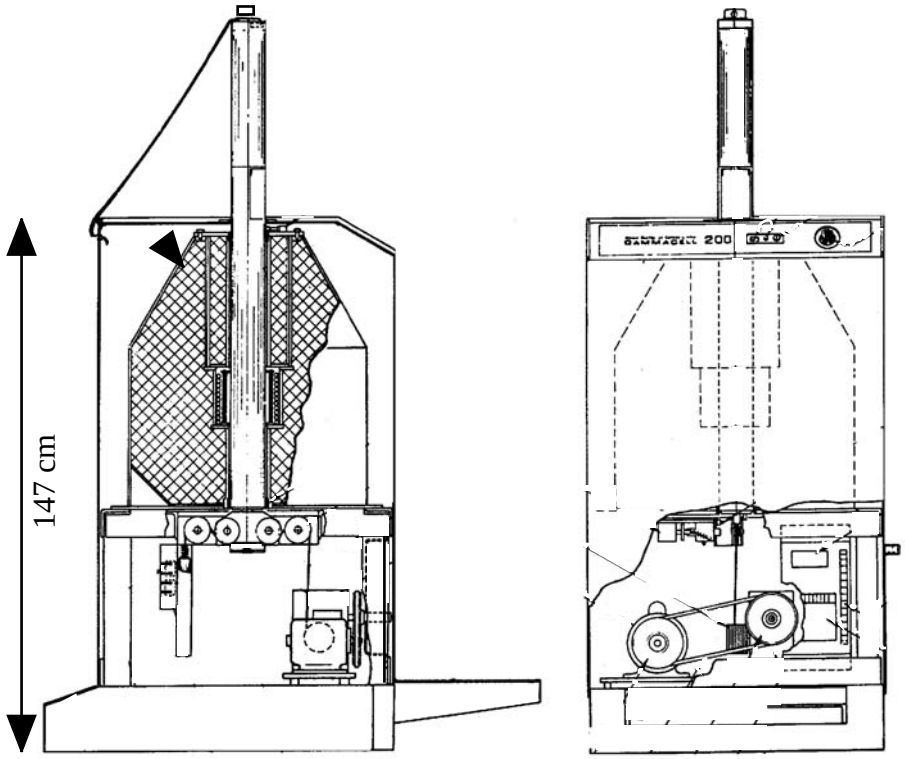

Figure 2.2. Gammacell 200 cobalt-60 irradiator from Atomic Energy of Canada, Ltd.; side (left) and front (right) views.

When received in 1970, the dose rate in the center of the chamber was 1.75 kGy/hr. The source was recharged in 1983 with a total Co-60 activity of 3600 Ci (130 TBq). Dosimetry of the source measured on May 21, 1990 gave a dose rate of 2.45 kGy/hr in the center of the irradiation chamber. More recent dosimetry was carried out on August 20, 1999 and gave a dose rate of 0.720 kGy/hr. The temperature within the source is approximately 2 ºC above room temperature.

2.2.2. The Gammacell 220 Irradiator

Figure 2.3 illustrates the Gammacell 220 irradiator (Nordion International Inc.) employed for dose rates of *ca* 10 kGy/h. The sample chamber has cylindrical dimensions with a height of 20 cm and a diameter of 15 cm. A mechanical drive system operates the raising and lowering of a central piston for loading and irradiating samples. Optical cables, wires, *etc.* can be inserted from the top of the irradiator to the sample cavity for *in situ* experiments.

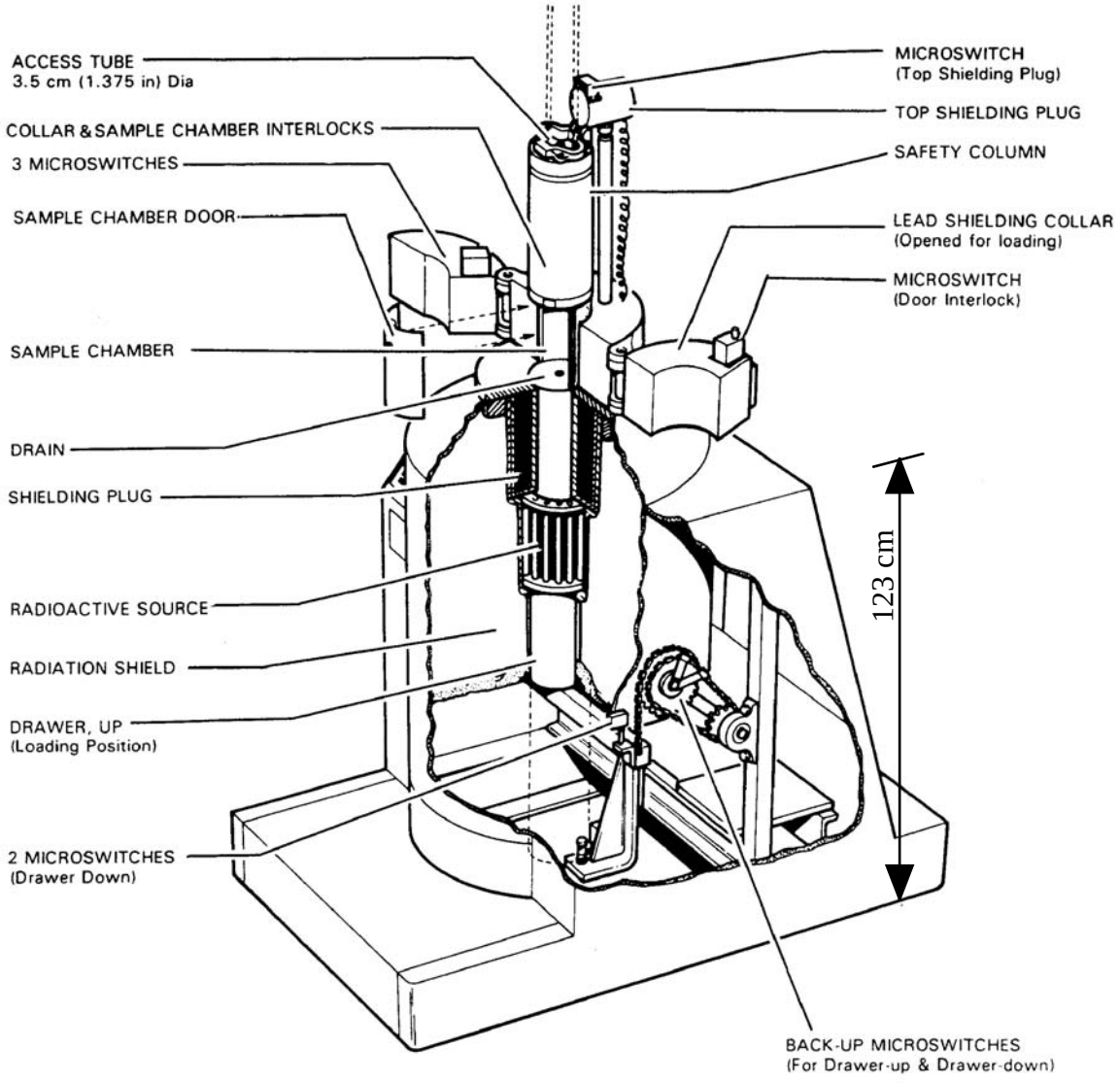

Figure 2.3. The Gammacell 220 cobalt-60 irradiator from Nordion International Inc.

The total activity from the set of 10 encapsulated sources on July 16, 1999 was 12075 Ci (446.78 TBq) corresponding to a central dose rate of 10.09 kGy/h. The most recent dosimetry of the source was carried out on August 30, 2001 and gave a dose rate of 7.617 kGy/hr. The gradient

in the dose rate formed by the placement of the source around the irradiation chamber is given in figure 2.4. The temperature within the source is approximately 8 ºC above room temperature.

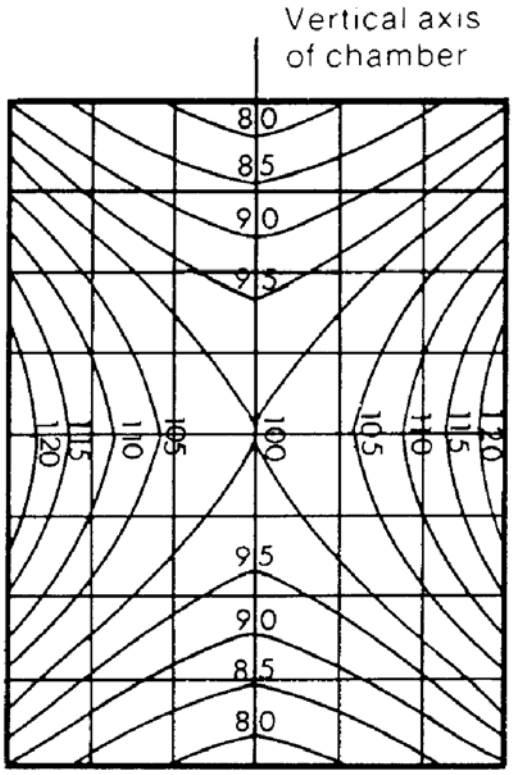

Figure 2.4. Isodose curves for the Gammacell 220 irradiator.

2.2.3. γ-Ray Dosimetry

As Co-60 decays, the amount of radioactive isotope within a γ-ray source decreases leading to a lowering of the activity, *A*, (and consequently the dose rate) as shown below.

$$A_t = A_0 \exp(-\lambda t) \tag{2.1}$$

In the above equation λ is the decay constant of Co-60 (4.169×10^{-9} sec^{-1}) and *t* is the time elapsed after determination of the source activity, A_0. Due to this natural decay, the activity of a source at the time of irradiation must be measured or calculated using equation 2.1.

The method used for determining the dose rate inside of the cobalt irradiators is based upon the oxidation of aerated solutions of ferrous sulfate in aqueous sulfuric acid. Known as the Fricke

dosimeter[1,2], this method of dosimetry can be used for absolute dose measurements with an accuracy of 1-2%. The standard Fricke dosimeter consists of a solution of 1.0 mM ferrous sulfate, 1.0 mM sodium chloride and 0.8 N sulfuric acid. The solution is irradiated and the increase in the UV absorption at 303 nm due to the formation of the ferric ion, Fe^{3+}, is monitored as a function of the irradiation time.

The primary reactive products formed by the radiolysis of water are hydroxyl radicals, solvated electrons, hydrogen atoms and hydrogen peroxide.

$$H_2O \sim\sim\sim> e^-, OH\bullet, H\bullet, H_2O_2 \quad \text{(A)}$$

Ferric ions are formed in the Fricke dosimeter solution via the reactions outlined below.

$$e^- + H^+ \rightarrow H\bullet \quad \text{(B)}$$

$$O_2 + H\bullet \rightarrow HO_2\bullet \quad \text{(C)}$$

$$Fe^{2+} + H^+ + HO_2\bullet \rightarrow Fe^{3+} + H_2O_2 \quad \text{(D)}$$

$$Fe^{2+} + H_2O_2 \rightarrow Fe^{3+} + OH^- + OH\bullet \quad \text{(E)}$$

$$Fe^{2+} + OH\bullet \rightarrow Fe^{3+} + OH^- \quad \text{(F)}$$

Due to the stoichiometry of the above reactions, the G-value (*i.e.* the number of species formed per 100 eV of absorbed energy) of ferric ion formation, $G(Fe^{3+})$, is equal to the G-value of hydroxyl radical, plus three times the sum of the G-value of solvated electrons and hydrogen atoms, plus two times the G-value of hydrogen peroxide. $G(Fe^{3+})$ has been experimentally determined to be 15.6 $(100\ eV)^{-1}$[2].

The absorbed dose in Gray (1 Gy = 1 J/kg) is calculated using this value of $G(Fe^{3+})$ in the following equation.

$$D(Gy) = \frac{N_A \times \Delta OD \times 100 \times e}{\varepsilon_{303} \times \rho \times G(Fe^{3+})} \quad (2.2)$$

In equation 2.2, N_A is Avogadro's number (6.022×10^{23} $mole^{-1}$), ΔOD is the change in the optical density at 303 nm in a 1 cm cuvette of the solution, ε_{303} is the molar extinction coefficient of the ferric ion at 303 nm (2164 $M^{-1}cm^{-1}$ at 25 ºC), ρ is the specific density of the dosimeter solution (1.024 kg/L at 25ºC) and e is the numerical value of the elementary charge in coulombs (1.6022×10^{-19}).

The useful dose range of the Fricke dosimeter is between 40 and 400 Gy. These limits arise due to the detection limits for optical absorption measurements on the low side and depletion of the

oxygen in the system on the high side. For γ-rays, the Fricke dosimeter has been shown to be reliable and independent of the dose rate for rates between 0.004 and 140 kGy/h.

For practical reasons, the dose rate is not determined via the Fricke dosimeter prior to every experiment but is calculated on the basis of the natural decay. If D'_0 is the dose rate determined at a given time using the Fricke dosimeter, then the dose rate after an elapsed time *t* is given by

$$D' = D'_0 \times (0.5)^{t/t_{0.5}} \tag{2.3}$$

In equation 2.3, $t_{0.5}$ is the half-life of Co-60.

The dose imparted to an irradiated sample is directly proportional to the electron density of the material. The dose rate in an irradiated material other than water, D'_m, is therefore determined by the ratio of the electron densities as given in equation 2.4 (see equation 1.9 in chapter 1).

$$D'_m = 1.80 \times D'_{H_2O} \left[\rho \sum_x Z_x \Big/ M_W \right]_m \tag{2.4}$$

It is more appropriate for kinetic considerations to use the dose rate in units of energy deposited per unit volume rather than per unit mass. The dose rate in joules per liter per second, D'_V, is the product of D'_m and the density ρ (kg/L). As such, the formation rate of a product P in units of moles per liter per second, $F_R(P)$, is given by

$$F_R(P) = \frac{D'_V G(P)}{100 N_A e} \tag{2.5}$$

2.3. Pulsed Electron Irradiation

"Continuous" irradiations usually involve exposure times of hours or minutes at least. Under these conditions the reaction intermediates formed will usually have reached their constant, "steady-state" concentrations. In pulse radiolysis on the other hand, exposure times are only a few microseconds or less and steady-state conditions usually do not apply. Variation of the pulse width (*i.e.* exposure time) is a direct means by which to influence the total number of reactive or excited species in an irradiated material. Furthermore, the time between subsequent pulses can be varied which provides a unique means by which to control specific molecular processes. In polymerization for example, varying the time between electron pulses will affect the rate of termination and consequently the size of the polymer formed. This has been shown for the pulsed electron-beam polymerization of styrene in latex particles[3]. Electron-beam pulse radiolysis studies

have also provided insight into the early processes occurring during radiation-induced polymerization and the kinetics thereof[4,5].

The Van de Graaff electron accelerator employed for the pulsed initiation of polymerization presented in this thesis is discussed below. In addition to providing information on the effects of high dose rates on monomer conversion and polymer molecular mass, the pulsed technique can provide valuable information on the rate constants of propagation and termination[6-8].

2.3.1. Van de Graaff Electron Accelerator

An illustration of the Van de Graaff accelerator used for pulsed electron-beam irradiations was given in chapter one of this thesis (figure 1.6). The terminal capacitor at the top of the accelerator is charged to 3 million volts via the mechanical transport of electrons by an insulating rubber belt. Electrons are emitted from the cathode and accelerated over the 3 MV potential in an evacuated, constant gradient acceleration tube. The accelerated electrons leave the drift tube with a velocity close to the speed of light through a thin (100 μm) aluminum window. The electron-beam can be focused, aligned and deflected by electromagnetic coils. When fully deflected, the electron beam is incident on a target connected to an electrometer which enables measurement of the beam charge. The typical current in the pulse is *ca* 4 A. Pulses of 0.2, 0.5, 2, 5, 10, 20, 50 and 250 ns duration are possible. Alternatively, the accelerator can be operated in continuous-current mode with a maximum DC current of 1 mA. For a more detailed description of this Van de Graaff accelerator, the reader is referred to the publications of the IRI accelerator group[9-13].

2.3.2. Electron-Beam Dosimetry

Dosimetry of the Van de Graaff accelerator electron beam is accomplished with FWT-60 thin film dosimeters (Far West Technology, Inc.). These 1 x 1 cm^2 nylon films are *ca* 50 μm thick and contain 10% by weight hexahydroxyethyl pararosaniline nitrile. In practice, the thin film dosimeter is placed at the same position as the irradiated sample. The colorless film becomes blue upon exposure to ionizing radiation. The dose is determined by monitoring the increase in the optical absorption at 510 nm. For this purpose, optical density readings of the film dosimeter are made with an FWT-92 Radiachromic Reader (Far West Technology. Inc.).

Calibration of the thin film dosimeters is achieved via use of the Fricke dosimeter and Co-60 γ-ray sources discussed above. In order to achieve electron equilibrium in the thin film dosimeter when irradiating with γ-rays, the film is placed between two plates of nylon (40 x 40 x 3 mm^3) of an equivalent electron density. The dose imparted to the thin film dosimeter during γ-ray irradiations is essentially due to secondary electrons produced in the nylon plates. The dose in the thin film

dosimeter, D_f, is therefore related to the dose in the Fricke dosimeter, D_F, by the ratio between mass energy absorption coefficients, μ_e, for nylon and the Fricke dosimeter as shown below.

$$D_f = D_F \frac{(\mu_e/\rho)_f}{(\mu_e/\rho)_F} \tag{2.6}$$

Equation 2.6 reduces to equation 2.7 by substituting the μ_e values of nylon and the Fricke dosimeter for *ca* 1 MeV photons (0.0291 and 0.0296 cm^2/g respectively).

$$D_f = 0.983 \times D_F \tag{2.7}$$

2.4. Fluorescence Techniques

The response of fluorescent and/or fluorogenic probe molecules to changes occurring during polymerization were monitored by both steady-state and time-resolved fluorescence techniques. *In situ* detection systems were developed which provide a convenient means by which to follow the reactions within shorter time intervals without interrupting the irradiation. Prior to the construction of the *in situ* set-ups samples were irradiated for an allotted time, removed from the source, measured and then reinserted into the source for further irradiation. In addition to saving time, the *in situ* detection systems permit monitoring reactions without interruption from a safe, remote location.

2.4.1. Steady-State Fluorescence

Fluorescence spectroscopy permits the measurement of molecular species present in trace amounts. The remarkable sensitivity of fluorescence spectroscopy, in addition to a large linear concentration range for detection, makes it an attractive method for monitoring molecular environments, reactions and processes.

Many aromatic molecules fluoresce in the UV region of the electromagnetic spectrum following the excitation processes discussed in chapter one. The excited states formed can return to the ground state via radiative (fluorescence or phosphorescence) or non-radiative (internal conversion, intra- or inter-molecular quenching) processes. The fluorescence intensity is determined by the fluorescence quantum yield of the molecule (*i.e.* the ratio between the rate constant for fluorescence to the sum of rate constants for all relaxation processes). If changes in the environment of a fluorophore affect the relative rates of the relaxation processes, its fluorescence emission can be used to monitor the course of polymerization. Alternatively, certain fluorophores form dipolar excited states which can be stabilized by dipoles of the surrounding solvent molecules.

The extent of this stabilization determines the maximum wavelength of fluorescence emission. Provided that the extent of this stabilization process is affected by changes in the polymerizing system (*e.g.* dielectric constant or viscosity), monitoring of the maximum wavelength of fluorescence emission can be used to follow the polymerization.

2.4.1.1. External Measurements

External fluorescence measurements of irradiated samples were made with a Photon Technology International (PTI) Quanta Master QM-1 fluorescence spectrometer. The spectrofluorimeter employs a 75 W Xenon arc lamp and a dual excitation light monochromator with variable slit widths. The emitted light is collected at a 90º angle to the excitation light and after passing through a monochromator with a variable slit width is measured using a PMT photo-detector. The useful range for emission measurements is 185-900 nm. All fluorescence spectra were corrected using PTI's Felix data acquisition program. The Quanta Master spectrofluorimeter was always used for accurate measurement of fluorescence quantum yields and spectra. 9,10-diphenylanthracene (DPA) was used as a fluorescence standard at optical densities of 0.1 or less for the determination of absolute fluorescence quantum yields.

Sample preparation involved the removal of oxygen via purging with argon gas for 15 minutes and sealing with a Teflon stopper and parafilm tape or alternatively using a vacuum line and three freeze-pump-thaw cycles. Samples were contained in either commercial or home-made 1 cm fluorescence cuvettes constructed of Suprasil quartz.

2.4.1.2. *In Situ* Measurements

The experimental set-up employed for obtaining *in situ* fluorescence spectra within Co-60 γ-ray sources is illustrated in figure 2.5. The excitation light source consists of a Short Arc Xenon Illuminator (PTI "Power Arc" 1010 A, 75W). The output of the source is blocked by a mechanical shutter assembly (Oriel 71446) which opens automatically for a duration of *ca* 1 second during each fluorescence measurement. A dichroic UV mirror (Oriel 66226) supported on a holder (Oriel 66246) reflects the UV light from the source at a 90º angle onto a 340 nm narrow band-pass filter (Schott UV-DAD 8-1). The excitation light is focused on the optical light guide (Top Sensor Systems UV/VIS: FC-UV 200-2) shown in figure 2.6. The light guide consists of six outer fibers and one inner fiber. The outer fibers are used to conduct excitation light to the sample in the irradiation chamber and the inner fiber is used to transport the emitted light to the detector. This arrangement is used in order to optimize the resolution of the spectrophotometer discussed below. The fibers are made of Suprasil quartz in order to prevent discoloring due to the influence of ionizing radiation.

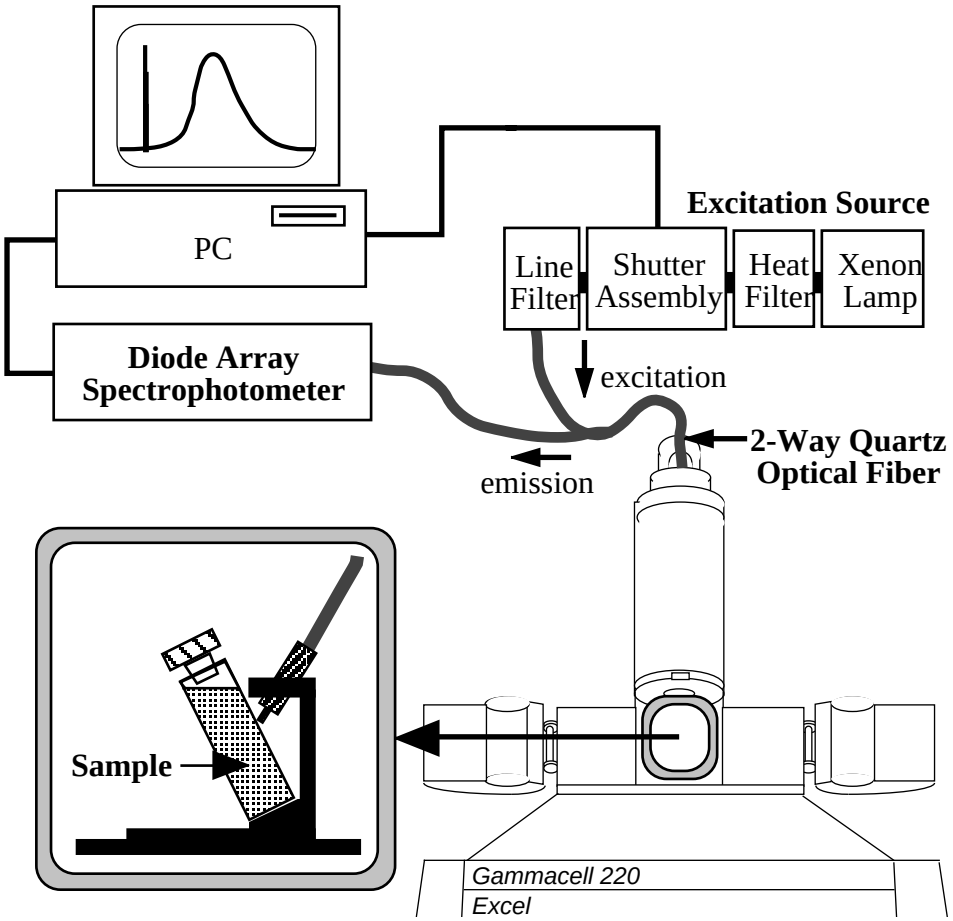

Figure 2.5. *In situ* set-up for fluorescence spectra measurements.

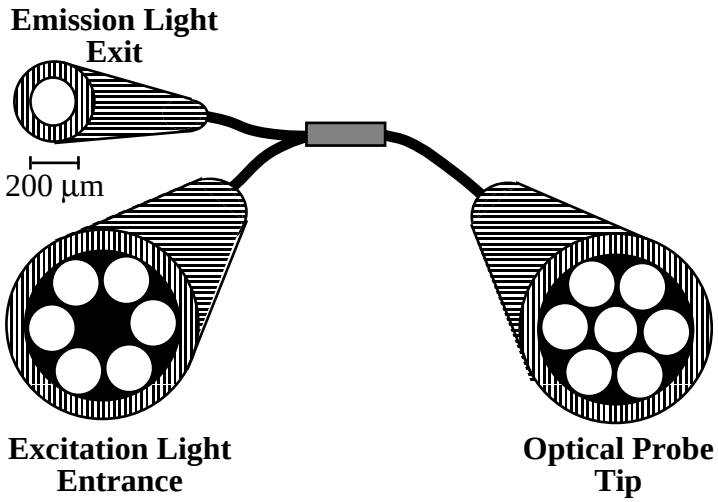

Figure 2.6. Optical light guide from Ocean Optics for *in situ* fluorescence measurements.

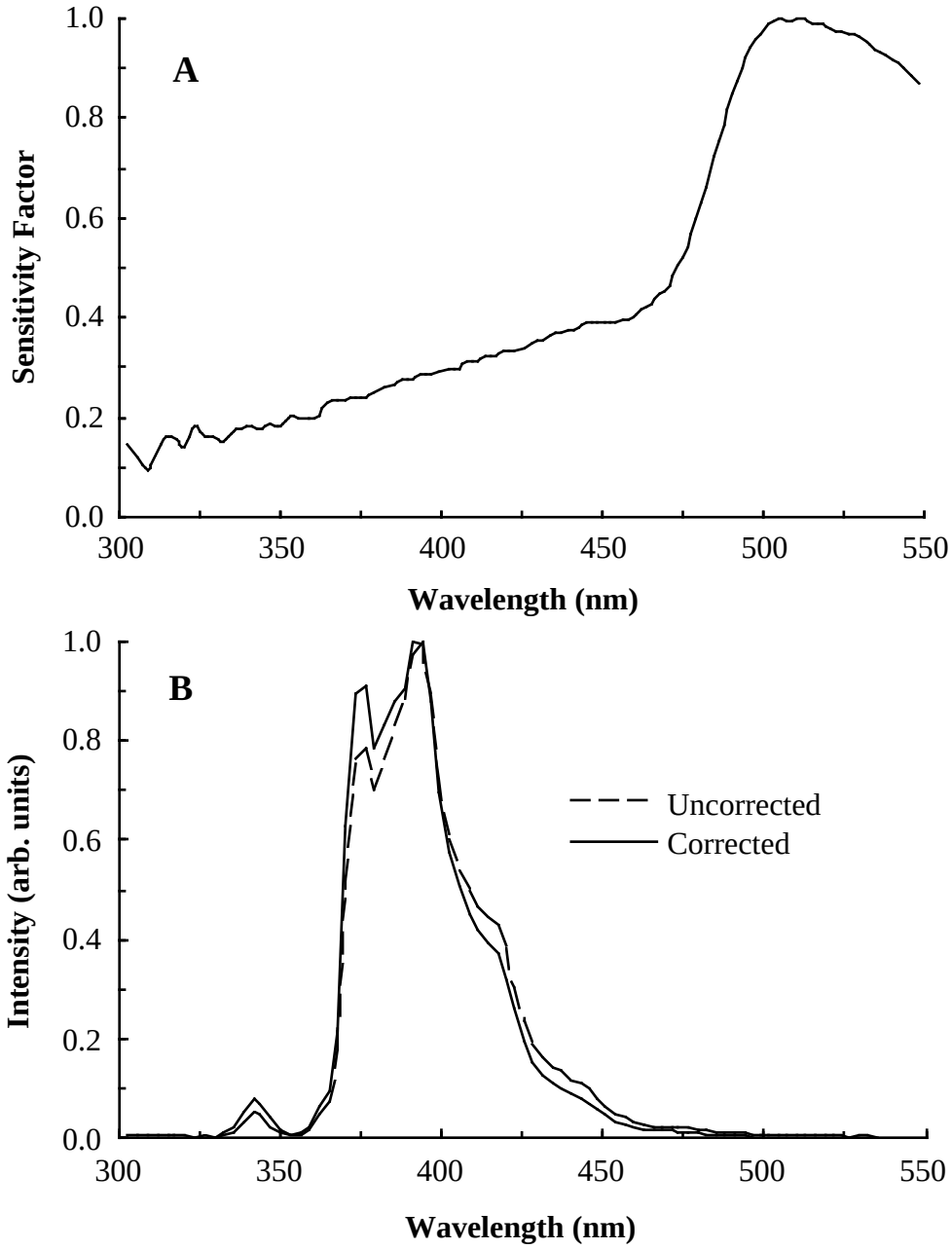

Figure 2.7. (A) Normalized sensitivity factor of the diode array spectrophotometer and (B) emission spectra from pyrene in methyl methacrylate; uncorrected and corrected.

In order to prevent the destruction of expensive fluorescence cuvettes when polymerizing samples to complete conversion, sample cells were constructed in-house from Heraeus Suprasil quartz. The degassing procedure was the same as mentioned above for the external measurements. The optical probe tip makes contact with the sample at a 70º angle to the cell surface (see insert in figure 2.5) in order to minimize the amount of excitation light entering the central optical fiber

which was used to transmit emitted light from the sample to the diode array spectrophotometer (Ocean Optics Europe S2000). The spectrophotometer is capable of measurements in the spectral regions of 350-550 nm and 250-850 nm with optical bandwidth resolutions of 3.3 nm and 10 nm respectively for a 200 μm fiber aperture. The detectors are 2,048-element CCD (charge-coupled device) linear arrays with an average sensitivity of 86 photons per count. The arrays were calibrated using a tungsten ribbon lamp at 2853 K as a standard source[14].

Data acquisition and storage were carried out in an automated manner using a PC and software developed in-house. By coinciding the start of data acquisition with the lowering of the sample into the source, emission spectra could be measured in an automated manner at variable time intervals (with a minimum of 6 seconds between measurements) for three individual stages of the data acquisition sequence. A single measurement was initiated by an electrical signal sent to the mechanical shutter assembly which would then open for *ca* 2 seconds. During this time the spectrophotometer would take a reading for the pre-programmed integration time. The set-up could be operated manually for obtaining reproducible spectra at 2 second time intervals.

Figure 2.7 illustrates an example fluorescence spectrum taken from the *in situ* set-up with 10 nm resolution. The top curve shows the normalized sensitivity factor due to the variable sensitivity of the photo-detector over the spectral range 300 to 550 nm. The bottom curve gives uncorrected and corrected emission spectra from pyrene in oxygen-free methyl methacrylate at an optical density of 2 in a 1 cm cuvette. The peak below 350 nm is due to scattered excitation light.

2.4.2. Time-Resolved Fluorescence

Excited states of molecules are formed by the excitation processes discussed in chapter one. Non-dissociative excited states of fluorophores will return to the ground state via radiative (fluorescence or phosphorescence) or non-radiative (internal conversion, intra- or inter-molecular quenching) processes. If the kinetics of these processes are dependent on the molecular environment, time-resolved fluorescence detection can provide a means to monitor the progress of polymerization by measuring the lifetime of the fluorescent state.

2.4.2.1. External Measurements

Time-resolved fluorescence decay measurements were accomplished using a nitrogen laser (Laser Photonics MegaPlus LN 1000) which produces pulses of 337 nm UV radiation with a pulse width at half height of *ca* 800 ps. The excitation light is incident on the sample at an angle of 90º to the detection system. Emitted light is focused onto a monochromator (American ISA Incorporated H-20 SA) with variable entrance and exit slits. In this way the bandwidth could be varied from 2 to 8 nm. The emitted light is detected using a single channel-plate photomultiplier (Photek PMT

113/UHF Ultrafast MCP Photomultiplier) with *ca* 100 ps rise and fall times. The signal is then read by a digital, real-time 1 GHz oscilloscope (Tektronix TDS 680B). Data acquisition was accomplished with the LabVIEW Package, version 5.1 from National Instruments Corporation.

Sample cells were either commercial quartz Suprasil 1 cm fluorescence cuvettes or constructed in-house from Heraeus Suprasil quartz. The degassing procedure is the same as mentioned above for the external steady-state fluorescence measurements.

2.4.2.2. *In Situ* Measurements

An experimental set-up was designed and constructed for *in situ* time-resolved fluorescence lifetime measurements. This consisted of a pulsed nitrogen laser (LTB Lasertechnik Berlin MSG 800) which provides a 337 nm excitation light pulse with a pulse width at half height of *ca* 500 ps. The excitation light is transmitted via an optical fiber with a 200 μm diameter connected to the multi-fiber optical light guide cable (Top Sensor Systems UV/VIS: FC-UV 200-2) described in figure 2.6. The excitation light is then directed to the sample cell via the inner optical fiber and the emitted light is carried away from the sample via the six outer fibers. This arrangement is used in order to optimize the sensitivity of the photon detection system. The probe tip makes contact with the sample cell at a 70º angle to the surface in order to minimize the amount of excitation light entering the outer optical fiber bundle. The emitted light exits the fiber bundle via a 350 nm UV cut-off filter and is detected by a silicon semiconductor photodiode (EG&G FWD-100Q) capable of 1 ns rise and fall times. The electrical signal is stored by a 1 GHz digital oscilloscope (Tektronix TDS 680B). Data analysis was accomplished on a PC.

Figure 2.8 illustrates the *in situ* set-up employed for time-resolved fluorescence detection. The sample holder is identical to that depicted in the inset of figure 2.5. An example measurement is provided in figure 2.9 for pyrene in methyl methacrylate at an optical density of 2 in a 1 cm cuvette.

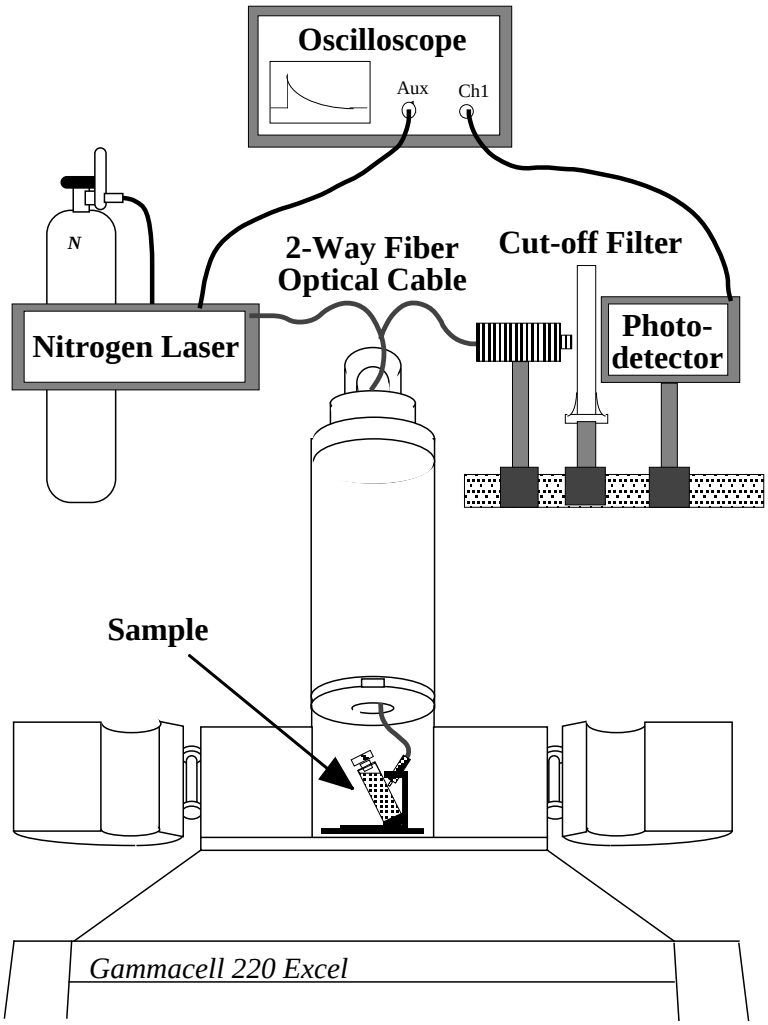

Figure 2.8. *In situ* set-up for time-resolved fluorescence detection.

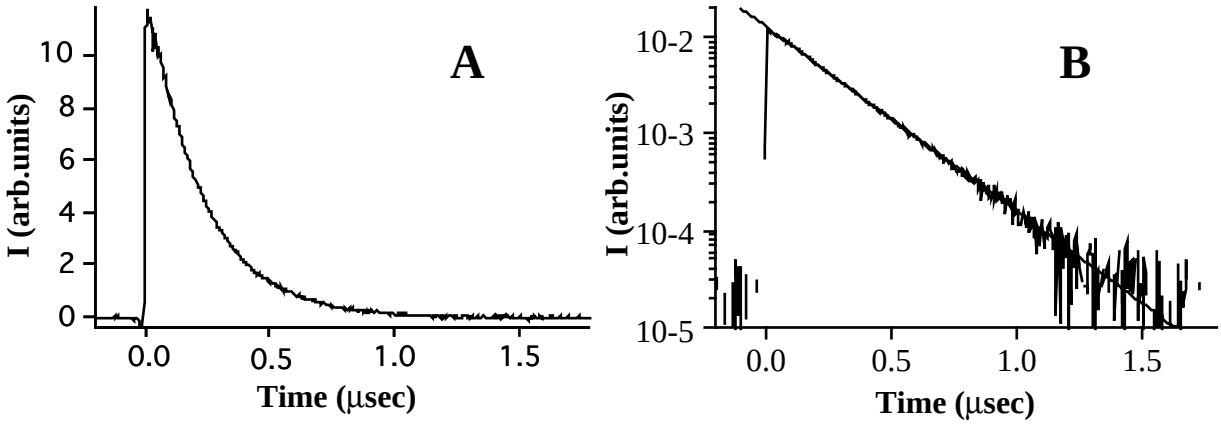

Figure 2.9. Time-resolved fluorescence decay of pyrene in methyl methacrylate (A) and single exponential fit (B) for fluorescence lifetime determination.

2.5. Monomer Conversion

The conversion of monomer in chain polymerization can be measured by either direct or indirect means. In the former, an analytical technique is used to quantitatively measure the amount of monomer or polymer in the system. Examples include residual monomer evaporation, product polymer precipitation, infra-red spectroscopy and nuclear magnetic resonance spectroscopy. Indirect methods of determining monomer conversion require that a physical property which undergoes change in a polymerizing system is correlated to the actual monomer conversion. Such methods require that the monomer conversion is determined by a direct method and then correlated to a given physical property, *i.e.* a calibration curve must be prepared. Examples of some physical properties that change upon polymerization include the density, viscosity and dielectric constant.

2.5.1. Residual Monomer Evaporation

If the monomer is volatile, one can determine the percent conversion directly via residual monomer evaporation. This involves polymerizing a known mass of monomer for an allotted time and then rapidly quenching the reaction, *e.g.* by exposing the sample to oxygen in free radical polymerization. Subsequently, the residual monomer is removed under vacuum and the residual mass is taken to be equal to the amount of monomer converted to polymer.

The direct determination of monomer conversion versus absorbed dose for the polymerizations presented in this thesis was accomplished by residual monomer evaporation. The monomer was distilled (atmospheric pressure and 100-101 ºC) in order to remove the inhibitor and subsequently degassed on a vacuum line by three freeze-pump-thaw cycles and then transferred into a glove bag under a nitrogen atmosphere. Samples of *ca* 2 g of monomer were placed into cylindrical scintillation vials (22 mm diameter). These were closed and sealed tightly with parafilm tape prior to extraction from the glove bag. Samples were immediately irradiated within the source for a given absorbed dose after which the polymerization was rapidly quenched by opening the vials and exposing the samples to atmospheric oxygen. The residual monomer was removed under vacuum at room temperature until a constant mass was observed (*ca* 3 days).

There are certain disadvantages to this simple experimental technique. For one, the quenching step must be accomplished efficiently and rapidly which can be difficult for systems polymerizing at a fast rate, *e.g.* acrylates and polymerizations undergoing autoacceleration. Another complication is evident in systems which undergo vitrification. In such a case, residual monomer can be trapped in the glassy matrix and the evaporation step could be inefficient.

2.5.2. Polymer Precipitation

Precipitation of the product polymer by the addition of a suitable non-solvent of the polymer is an alternative method of determining monomer conversion. The major disadvantage to this technique is that the polymer must be completely precipitated and isolated. In some systems however, the product polymer consists of many small chains which have a solubility intermediate between that of the monomer and larger polymer chains.

An attempt to obtain a conversion versus absorbed dose plot for methyl methacrylate, MMA, via polymer precipitation gave systematically low data points when compared to the residual monomer evaporation procedure. This is explained by the fact that poly(methyl methacrylate), PMMA, undergoes chain-scission when exposed to ionizing radiation. Small chain fragments are likely to exhibit a solubility similar to that of the monomer. This was confirmed by observing a tacky residue from all samples after complete evaporation of all volatile components.

2.5.3. Fluorogenic Probes

In this thesis the use of fluorogenic molecules for monitoring radiation-induced polymerization is presented. Unlike charge-transfer, viscosity or free-volume sensitive fluorophores, fluorogenic probes enable monitoring of monomer polymerization at low conversion and even in dilute solution, *i.e.* conditions in which the dielectric constant and/or viscosity do not change by a significant amount.

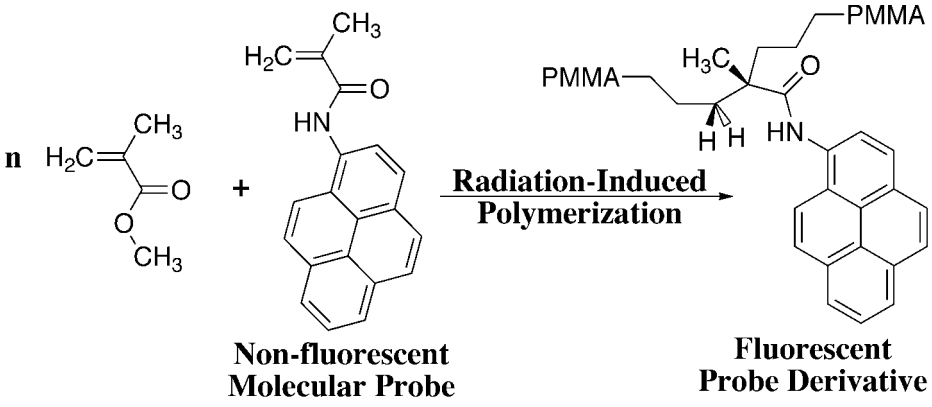

Figure 2.10. Induction of fluorescence in the fluorogenic probe PyMA during the polymerization of MMA.

The non-fluorescent fluorogenic probe molecules become incorporated, *i.e.* copolymerized, into growing polymer chains. In doing so they undergo a chemical change which results in them becoming fluorescent. Consequently, the integrated fluorescence intensity from the sample is a quantitative indication of the extent of monomer conversion. Figure 2.10 depicts the fluorogenic behavior of *N*-(1-pyrene)methacrylamide, PyMA, during the polymerization of MMA. Figure 2.11

illustrates the increase in the fluorescence intensity from an MMA solution of PyMA (OD at 337 nm = 2) with increasing dose from the Gammacell 200 irradiator.

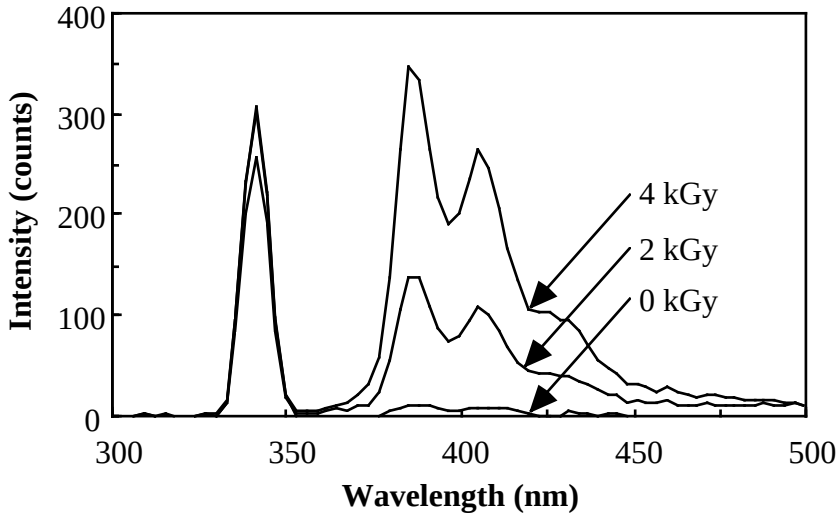

Figure 2.11. Increase in fluorescence intensity with increasing dose from an MMA solution of PyMA (OD at 337 nm = 2).

2.6. Polymer Molecular Mass Determination

The molecular mass of polymeric materials is defined by averages due to the fact that samples invariably consist of molecules with a distribution of sizes. The two averages most often used to characterize a polymer sample are the number-average ($\overline{M}_n$) and weight-average ($\overline{M}_w$) molecular masses. These are defined in equations 2.8 and 2.9 respectively.

$$\overline{M}_n = \frac{\sum N_x M_x}{\sum N_x} \tag{2.8}$$

$$\overline{M}_w = \frac{\sum N_x M_x^2}{\sum N_x M_x} \tag{2.9}$$

In equation 2.8, $\overline{M}_n$ is the sum of the products of the number of molecules, N_x, of a given mass, M_x, (the total mass of the sample) divided by the total number of molecules. The weight-average molecular mass is averaged by the weight fractions of polymer molecules of a given mass and is therefore biased to larger polymer molecules. An indication of the molecular mass distribution in a polymer sample is given as the polydispersity index, PDI, which is $\overline{M}_w$ divided by $\overline{M}_n$. The PDI would be equal to unity for a monodisperse polymer.

Gel permeation chromatography (GPC, also known as size-exclusion chromatography) was chosen as the method by which polymer molecular mass distributions were determined for the experiments described in this thesis. The column (Waters Styragel HT 6E) was calibrated against polystyrene standards (Polymer Labs) and the universal calibration method[15] was employed for the determination of absolute molecular masses. A high-pressure liquid chromatography pump (Waters 515 HPLC Pump) and refractive index detector (Waters 410 Differential Refractometer) were employed, along with degassed tetrahydrofuran as the eluent. Data acquisition was accomplished with Baseline 810 software from Millipore, a division of Dynamic Solutions.

References

(1) Fricke, H.; Morse, S. *Am. J. Roentg. Radium Ther. Nucl. Med.* **1927**, *18*, 430.

(2) *Manual on Radiation Dosimetry*; Holm, N. W.; Berry, R. J., Eds.; Marcel Dekker, Inc.: New York, 1970.

(3) van Herk, A. M.; de Brouwer, H.; Manders, B. G.; Luthjens, L. H.; Hom, M. L.; Hummel, A. *Macromolecules* **1996**, *29*, 1027.

(4) Takács, E.; Emmi, S. S.; Wojnárovits, L. *Radiat. Phys. Chem.* **1999**, *55*, 621.

(5) Takács, E.; Wojnárovits, L.; Dajka, K. *Macromol. Chem. Phys.* **2000**, *201*, 2170.

(6) Takács, E.; Wojnárovits, L. *Radiat. Phys. Chem.* **1996**, *47*, 441.

(7) van Herk, A. M. *J. Macromol. Sci.: Rev. Macromol. Chem. Phys.* **1997**, *C37*, 633.

(8) van Herk, A. M. *Macromol. Theory Simul.* **2000**, *9*, 433.

(9) Luthjens, L. H.; Hom, M. L.; Vermeulen, M. J. W. *Rev. Sci. Instrum.* **1978**, *49*, 230.

(10) Luthjens, L. H.; Hom, M. L.; Vermeulen, M. J. W. *Rev. Sci. Instrum.* **1986**, *57*, 2230.

(11) Luthjens, L. H.; Vermeulen, M. J. W.; Hom, M. L. *Rev. Sci. Instrum.* **1980**, *51*, 1183.

(12) Luthjens, L. H.; Vermeulen, M. J. W.; Hom, M. L. *Rev. Sci. Instrum.* **1982**, *53*, 476.

(13) Luthjens, L. H.; Vermeulen, M. J. W.; Hom, M. L. *Nucl. Instr. Meth. Phys. Res. A* **2000**, *455*, 495.

(14) Kruithof, A. A. Modern Light Sources. In *Advanced Optical Techniques*; Heel, A. C. S. V., Ed.; North-Holland Publishing Company: Amsterdam, 1967; pp 309-384.

(15) Pasch, H.; Trathnigg, B. *HPLC of Polymers*; Springer-Verlag: Berlin, 1998.

Chapter Three

Materials

3.1. Introduction

Chapter three describes the chemical materials employed for experiments mentioned in this thesis. The monomers are discussed in regard to their commercial sources and methods of purification. Fluorescent and fluorogenic probe molecules are described with emphasis given to their photophysical properties. Furthermore, synthetic procedures are provided for the probe molecules synthesized by the author of this thesis.

3.2. Monomers

Methyl methacrylate, MMA, was purchased from both Aldrich (synthesis grade, 99%) and Merck (synthesis grade, 99%). Immediately prior to use, the monomer was distilled at atmospheric pressure and 100-101 ºC in order to remove the hydroquinone stabilizer. Because of their much more rapid rates of thermal polymerization, the stabilizer in both methyl acrylate (MA; Aldrich, 99%) and the difunctional tetraethylene glycol diacrylate (TEGDA; Scientific Polymer Products, Inc.) was removed immediately prior to use by passing drop-wise through a column containing HR-4 chromatographic packing (Scientific Polymer Products, Inc.).

3.3. Commercially Available Probe Molecules

The following sections describe the sources and properties of the commercially available probe molecules studied in this thesis.

3.3.1. Aromatic Hydrocarbons

Pyrene, Py, was purchased from Fluka Chemika (>99%) and both anthracene, An, and 9,10-diphenylanthracene, DPA, were purchased from Merck (>96% and 98% respectively). All of these fluorescent molecules were used as obtained without any further purification. The molecular structures of Py, An and DPA are given in figure 3.1.

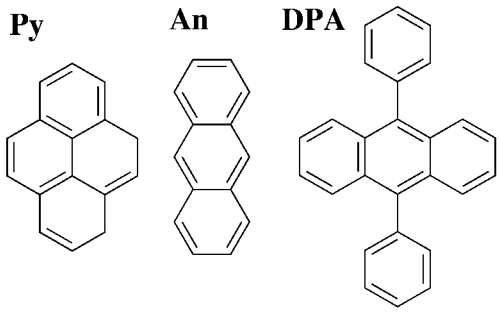

Figure 3.1. Molecular structures of pyrene (Py), anthracene (An) and 9,10-diphenylanthracene (DPA).

Pyrene is an interesting fluorescent probe molecule for several reasons. For instance, it is capable of forming an excited bi-molecular encounter pair (known as an excimer) which fluoresces at longer wavelengths than monomeric pyrene. The rate and extent of excimer formation depends upon the concentration, mobility and proximity of pyrene fluorophores. This is illustrated in figure 3.2 in which the much lower mobility of pyrene in poly(methyl methacrylate), PMMA, relative to that in MMA leads to a suppression of the long wavelength excimer fluorescence. Excimer

fluorescence from pyrene can therefore be used for monitoring bulk polymerizations of monomers such as MMA[1-3].

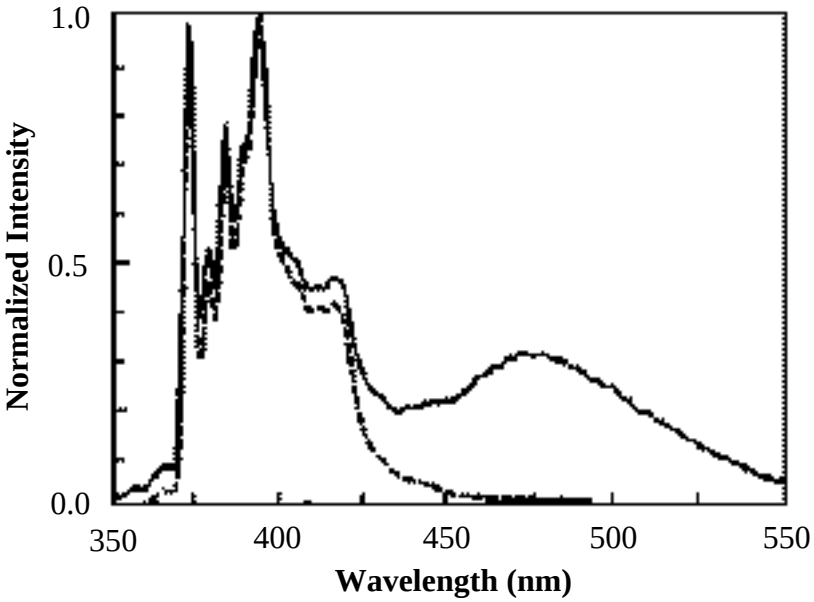

Figure 3.2. Normalized emission spectrum of pyrene (1.0 x 10^{-3} M) in MMA (solid curve) and PMMA (dashed curve).

Another interesting property of pyrene is its anomalously large Ham effect[4] (*i.e.* the vibrational fine structure in the electronic spectra of this compound is sensitive to solvent properties). The relative intensities of the emission bands of pyrene corresponding to fluorescence peaks at 375 and 384 nm have been reported to be a measure of solvent polarity[5].

Furthermore, the long lifetime and temperature-sensitive quantum yield of fluorescence make pyrene an interesting probe molecule for studying various types of molecular systems[6]. The long lifetime can however be a problem since this is sensitive to small amounts of oxygen and other impurities. The lifetime in de-aerated MMA was found to be 258 ns. The fluorescence quantum yield has been determined to be 0.35 using DPA as a reference fluorophore.

Anthracene, An, and 9,10-diphenylanthracene, DPA, were chosen as alternative probe molecules because of their considerably shorter fluorescence lifetimes (less than 10 ns in MMA) when compared to pyrene. Consequently, these probes are less sensitive to trace amounts of oxygen and other impurities. In addition to its use as a probe molecule, DPA was used as a standard reference compound for establishing fluorescence quantum yields (the fluorescence quantum yield of DPA in degassed cyclohexane is 0.91 ± 0.02[7]).

3.3.2. *N*-(1-pyrene)maleimide

The fluorogenic probe molecule *N*-(1-pyrene)maleimide, MPy, was purchased from Molecular Probes, Inc. and used as obtained without further purification. The molecular structure of MPy is provided in figure 3.3. This non-fluorescent molecule can react via copolymerization with various vinyl monomers to form a fluorescent succinimide derivative as shown in the figure for MMA polymerization. Consequently, an induction of fluorescence is observed when MMA is polymerized with trace amounts of this probe present as shown in figure 3.4.

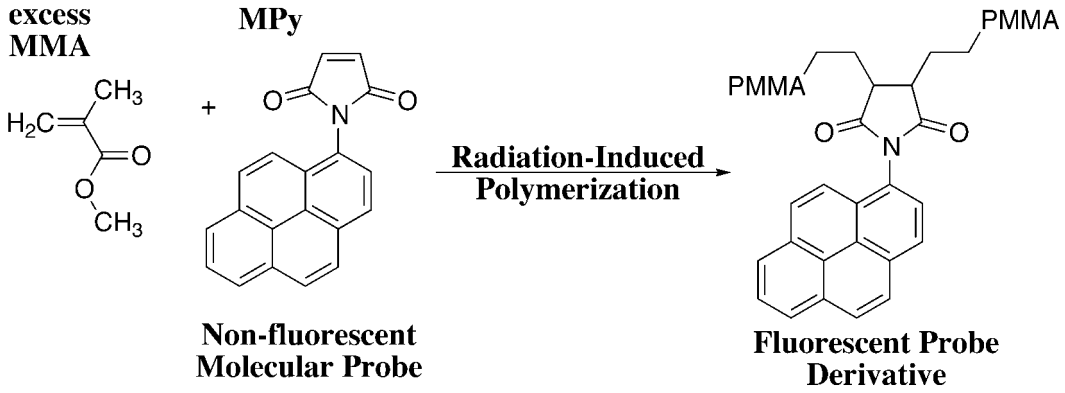

Figure 3.3. Induction of fluorescence in fluorogenic *N*-(1-pyrenee)maleimide during the polymerization of MMA.

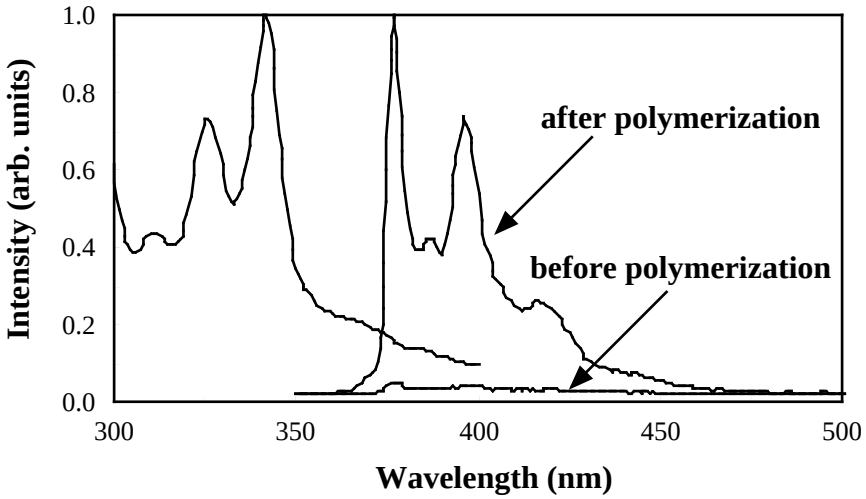

Figure 3.4. Absorption spectrum of MPy in MMA (1 x 10^{-5} M) and fluorescence spectra before and after polymerization.

3.4. Non-commercial Molecular Probes

The following sections describe probe molecules which were synthesized either at the University of Amsterdam in the group of Prof. J.W. Verhoeven or by the author.

3.4.1. Fluoroprobe and Maleimido-Fluoroprobe

Fluoroprobe, FP, is a donor-spacer-acceptor molecule which exhibits strong charge-transfer fluorescence[8,9]. FP and the fluorogenic derivative maleimido-fluoroprobe, MFP, were both synthesized in the group of Prof. J.W. Verhoeven of the Department of Organic Chemistry at the University of Amsterdam (molecular structures are given in figure 3.5). The syntheses of FP and MFP have been reported by G.F. Mes, *et al.*[8] and H.J. Verhey, *et al.*[10] respectively.

Photoexcitation of FP leads to rapid intramolecular electron transfer from the anilino group to the cyano-naphthalene chromophore resulting in a highly polar excited state. Nanosecond time-resolved microwave conductivity measurements have shown that the dipole moment thus produced is as high as 25 ± 2 D[8]. Substantial stabilization of the charge-transfer excited state of FP can occur via interactions with surrounding solvent dipoles. Consequently, its fluorescence exhibits pronounced solvatochromism resulting in large shifts to the red with increasing solvent polarity (see table 3.1).

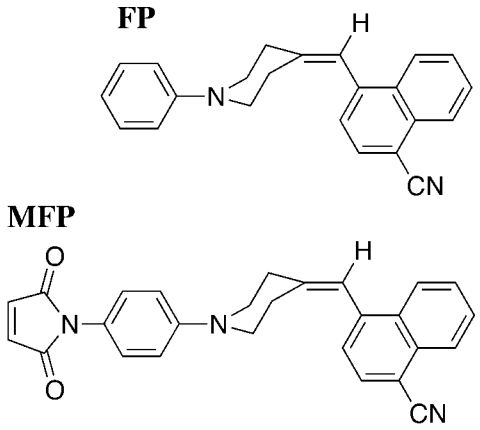

Figure 3.5. Molecular structures of fluoroprobe, FP, and maleimido fluoroprobe, MFP.

Substitution of the maleimido group in FP results in complete quenching of fluorescence as observed for the commercial probe molecule MPy. The non-fluorescent character of MFP has been attributed to a low-energy $n \rightarrow \pi^*$ transition within the maleimido group which leads to radiationless-deactivation via intersystem crossing[10]. When the double bond of the maleimido group of MPF becomes saturated, *e.g.* copolymerized with vinyl monomers or condensed with an amine or thiol, the charge-transfer fluorescence characteristic of FP reappears (see table 3.1).

Table 3.1. Solvatochromism of fluoroprobe and a fluorescent derivative of maleimido-fluoroprobe (condensation product with isopropylamine).

		Fluoroprobe[2.]		MFP-isopropylamine[3.]	
Solvent	$E_T(30)$[1.]	λ_{max}(nm)	Φ_{fl}	λ_{max}(nm)	Φ_{fl}
cyclohexane	30.9	412	0.13	411	0.13
di-n-butyl ether	33.0	468	0.60	461	0.43
diisopropyl ether	34.1	482	0.40	481	0.37
diethyl ether	34.5	506	0.24	516	0.23
tetrahydrofuran	37.4	574	0.12	565	0.12
ethyl acetate	38.1	573	0.11	560	0.07

1. A solvent polarity parameter (C. Reichart, Solvent Effects in Organic Chemistry, from *Monographs in Modern Chemistry*, **1979**, vol. 3, ed. H.F. Ebel).
2. G.F. Mes, *et. al.*, J. Am. Chem. Soc. **1984**, 106, 6524-6528.
3. M. Goes, *et.al.*, Eur. J. Org. Chem. **1998**, 2373-2377.

3.4.2. *N*-(1-pyrene)methacrylamide

N-(1-pyrene)methacrylamide (PyMA, structure given in reaction A) was synthesized with the intention of producing a fluorogenic probe molecule incorporating the pyrene moiety with a similar rate of copolymerization to MMA. It was thought that the enone functionality (α,β-unsaturation to a carbonyl group) of the methacrylamide group would probably quench the pyrene fluorescence which would then appear when the carbon-carbon double bond became saturated via copolymerization. This was based upon the fact that acrylamide had been found to be an efficient intermolecular quencher of fluorescence for a number of simple aromatic fluorophores in organic solvents[11]. As predicted, PyMA was found to exhibit the desired fluorogenic character.

PyMA was synthesized from 1-aminopyrene (Fluka Chemica, 98.0%) and methacryloyl chloride (Aldrich, 80%) as shown in reaction A. Triethylamine, NEt_3, (Aldrich, 99.5%) was dried over 4 Å molecular sieves. Dichloromethane (CH_2Cl_2) was dried and purified by distillation over phosphorous pentoxide, P_2O_5.

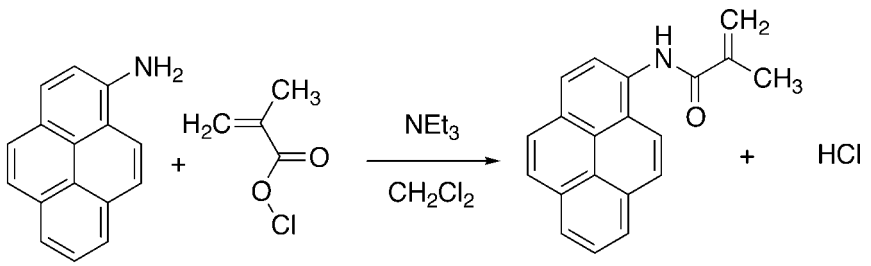

(A)

A solution of 1.00 g of 1-aminopyrene (4.60 mmol) in 20 mL of anhydrous CH_2Cl_2 was prepared. A second solution of 0.60 mL of freshly distilled methacryloyl chloride (5.5 mmol) and 0.42 mL of NEt_3 (5.5 mmol) in 5 mL CH_2Cl_2 was slowly added to the 1-aminopyrene solution at ambient temperature. The initially clear, yellow 1-aminopyrene solution became cloudy as triethylammonium chloride precipitated from solution. The reaction mixture was shaken with 50 mL of 10% aqueous hydrochloric acid and subsequently with an excess of distilled water. Next the mixture was filtered into a separatory funnel and the bottom CH_2Cl_2 layer was collected. The solvent was removed by evaporation to yield 1.10 g of pale yellow crystals. Recrystallization from toluene was performed twice resulting in a 39% yield (0.51 g) of almost colorless PyMA crystals; m.p. = 173.5-175.5 ºC. ^{1}H NMR ($CDCl_3$, 400 MHz): 8.43 (d, *J* = 11.2 Hz, 1H), 8.18 (d, *J* = 10.3 Hz, 1H), 8.17 (d, *J* = 10.4 Hz, 1H), 8.15 (d, *J* = 10.4 Hz, 1H), 8.14_3 (d, *J* = 10.2 Hz, 1H), 8.13_9 (d, *J* = 11.2 Hz, 1H), 8.06 (d, *J* = 12.3 Hz, 1H), 8.01 (br s, 1H), 7.99 (t, *J* = 10.1 Hz, 1H), 7.97 (d, *J* = 12.3 Hz, 1H), 6.03 (s, 1H), 5.59 (s, 1H), 2.21 (s, 3H).

The absorption spectrum of PyMA in MMA is shown in figure 3.6. As predicted, PyMA is non-fluorescent in MMA until the carbon-carbon double-bond reacts via radical chain polymerization as indicated by the induction of fluorescence as shown in figure 3.6.

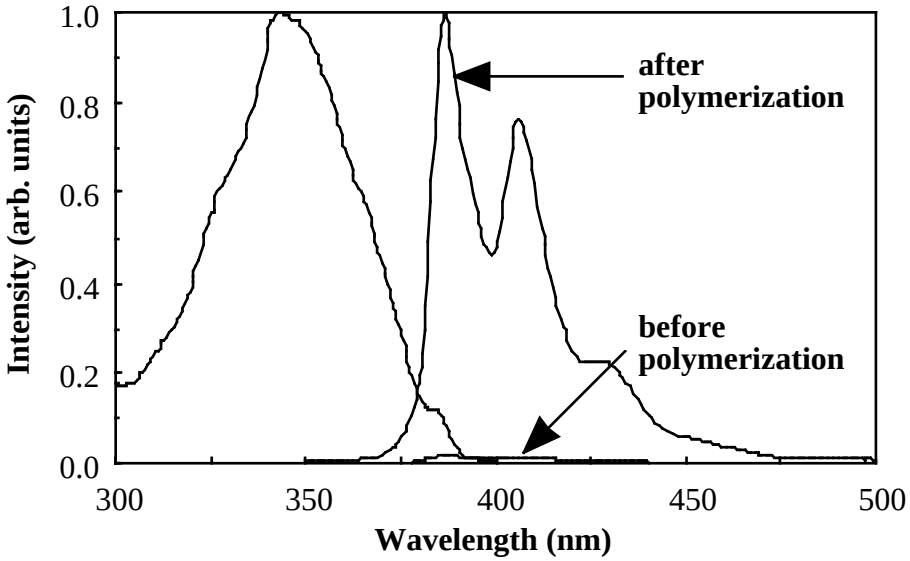

Figure 3.6. Absorption spectrum of PyMA in MMA (1 x 10-5 M) and fluorescence spectra before and after polymerization.

The mechanism by which the methacrylamide group quenches pyrene fluorescence is not entirely understood. Whether the quenching mechanism involves a low-energy $n \rightarrow \pi^*$ transition which leads to radiationless-deactivation via intersystem crossing[10,9] or a partial charge-transfer interaction in the excited state[11-14,9] remains an unresolved question.

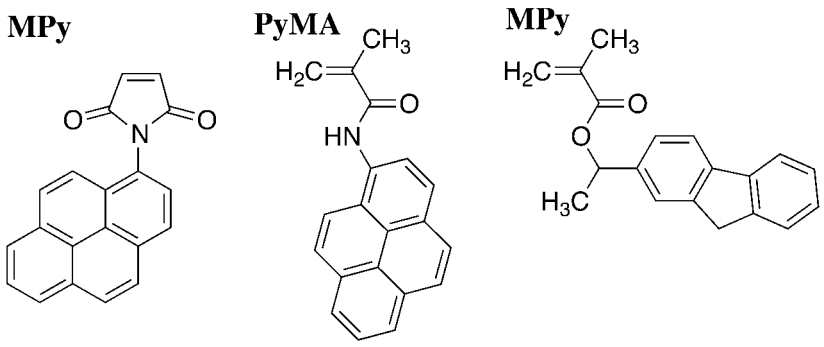

Figure 3.7. Structures of *N*-(1-pyrene)maleimide (MPy), *N*-(1-pyrene)-methacrylamide (PyMA) and (3-fluorenyl)ethyl methacrylate (FLEMA).

The work of Miller *et al.*[12] demonstrated how the *partial* self-quenching of fluorene fluorescence in (2-fluorenyl)ethyl methacrylate (FLEMA, structure given in Fig. 3.7) ceases once the probe is incorporated into growing polymer chains. This supports the hypothesis that fluorescence quenching is caused by the enone functionality. In comparison to FLEMA, the enone functionality in both MPy and PyMA is more closely coupled to the fluorophore, *i.e.* the methylene spacer between fluorophore and quenching species is absent. This is probably the reason why *complete* quenching of fluorescence occurs for both MPy and PyMA, whereas only partial quenching is observed with FLEMA.

3.4.3. *N*-(2-anthracene)methacrylamide

The pyrene fluorophore, when activated by copolymerization of MPy and PyMA, exhibits a very long singlet-state lifetime (*ca* 150 ns in MMA). This leads to considerable sensitivity of the observed fluorescence intensity and lifetime from such probes to low concentrations of oxygen and other possible trace impurities. Since anthracene has a much shorter natural fluorescence lifetime (*ca* 4 ns), it was thought that a fluorogenic probe incorporating the anthracene moiety would be less sensitive to low concentrations of quenching species.

The fluorogenic probe *N*-(2-anthracene)methacrylamide, AnMA, was synthesized from 2-aminoanthracene (Aldrich, 96%) and methacryloyl chloride (Aldrich, 80%) as shown in reaction B below. The NEt_3 (Aldrich, 99.5%) was dried over 4 Å molecular sieves and CH_2Cl_2 was dried and purified by distillation over P_2O_5.

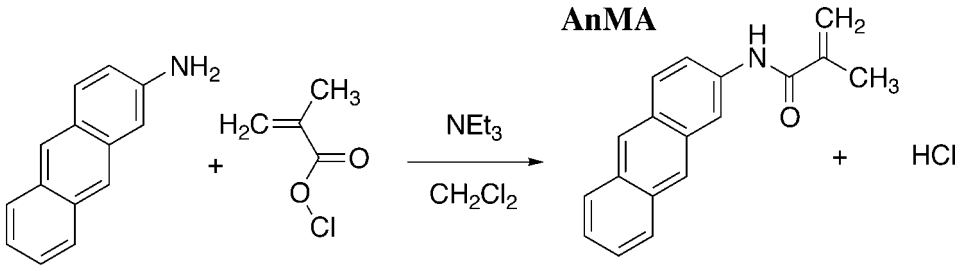

(B)

The 2-aminoanthracene reagent was purified from oxidation products by passing through a chromatography column packed with silica gel using a 4-to-1 mixture of CH_2Cl_2 and hexane as the eluent. Eluent fractions containing the fluorescent starting material were combined and the solvent was removed by evaporation under reduced pressure. The remaining solid was recrystallized using the same solvent mixture, isolated by filtration and dried under vacuum.

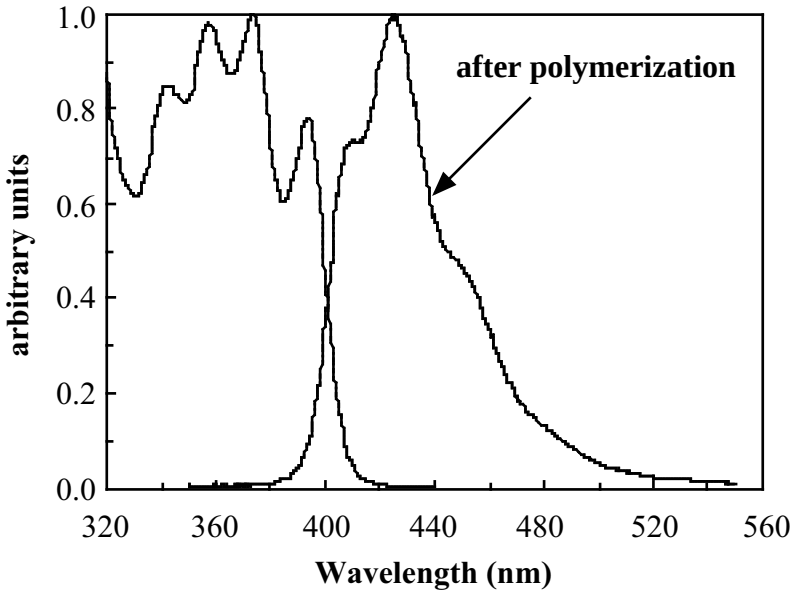

Figure 3.8. Absorption spectrum of AnMA and the emission spectrum after copolymerization.

A solution of 328 mg of the purified 2-aminoanthracene (1.70 mmol) in 60 mL of anhydrous CH_2Cl_2 was prepared. A 20 mL solution containing 1.2 equivalents of freshly distilled methacryloyl chloride and anhydrous NEt_3 (0.22 mL and 0.29 mL respectively) was then prepared and slowly added to the stirred 2-aminoanthracene solution at room temperature. Within 10 minutes triethylammonium chloride precipitated from the solution. The reaction mixture was then shaken with 30 mL of 10% aqueous hydrochloric acid and subsequently with an excess of distilled water prior to filtering into a separatory funnel. The bottom CH_2Cl_2 layer was collected and the solvent was removed under reduced pressure. The solid was recrystallized twice from the

CH_2Cl_2/hexane mixture rendering 130 mg of almost colorless AnMA crystals with a 16% yield; m.p. = 253-254 ºC. ^{1}H NMR ($CDCl_3$, 400 MHz, not all peaks could be sufficiently resolved from one another): 8.48 (d, 1H), 8.37 (d, 1H & s, 1H), 7.99 (s, 1H), *ca* 8 (d, 1 H), 7.96 (s, 1H), 7.66 (br s, 1H), 7.46 (t, 1H), *ca* 7.5 (d, 1H), 7.43 (t, 1H), 5.87 (s, 1H), 5.25 (s, 1H), 2.13 (s, 3H).

The absorption spectrum of AnMA is shown in figure 3.8. Similar to MPy and PyMA, AnMA is completely non-fluorescent until the carbon-carbon double bond of the methacrylamide group becomes saturated upon copolymerization. The fluorescence spectrum of the reacted probe derivative is also shown in figure 3.8.

References

(1) Valdes-Aguilera, O.; Pathak, C. P.; Neckers, D. C. *Macromolecules* **1990**, *23*, 689.

(2) Wang, F. W.; Lowry, R. E.; Grant, W. H. *Polymer* **1984**, *25*, 690.

(3) Stroeks, A.; Shmorhun, M.; Jamieson, A. M.; Simha, R. *Polymer* **1988**, *29*, 467.

(4) Nakajima, A. *Bull. Chem. Soc. Japan* **1971**, *44*, 3272.

(5) Dong, D.; Winnik, M. *Can. J. Chem.* **1984**, *62*, 2560.

(6) Kropp, J. L.; Dawson, W. R.; Windsor, M. W. *J. Phys. Chem.* **1969**, *73*, 1747.

(7) Meech, S. R.; Phillips, D. *J. Photochem.* **1983**, *23*, 193.

(8) Mes, G. F.; de Jong, B.; van Ramesdonk, H. J.; Verhoeven, J. W.; Warman, J. M.; Haas, M. P. d.; Dool, Horsman-van den Dool, L. E. W. *J. Am. Chem. Soc.* **1984**, *106*, 6524.

(9) Goes, M.; Lauteslager, X. Y.; Verhoeven, J. W.; Hofstraat, J. W. *Eur. J. Organic Chem.* **1998**, 2373.

(10) Verhey, H. V.; Bekker, C. H. W.; Verhoeven, J. W.; Hofstraat, J. W. *New J. Chem.* **1996**, *20*, 809.

(11) Eftink, M.; Selva, T.; Wasylewski, Z. *Photochem. Photobiol.* **1987**, *46*, 23.

(12) Miller, K.; Burch, E.; Lewis, F.; Torkelson, J. *J. Polymer Sci. B Polymer Phys.* **1994**, *32*, 2625.

(13) Aloisi, G.; Masetti, F.; Mazzucato, U. *Chem. Phys. Lett.* **1974**, *29*, 502.

(14) Du, F. S.; Cai, H.; Li, Z. C.; Li, F. M. *J. Polym. Sci. A* **1998**, *36*, 1111.

Chapter Four

Monomer Conversion in Methyl Methacrylate

4.1. Introduction

In this chapter the experimental results for monomer conversion and polymer molecular weight on irradiation of methyl methacrylate, MMA, are presented. This information is used in subsequent chapters for comparison with results obtained using fluorogenic probe molecules under identical irradiation conditions. It is worth pointing out that one of the aims of using fluorogenic probe molecules is to allow the *in situ* or on-line monitoring of polymerization without the requirement of interrupting the process for sample analysis as was necessary to obtain the data presented in this chapter.

The results are presented in two separate sections: the first deals with polymerization under conditions of "continuous" or "steady-state" γ-radiolysis for which the concentration of reactive, free radical intermediates reaches a constant value on a timescale short compared with the irradiation time; the second concerns nanosecond pulsed electron-beam irradiation using the Van de Graaff accelerator for which the lifetimes of the free radical intermediates are considerably longer than the pulse duration. Data are also presented on the molecular mass distribution of the poly(methyl methacrylate), PMMA, products. The relationship between the measurements and the kinetics of the underlying reactions controlling the rate and degree of polymerization are discussed.

4.2. γ-Ray Radiolysis

A well-documented phenomenon in the polymerization of MMA is the occurrence of autoacceleration of the polymerization process above a certain fractional conversion of the monomer. This is commonly known as the "gel" or "Trommsdorff" effect (discussed in detail at the end of this chapter) and occurs irrespective of whether polymerization is initiated thermally, photolytically or radiolytically. Because of this it is convenient to separate a discussion of MMA polymerization into sections dealing with conversions below and above the gel effect region.

4.2.1. Low Monomer Conversion (< 30%)

As mentioned in section 2.5. of chapter 2, the residual monomer evaporation technique of estimating the fractional monomer conversion, C_M, gave consistently higher values than the method of polymer precipitation. It was concluded that the former method, which could possibly yield somewhat too high values at very high conversions due to monomer entrapment in the vitreous matrix, was to be preferred particularly in the low conversion region. Consequently only data obtained using the monomer evaporation technique are given in this chapter.

In Figures 4.1 and 4.2 C_M is shown as a function of dose for conversions less than 35% using the Gammacell 200 and 220 irradiators with dose rates of 0.754 and 9.82 kGy/h respectively. The good agreement of the data with the straight lines drawn through the points indicates the close to linear dependence of C_M on dose in the early stage of polymerization in both cases. The slopes of the straight lines yield values of $-dC_M/dD$ of 6.95×10^{-5} and 2.22×10^{-5} Gy^{-1} for the low and high dose rates respectively.

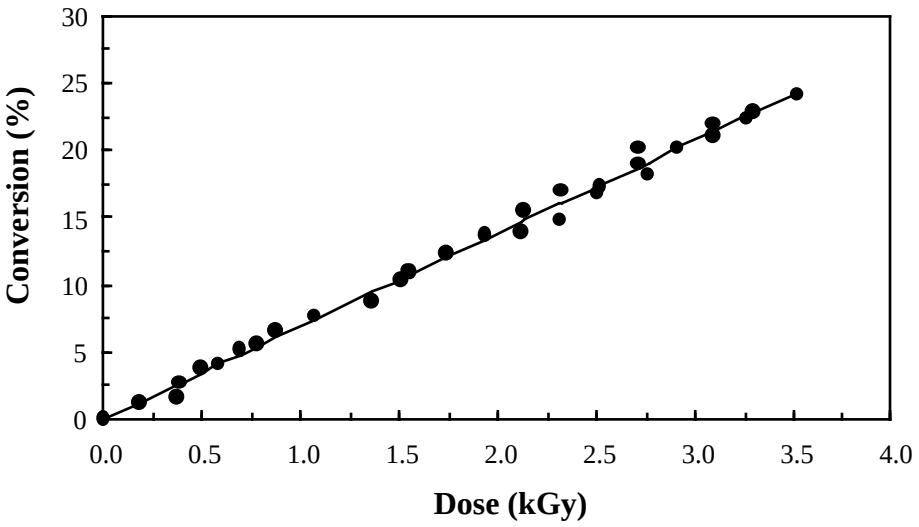

Figure 4.1. Conversion of MMA to PMMA versus γ-ray dose in the Gammacell 200 irradiator (dose rate of 0.754 kGy/h).

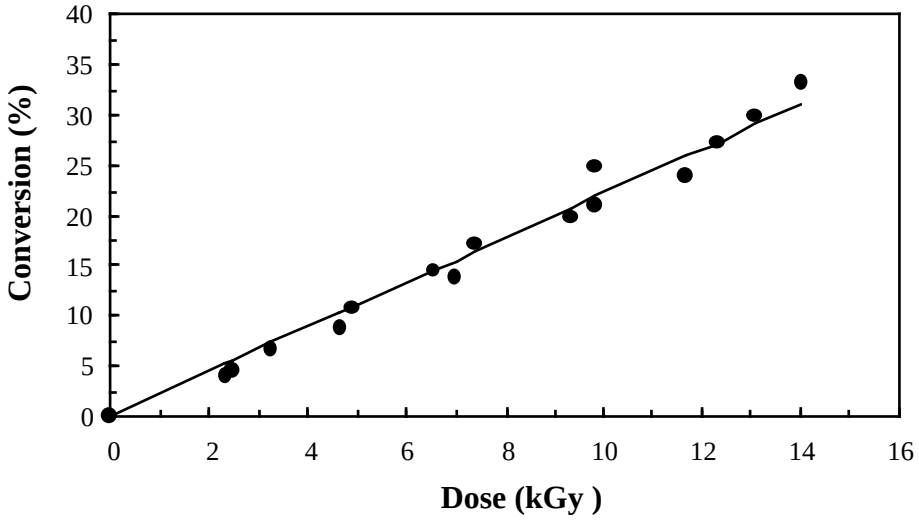

Figure 4.2. Conversion of MMA to PMMA versus γ-ray dose in the Gammacell 220 irradiator (dose rate of 9.82 kGy/h).

Rather than being expressed as the fractional change in concentration per Gray, the change in concentration of a reactant or product on irradiation is usually expressed as either the number of moles per joule of absorbed energy, the "*g*" value, or the number of molecules per 100 eV of absorbed energy, the "*G*" value. While the former is the SI accepted parameter, the latter is still more familiar to many of those working in the field and is most frequently found in the literature. The two units are related by

$$g = G/100eN_A = 1.038x10^{-7}G \tag{4.1}$$

with e and N_A the numerical value of the elementary charge ($1.60x10^{-19}$) and Avogadro's number ($6.02x10^{23}$ molecules/mole) respectively. Use of the g value results in simpler mathematical expressions and therefore it will be used here. In the present case, the g value for monomer conversion is related to dC_M / dD by

$$g(-MMA) = 1000[dC_M / dD] / W_{MMA} \tag{4.2}$$

with W_{MMA} the molecular mass of MMA (100.13 g/mole). Because of its familiarity, the G value will be mainly used in the text for discussion of the results. Using 4.1 and 4.2, the G values for monomer conversion for the low and high dose rates are determined to be 6690 and 2140 $(100\ eV)^{-1}$ respectively.

The present results will be discussed further and compared with previous results after first considering the underlying processes and kinetics of the polymerization process.

4.2.2. Steady-State Polymerization Kinetics

The process of free radical polymerization on γ-radiolysis involves four distinguishable steps; primary free radical formation, initiation, propagation and termination. Primary free radicals, $R\bullet$, are produced at a rate, F_R (mole/L s), which is determined by the g value of free radical formation and the dose rate D' (Gy/s) according to equation 4.3.

$$F_R = g(R\bullet)\rho D' \tag{4.3}$$

with ρ (kg/L) the density of MMA. These primary free radicals initiate polymerization by reacting with a monomer molecule, M, with a rate constant k_i,

$$R\bullet + M \xrightarrow{k_i} RM\bullet \tag{A}$$

Propagation, represented by reaction B, then follows by the repeated addition of monomer units to the growing (macro-)radical.

$$RM_n\bullet + M \xrightarrow{k_{pn}} RM_{n+1}\bullet \tag{B}$$

The propagation rate constant is denoted k_{pn} with the subscript n indicating the possibility that it is dependent on the size of the propagating free radical. Studies involving pulsed laser polymerization (PLP) have in fact shown that the propagation rate constant is almost independent of the size of the propagating free radical during the early stage of polymerization[1,2]. The value of k_{pn} does however

decrease significantly in the late stage of bulk polymerization due to a large increase in viscosity[3-5]. Since the concern here is with the early, low viscosity stage of polymerization k_{pn} may be taken to be close to constant. The possibility of a slight dependence of k_{pn} on n is nevertheless indicated by denoting k_p as an average value, $\langle k_p \rangle$.

In the pure bulk monomer termination of polymerization occurs either by combination or disproportionation reactions, represented jointly by reaction C.

$$RM_n\bullet + R'M_m\bullet \xrightarrow{k_{tnm}} P_{nm} \text{ or } P_n + P_m \qquad \text{(C)}$$

The overall rate constant of termination, k_{tnm}, is known to be dependent on the chain-lengths of the reacting radicals (see figure 1.13)[6-9], and the subscripts n and m are used to indicate this.

The above reaction mechanism leads to the following expression for the rate of change of the total free radical concentration in the system.

$$d\sum_n [RM_n\bullet]/dt = F_R - \sum_n \left([RM_n\bullet] \sum_m (2k_{tnm}[RM_m\bullet]) \right) \qquad (4.4)$$

Note that the propagation reaction does not appear in equation 4.4 since this does not result in a net change in the free radical concentration. Defining an average value of the termination rate constant by equation 4.5

$$\langle k_t \rangle = \sum_n \left([RM_n\bullet] \sum_m k_{tnm}[RM_m\bullet] \right) \Big/ \sum_n ([RM_n\bullet] \sum_m [RM_m\bullet]) \qquad (4.5)$$

results in equation 4.6 for the rate of change of the total free radical concentration in the system.

$$d\sum_n [RM_n\bullet]/dt = F_R - 2\langle k_t \rangle \left(\sum_n [RM_n\bullet] \right)^2 \qquad (4.6)$$

According to the "steady-state approximation", under continuous irradiation conditions the concentration of free radicals reaches an equilibrium value $[RM_n\bullet]_{ss}$ which is given by

$$[RM_n\bullet]_{ss} = (F_R / 2\langle k_t \rangle)^{1/2} \qquad (4.7)$$

The rate of decrease in the monomer concentration, [M], during the early stage of polymerization is given by equation 4.8.

$$-d[M]/dt = \langle k_p \rangle [RM_n\bullet][M] \tag{4.8}$$

Substitution in equation 4.8 of the steady-state free radical concentration gives

$$-d[M]/dt = \langle k_p \rangle \left(F_R / 2\langle k_t \rangle\right)^{1/2}[M] \tag{4.9}$$

One can then derive the fractional conversion of monomer as a function of time $C_M(t)$ under steady-state conditions by integration of equation 4.9.

$$C_M(t) = 1 - \exp\left(-\langle k_p \rangle \left(F_R/2\langle k_t \rangle\right)^{1/2} t\right) \tag{4.10}$$

For short times, quadratic terms in the series expansion of the exponential function in equation 4.10 can be neglected. This leads to the following, limiting expression for the monomer conversion at low conversions.

$$C_M(t) = \langle k_p \rangle \left(F_R/2\langle k_t \rangle\right)^{1/2} t \tag{4.11}$$

Equation 4.11 can be written in terms of the total accumulated dose by substituting for D ($D = D't$) and for F_R from equation 4.3.

$$C_M(D) = \langle k_p \rangle \left(\rho g(R\bullet)/2\langle k_t \rangle\right)^{1/2} D/\sqrt{D'} \tag{4.12}$$

According to 4.12, plots of the monomer conversion against the parameter $D/\sqrt{D'}$ for different dose rates at the same temperature should have the same slope given by,

$$dC_M \Big/ d\left(D/\sqrt{D'}\right) = \langle k_p \rangle \left(\rho g(R\bullet)/2\langle k_t \rangle\right)^{1/2} \tag{4.13}$$

Accordingly, the data given in figures 4.1 and 4.2 have therefore been replotted against $D/\sqrt{D'}$ in figure 4.3.

The slightly greater slope for the high dose rate data can be explained by the higher temperature in the Gammacell 220 source (34^0C compared with 25^0C) and the known activation energy of 4.9 kcal/mole found for the propagation rate constant[10].

For simplicity of presentation the results can best be discussed in terms of the parameter P_{ss} which is defined as

$$P_{ss} = \langle k_p \rangle^2 g(R\bullet)/2\langle k_t \rangle \tag{4.14}$$

$$P_{ss} = \left(dC_M / d\left(D / \sqrt{D'} \right) \right)^2 / \rho \qquad (4.15)$$

From the slope for the low dose rate data and the known density of 0.94 kg/L, a value of $1.07x10^{-9}$ L/J s is determined for P_{ss}. This is in good agreement with the value of $1.00x10^{-9}$ L/J s which is obtained for the same dose rate and ambient temperature by interpolation from a large collection of published data covering the dose rate range from 10^{-4} to 2 Gy/s (Chapiro reference, figure V.7.). Using the literature value of 342 L/mole s for the propagation rate constant as determined from PLP experiments on bulk MMA at 25^0C [11], allows an estimate of $9.1x10^{-15}$ mole^2 s/L J to be made for the product $g(R\bullet)/2\langle k_t \rangle$ from the value of P_{ss} determined. Separate estimates of $g(R\bullet)$ and $\langle k_t \rangle$ can be made on the basis of the polymer molecular mass and the pulse-radiolysis experiments as described in the following sections.

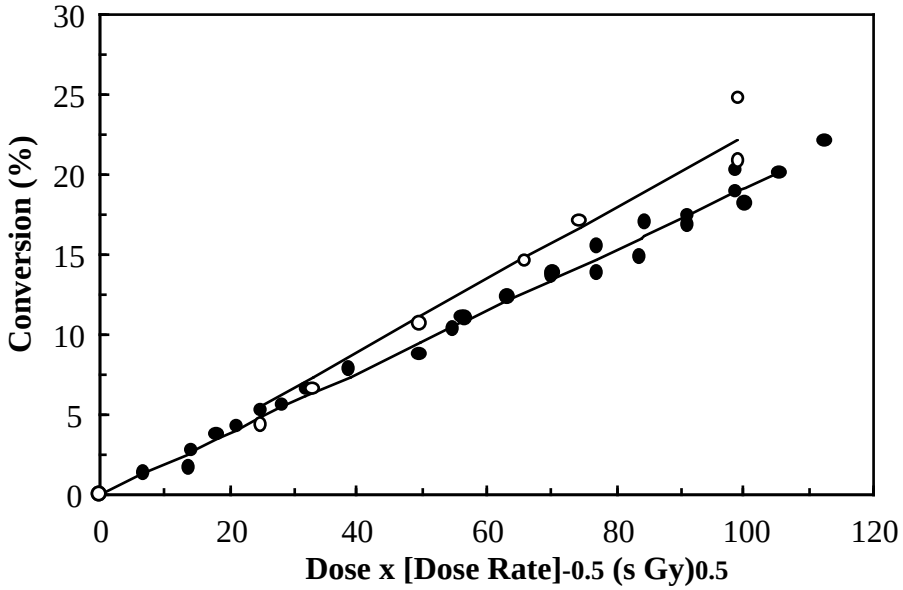

Figure 4.3. MMA conversion versus the scaled dose for both the Gammacell 200 (filled circles) and Gammacell 220 (open circles) sources.

4.2.3. Low Conversion Polymer Molecular Mass

GPC traces are shown in figures 4.4 and 4.5 for PMMA samples obtained at low monomer conversions for the two dose rates studied. As can be seen the molecular mass distribution changes very little up to approximately 20% conversion. The values of the number-average molecular mass, M_n, for the lowest conversions are 154 and 55 kDa for the low and high dose rates respectively.

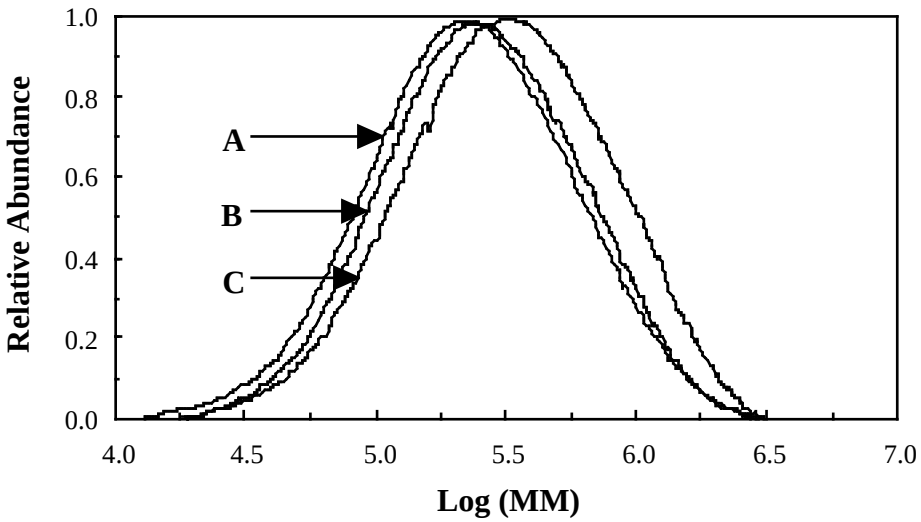

Figure 4.4. GPC traces for PMMA samples produced in the Gammacell 200 irradiator at various extents of monomer conversion; (**A**) 5.5 %, (**B**) 10.9 %, (**C**) 22.3 %.

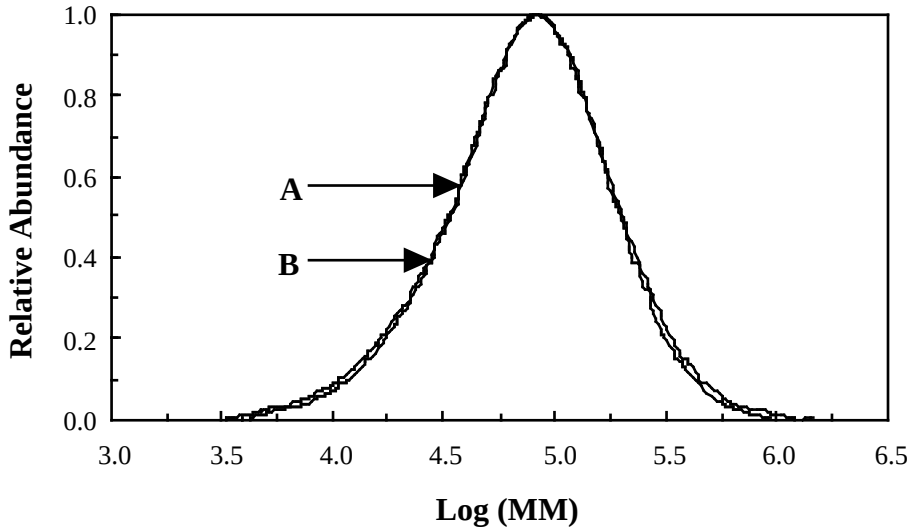

Figure 4.5. GPC traces for PMMA samples produced in the Gammacell 220 irradiator at various extents of monomer conversion; (**A**) 10.7 %, (**B**) 24.7 %.

The molecular mass of the polymer formed under steady-state irradiation conditions depends upon the relative rates of propagation and termination. The average number of propagation steps prior termination, *l*, is given by

$$l = \langle k_p \rangle [M] \Big/ \sqrt{2\langle k_t \rangle F_R} \tag{4.16}$$

For termination by disproportionation, M_n will therefore be given by 4.17 in which W_{MMA} is the molecular mass of the MMA monomer.

$$M_n = [M]W_{MMA}\langle k_p\rangle \Big/ \sqrt{2\langle k_t\rangle F_R} \tag{4.17}$$

Termination by combination will result in a value of M_n twice that given by 4.17. Most materials, including MMA, undergo both disproportionation and combination. If the fraction of termination reactions occurring via combination is f_c then the overall value of M_n will be given to a first approximation by

$$M_n = (1+ f_c)([M]W_{MMA})\langle k_p\rangle \Big/ \sqrt{2\langle k_t\rangle F_R} \tag{4.18}$$

$$= (1+ f_c)([M]W_{MMA})\langle k_p\rangle \Big/ \sqrt{2\langle k_t\rangle \rho D' g(R\bullet)} \tag{4.19}$$

According to 4.19, M_n should therefore be inversely proportional to the square root of the dose rate. The ratio between the M_n values of 2.8 found in the present work for the low and high dose rates is somewhat lower than the value of 3.6 expected based on the inverse ratio of the square root of the dose rates. Again, this difference may be ascribed, at least in part, to the higher temperature in the high dose rate source which, because of the thermal activation of the propagation reaction, would result in a relatively too high value of M_n.

The following expression can be derived by taking the derivative with respect to dose of equation 4.11, $(t = D/D')$, with substitution from equation 4.2.

$$\langle k_p\rangle / \sqrt{2\langle k_t\rangle} = W_{MMA} D' g(-MMA)/1000\sqrt{F_R} \tag{4.20}$$

Substitution from equation 4.18 and rearrangement results in the following expression for the yield of primary, initiating free radicals

$$g(R\bullet) = (1+ f_c) W_{MMA} g(-MMA)/M_n \tag{4.21}$$

Using the above values of M_n, the values of $G(\text{-}MMA)$ determined in section 4.2.1. (6690 and 2140 $(100\ eV)^{-1}$) and the value of 0.33 for f_c[12] yields $G(R\bullet)$ values of 5.8 and 5.2 $(100\ eV)^{-1}$ for the low and high dose rates respectively. These values are very close to the free radical yields in MMA of 5.5 and 6.7 $(100\ eV)^{-1}$ determined using the DPPH (*i.e.* diphenylpicrylhydrazyl: a scavenger of free radicals) method[10,13]. As will be seen, the present values are also close to the value of 5.0 $(100\ eV)^{-1}$ derived from the results of the pulse experiments.

4.2.4. High Monomer Conversion (> 30%)

Complete conversion curves for the low and high dose rate sources are shown in Figures 4.6 and 4.7. In both cases the rate of polymerization increases dramatically above approximately 30% conversion.

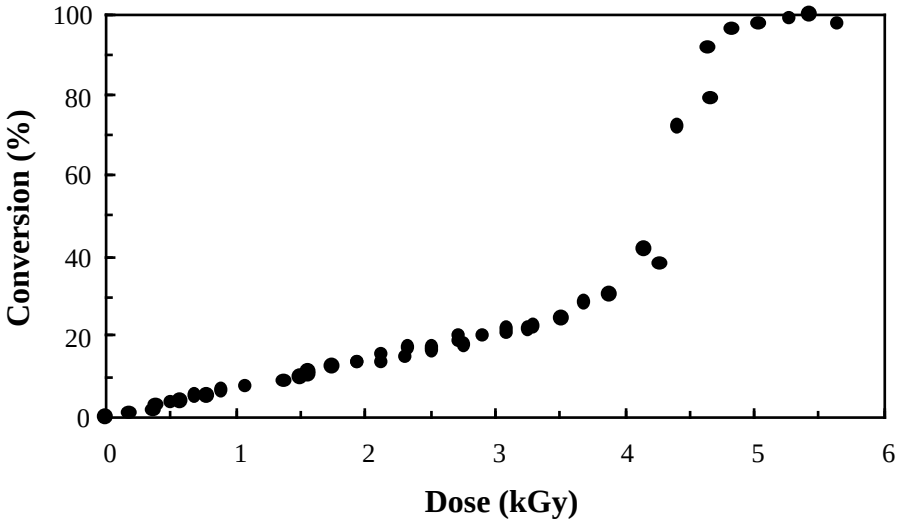

Figure 4.6. Conversion of MMA versus γ-ray dose in the Gammacell 200 irradiator (dose rate 0.754 kGy/h).

This autoacceleration phenomenon, known as the "gel" or "Trommsdorff" effect, is ascribed to a sudden increase in the radical concentration caused by a decrease in the termination rate constant. The precise mechanism is still under discussion and different theories behind the effect are discussed in detail at the end of this chapter. The maximum polymerization rate occurs for total accumulated doses, D_{max}, of 4.4 and 17 kGy for dose rates of 0.209 and 2.73 Gy/s respectively. The ratio of the D_{max} values of 3.8 is close to the ratio of the square roots of the dose rates. Interestingly, the conversion of close to 30%, above which the dramatic increase in the polymerization rate occurs, is independent of dose rate or whether polymerization is achieved by radiolytic, photolytic or thermal means. Perhaps surprisingly, the molecular weight of the polymers formed in the low conversion regime appears to have little influence on the conversion at which the gel effect occurs.

The rate of polymerization eventually slows down as monomer is consumed and the polymerizing system becomes a viscous glass. As mentioned previously, the monomer conversions determined after vitrification has occurred using the monomer evaporation technique could be too high due to monomer entrapment in the rigid matrix. The actual value of the final conversion for the highest doses in figures 4.6 and 4.7 may therefore be somewhat lower than the value of 100% indicated. Other methods of determining the monomer conversion have indicated that the ultimate value of C_M is in fact closer to 90% for MMA[14,15].

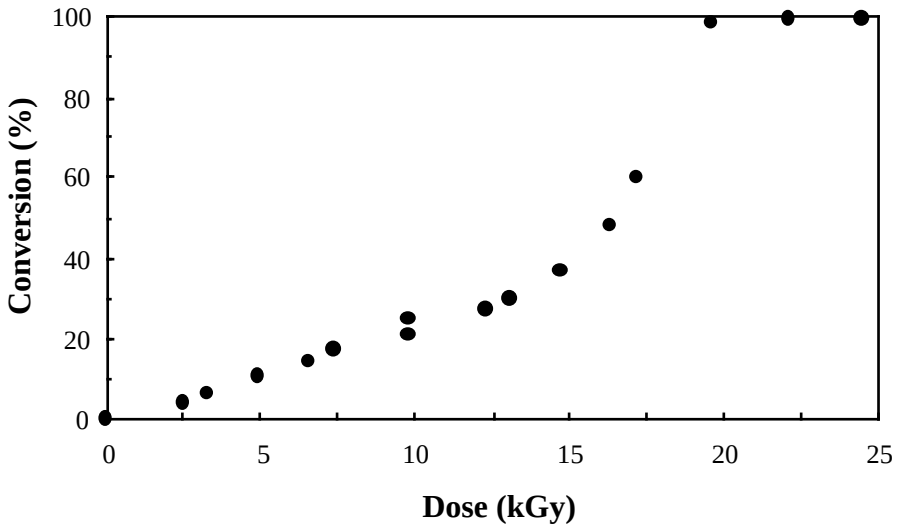

Figure 4.7. Conversion of MMA versus γ-ray dose in the Gammacell 220 irradiator (dose rate 9.82 kGy/h).

It is important to point out that the present experiments were carried out under non-isothermal conditions. Autoacceleration is therefore accompanied by a considerable increase in temperature which serves to further enhance the rate of polymerization. Since neither steady-state kinetics nor isothermal conditions apply, the gel region is not amenable to modeling using conventional homogeneous kinetic treatments.

4.2.5. High Conversion Polymer Molecular Mass

GPC traces are shown in figures 4.8 and 4.9 for irradiated MMA samples prior to and above the onset of the gel effect for the low and high dose rate conditions respectively. In both cases the gel effect is seen to be accompanied by the formation of significantly higher molecular mass polymeric material. In this regard it is worth mentioning that the column used for the GPC measurements was not suitable for separating polymers with molecular masses close to or in excess of approximately one million Dalton since molecular masses of this magnitude have similar retention times in the column. Because of this, the close to an order of magnitude increase in the molecular mass which is indicated by the results in figures 4.8 and 4.9 is therefore a lower limit to the actual change occurring.

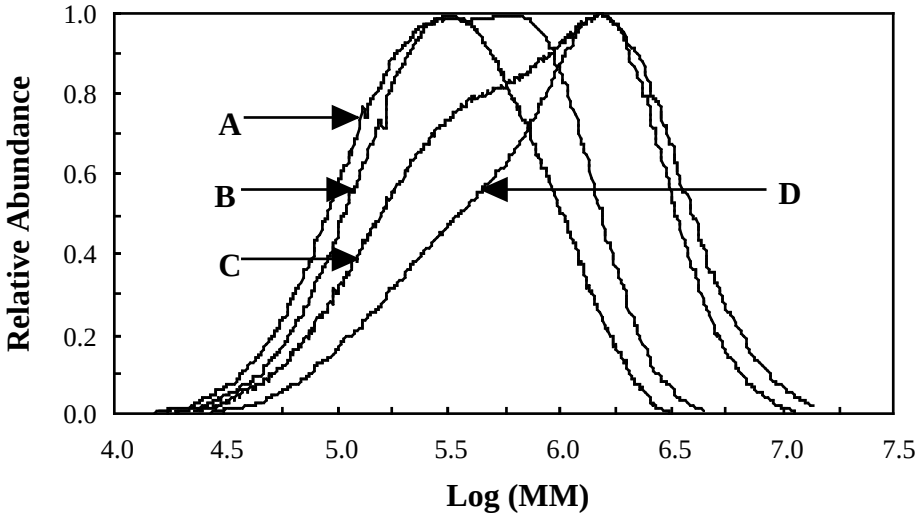

Figure 4.8. GPC traces for PMMA produced in the Gammacell 200 irradiator at various extents of monomer conversion; (**A**) 22.3 %/3.27 kGy, (**B**) 62.4 %/4.65 kGy, (**C**) 97.5 %/5.04 kGy, (**D**) 100 %/6.20 kGy.

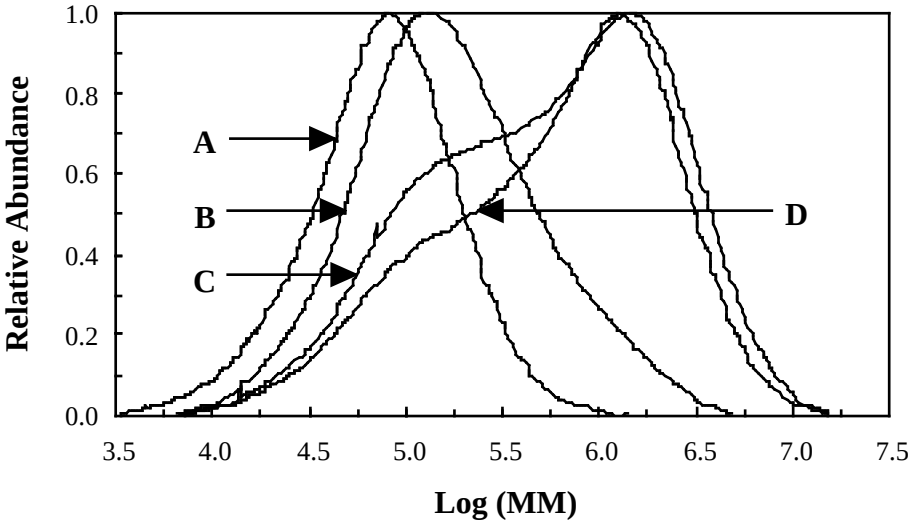

Figure 4.9. GPC traces for PMMA produced in the Gammacell 220 irradiator at various extents of monomer conversion; (**A**) 24.7 %/9.8 kGy, (**B**) 60.3 %/17.2 kGy (**C**) 97.9 %/19.6 kGy, (**D**) 99.1 %/22.1 kGy.

Such a large change in the polymer molecular mass can in part be explained by the formation of radiation-induced cross-links. This explanation is not necessarily in conflict with the known tendency for PMMA to undergo chain scission rather than cross-linking (see section 1.7.2 in Chapter 1). In this respect it is worth mentioning that studies of radiation-induced cross-linking or chain-scission are typically carried out on pre-formed polymer samples at doses in excess of 10

kGy. An additional factor which could possibly explain the drastic increase in the molecular mass is that when a small amount of monomer is present in the irradiated system, reaction diffusion[16,17,5] occurs more readily than chain-scission. This would remove the free radical center from the vicinity of main-chain tertiary carbons and thereby inhibit an established mechanism for chain-scission[10]. Reaction with other macro-radicals would effectively lead to H-shaped cross-links. If this mechanism were to continue, network formation is conceivable.

4.3. Pulsed Electron-Beam Radiolysis

Pulsed irradiation techniques are often applied for the fundamental study of the reaction kinetics of polymerizing systems. In pulse-radiolysis steady-state kinetics do not apply and a relaxation-kinetic treatment has to be used. As will be shown, the parameter $\langle k_p \rangle G(R\bullet)$ can be determined by combining the γ-radiolysis and pulse-radiolysis results.

4.3.1. Pulse Radiolysis Monomer Conversion

Figure 4.10 shows the monomer conversion as a function of dose using 50 ns pulses of 3 MeV electrons delivering a dose of *ca* 15 Gy per pulse at a repetition frequency of 5 Hz. The maximum conversion reached in these experiments was 33% at an accumulated dose of 140 kGy. As for the γ-irradiations, the conversion is seen to increase with dose in a close to linear manner for conversions up to approximately 30%. The polymerization rate determined from the slope of the straight line through the data in figure 4.10 is 1.9×10^{-6} Gy^{-1}. This corresponds to a *G*-value of monomer consumption of 1.8×10^{2} $(100\ eV)^{-1}$, which is more than an order of magnitude lower than found for the high dose rate gamma-irradiation source.

The highest achieved conversion, corresponding to 33% conversion, does appear to lie somewhat higher than expected based on the straight line drawn through the lower data points. This could possibly be taken to indicate the onset of the gel effect even under pulse-radiolysis conditions. However, the difference is close to the error limits in the reproducibilty of the conversion determinations. Unfortunately, doses above 140 kGy were not achieved for practical reasons.

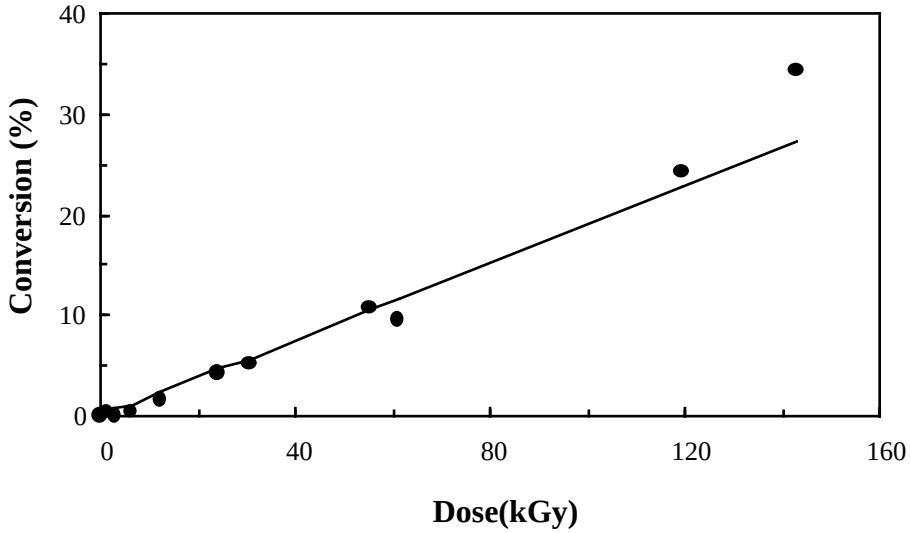

Figure 4.10. Conversion of MMA to PMMA via pulsed electron-beam polymerization (5 Hz and *ca*15 Gy/pulse).

4.3.2. Pulsed Polymerization Kinetics

In the pulse radiolysis experiments the abundance of termination reactions occurring within the 50 ns pulses used is negligible. The concentration of free radicals produced within a pulse with a dose ΔD is therefore,

$$\sum_n [RM_n\bullet]_0 = \rho \Delta D g(R\bullet) \tag{4.22}$$

A rough estimate of $\sum_n [RM_n\bullet]_0$ can be made by using 15 Gy for ΔD, the dose per electron-beam pulse, and assuming an approximate value of 5 $(100\ \text{eV})^{-1}$ for the G value of free radical formation. This results in a $\sum_n [RM_n\bullet]_0$ of *ca* 7 μM.

The decay rate of free radicals after the pulse is given by

$$d\sum_n [RM_n\bullet]/dt = -2\langle k_t \rangle \left(\sum_n [RM_n\bullet]_t \right)^2 \tag{4.23}$$

which on integration yields the concentration of free radicals present at time t,

$$\sum_n [RM_n\bullet]_t = \sum_n [RM_n\bullet]_0 \Big/ \left(1 + 2\langle k_t \rangle \sum_n [RM_n\bullet]_0 t \right) \tag{4.24}$$

Substitution of this expression for the free radical concentration in the rate expression for monomer polymerization given here in equation 4.25

$$d[M]/dt = -\langle k_p \rangle [M] \sum_n [RM\bullet]_t \tag{4.25}$$

and subsequent integration leads to equation 4.26 for the monomer conversion as a function of elapsed time after a single pulse.

$$\Delta C_M(t) = 1 - \left(1 + 2\langle k_t \rangle \sum_n [RM_n\bullet]_0 t\right)^{-\langle k_p \rangle / 2\langle k_t \rangle} \tag{4.26}$$

It is apparent from equation 4.26 that, provided there are no free radical scavengers present, the conversion of monomer following a single pulse should go to completion given sufficient time. In the case of repetitive pulsing however, subsequent pulses produce radicals which stop the propagation of those remaining from the previous pulse by radical-radical reaction. If the time between pulses is τ (0.2 s for 5 Hz repetition rate), the conversion per pulse will therefore be

$$\Delta C_M(\tau) = 1 - (1 + 2\langle k_t \rangle \sum_n [RM_n\bullet]_0 \tau)^{-\langle k_p \rangle / 2\langle k_t \rangle} \tag{4.27}$$

Since $\langle k_p \rangle / 2\langle k_t \rangle$ is much smaller than 1, this expression is given to a good approximation by

$$\Delta C_M(\tau) = \langle k_p \rangle \ln\left[1 + 2\langle k_t \rangle \sum_n [RM_n\bullet]_0 \tau\right] \Big/ 2\langle k_t \rangle \tag{4.28}$$

Substituting in (4.28) for $\sum_n [RM_n\bullet]_0$ from (4.22) and the parameter P_{ss} (previously defined in equation 4.14 for steady-state, γ-radiolysis experiments) results in the following expression for $\Delta C_M(\tau)$,

$$\Delta C_M(\tau) = P_{ss} \ln\left\{1 + \left[\left(\langle k_p \rangle g(R\bullet)\right)^2 \rho \Delta D \tau / P_{ss}\right]\right\} \Big/ \langle k_p \rangle g(R\bullet) \tag{4.29}$$

For a train of pulses with a total accumulated dose D, the monomer conversion will be given by

$$C_M(\tau) = D P_{ss} \ln\left\{1 + \left[\left(\langle k_p \rangle g(R\bullet)\right)^2 \rho \Delta D \tau / P_{ss}\right]\right\} \Big/ \langle k_p \rangle g(R\bullet) \Delta D \tag{4.30}$$

As can be seen in the above equation, the slope of the dose dependence for pulsed irradiation is dependent on (a) P_{ss}, the value of which has been determined in the steady-state γ-radiolysis experiments (1.07×10^{-9} L/J s), (b) the known values of ΔD and τ, and (c) the product $\langle k_p \rangle g(R\bullet)$. The value of $\langle k_p \rangle g(R\bullet)$ required to fit the slope of the straight line in figure 4.10 is 1.76×10^{-4} $M^{-1}s^{-1}$. This corresponds to a value of $\langle k_p \rangle G(R\bullet)$ of 1700 $M^{-1}s^{-1}(100\ eV)^{-1}$.

Using the literature value of 342 $M^{-1}s^{-1}$ for k_p as determined from PLP experiments with bulk MMA at 25ºC[11] gives a *G*-value for initiating radicals of 5.0 $(100\ eV)^{-1}$. This is 10% less than the average value of 5.5 $(100\ eV)^{-1}$ determined from the polymer molecular weight and monomer conversion determinations in the γ-radiolysis experiments. The lower value may be the consequence of the much higher dose rate in the electron-beam pulse experiments. However, the difference is small and within the error limits of the measurements.

4.3.3. Polymer Molecular Mass Produced by Pulsed Irradiation

Figure 4.11 illustrates some interesting aspects of producing PMMA by pulsed electron-beam irradiation. The chromatograms are presented using the elution time scale along the x-axis, therefore it is important to keep in mind that a shorter elution time implies a larger molecular mass for the polymer. The elution profiles are all broad with polydispersities, *i.e.* the ratio between the weight-average and number-average molecular weights, in excess of 3 for each sample.

The effect of varying the pulse repetition rate is shown in part A of figure 4.11 in which all samples had been irradiated to the same total dose of 55 kGy. It is apparent that there is a significant difference in the position and shape of the chromatograms by comparing that for polymerization at 1 Hz, corresponding to 15.88% monomer conversion, with those at 5 and 10 Hz, corresponding to monomer conversions of 10.70% and 10.00% respectively. This can be attributed to the earlier termination of growing polymer chains by primary radicals created in subsequent pulses at higher repetition rates. For primary radical termination, PRT, the peak (modal) molecular mass of the polymer chains[18] $\overline{M}_p$ is given by

$$\overline{M}_p = W_{MMA} k_p [M] \tau \tag{4.31}$$

with W_{MMA} the molecular mass of the monomer, $[M]$ the monomer concentration and τ the time between pulses. For polymerizations at 5 and 10 Hz this gives molecular masses of 64 and 32 kDa respectively. The corresponding peaks in the molecular masses corresponding to the maxima in the elution curves shown in figure 4.11 are 69 and 45 kDa, *i.e.* close to the predicted values.

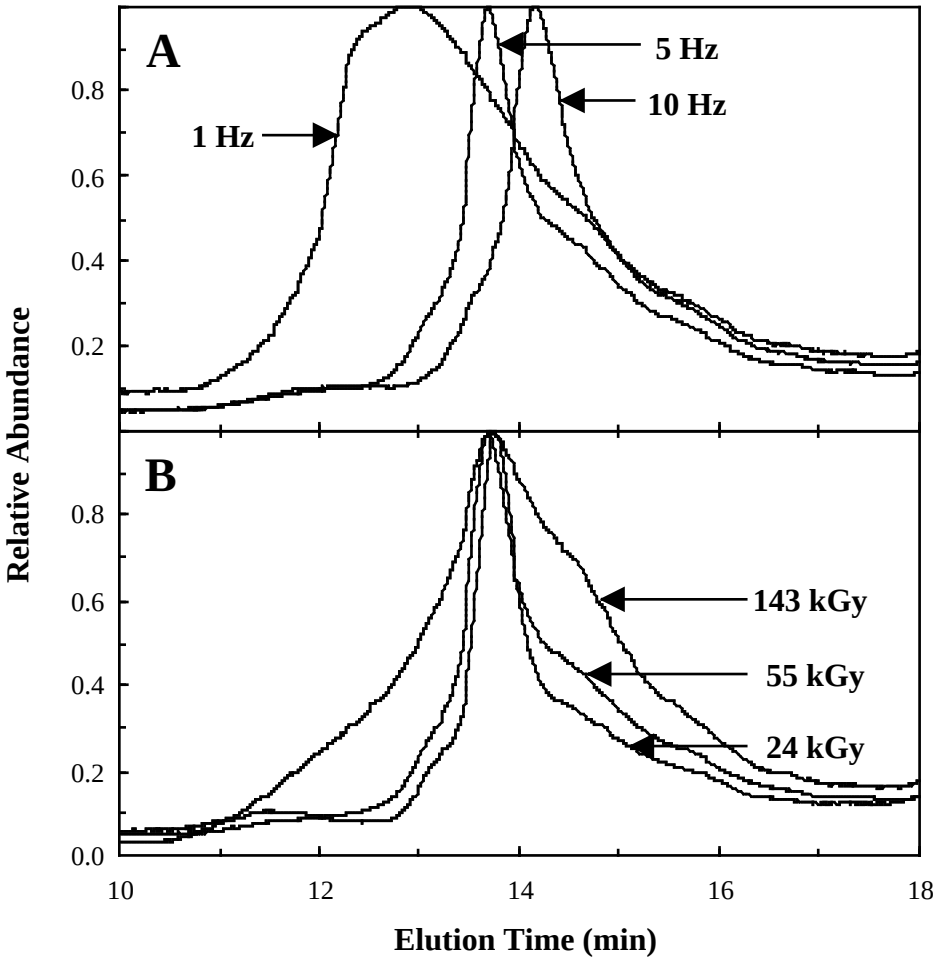

Figure 4.11. GPC traces for PMMA produced via pulsed irradiation with the van de Graaff electron accelerator under various irradiation conditions; (**A**) pulse frequency effect for identical accumulated doses of 55 kGy, (**B**) accumulated dose effect for 5 Hz pulsed irradiation.

Illustrated in part B of figure 4.11 is the effect of increasing the total dose on the shape of the molecular mass distribution for a fixed pulse repetition rate of 5 Hz. The slight variation in the shape of the elution profiles observed between 24 and 55 kGy, corresponding to monomer conversions of 4.21% and 10.70% respectively, can be attributed to the occurrence of chain-scission and macromolecular radical formation. At 143 kGy, corresponding to 34.39% conversion, higher molecular mass polymer also begins to be formed which indicates that the consequences of the gel effect must also be taken into account.

4.4. Theories Related to the Gel Effect

The bulk polymerization of several monomers (*e.g.* MMA and styrene) is accompanied by an abrupt increase in the rate of polymerization and lifetime of the kinetic chain at intermediate

extents of conversion. This leads to a rise in reaction temperature with potentially disastrous effects. Control of this autoacceleration of the polymerization rate is imperative not only for safety reasons but also for optimizing the properties of the polymer product.

The earliest report in the literature in regard to the autoacceleration of MMA polymerization was given by Norrish and Brookman in 1939[19]. Since that time various hypotheses have been proposed to explain the origin this effect[20,21,4,22]. Early experiments conducted under isothermal conditions demonstrated the importance of increasing bulk viscosity for the onset of autoacceleration[23]. An increase in viscosity could affect a decrease in the rate constant of termination which would lead to an increase in the free radical lifetime and the molecular mass of the polymer formed[24]. This sensitivity of the rate constant of termination to viscosity, even in solvents of low viscosity (*i.e.* less than 4×10^{-4} Pa s), was verified by both non-stationary phase and steady-state kinetic experiments on MMA[25,26]. Later to be known as the Norrish-Smith[19], Trommsdorff[14] or gel[15] effect, the focus of ensuing research was to develop an interpretation of this autoacceleration based upon molecular dynamics.

The reaction between two polymeric species at low concentration can be described by a three-step process (figure 1.13 in chapter one)[27]. The first step involves diffusion of the reacting polymer chains toward each other to form a contact pair, a process which is determined by the diffusion constants of the molecules in solution. The next step involves movement of the reactive segments of the polymers to within a minimum distance of each other as defined by a reaction volume. The rate of this step is determined by the flexibility of the chains and the micro-viscosity of the medium. The third step involves chemical reaction. For many chemical reactions in typical solvents the last step is the slowest due to large activation energies. For the bimolecular reaction between two polymeric free radicals however, the first and second steps can be slower and therefore rate determining.

In order to establish a better understanding of the gel effect, effort was directed at connecting the onset of the decrease in the termination rate constant with the onset of a change in a specific property of the polymerizing system. Two hypotheses have received popularity among researchers; one based upon the formation of a physical network of macromolecules due to polymer entanglements and the other based upon the polymerizing system reaching a critical free volume value. Both are discussed below.

4.4.1. The Entanglement Hypothesis

The rheological behavior of concentrated polymer solutions (*i.e.* those characterized by viscoelasticity) is characterized by the existence of physical entanglements. The presence of polymer entanglements is attributed to the compliance of a rheological property to the following empirical equation[28].

$$K_{cr} = \overline{X}_{n,cr}^{\alpha}\varphi_{cr} \qquad (4.32)$$

In 4.32, $\overline{X}_{n,cr}$ and φ_{cr} are critical values for the number-average degree of polymerization and the volume fraction of a polymer in solution respectively. K_{cr} and α are constants specific to a given polymer-solvent pair.

Several researchers proposed that the rate of bimolecular termination during free radical polymerization would be severely retarded by the formation of entanglements between polymer chains[29,30]. It is argued that if such entanglements exist which hinder the center-of-mass diffusion of macromolecular free radicals, an increase in the concentration of free radical species will occur and consequently an increase in the polymerization rate and polymer molecular mass will be observed. Using values of K_{cr} and α for MMA and PMMA[31], the relation given in equation 4.32 was found to hold well for determining the onset of the gel effect in the polymerization of MMA for various values of $\overline{X}_{n,cr}$ and φ_{cr}, therefore providing reasonable support for the entanglement hypothesis[30,21].

Despite some successes in modeling monomer conversion and polymer molecular mass[4], the entanglement hypothesis fails to explain certain experimental results. In particular, the gel effect can be observed in polymerizations in which the existence of polymer entanglements is prevented by the use of suitable concentrations of initiator and chain-transfer agents.[32].

Another explanation for the onset of the gel effect closely related to the entanglement theory has been proposed[33,34] which takes into account the chain-length dependence of the termination rate constant[9]. In this hypothesis the termination reaction at intermediate conversion is dominated by short (*i.e.* mobile, non-entangled) chains reacting with long (*i.e.* non-mobile, entangled) chains. Therefore the gel effect is related to a depletion of short chains in the system. Again, this theory cannot explain the observation of the gel effect under conditions where polymer entanglements are absent.

4.4.2. The Free-Volume Hypothesis

Free volume can be viewed as the space in a material which is not occupied by the van der Waals volumes of the constituent molecules. As a polymeric material is heated the free volume increases linearly above and below the glass transition temperature due to increased random motion of the molecules which leads to an expansion of the material. Amorphous polymeric materials consist of chains containing bends, kinks and chain ends which results in molecular packing which is less efficient, *i.e.* with more free volume, than that in a molecular crystal. Alternatively, polymeric materials consist of long molecular chains which inherently have a restricted mobility and less free volume than that in low molecular mass liquids. Free volume and other characteristics of polymeric materials such as cross-links and molecular mass result in the unique properties of polymeric materials (*e.g.* viscoelasticity, rubber-like elasticity and the melt and glass transition

temperatures).

The essential idea behind the free volume explanation for the gel effect is that the restricted mobility associated with the decrease in free volume as monomer is converted into polymer accounts for the observed decrease in the termination rate constant[35]. It is certainly true that temperature effects, which can be directly related to free volume, have an influence on the gel effect. Further support for the free volume hypothesis was provided by experiments conducted under conditions so as to produce only small molecular mass polymer. The experimental evidence suggests that the gel effect readily occurs even in the absence of chain entanglements[32].

Free volume has been successful as a basis for modeling the gel effect in that it adequately handles effects of temperature on the termination reaction[36,37]. However, all models based upon free volume-related transport properties involve at least one empirical parameter[38] which makes it possible to "fit" experimental data. Furthermore, additional molecular-level insight into the causes of the gel effect is required in order to explain other factors not predicted by free volume, *i.e.* the effects of chain transfer and solvent quality on termination[36]. Finally, free volume is a model (albeit a remarkably successful model[39]) designed to describe transport and/or frictional properties in polymer systems. Other models could be proposed to describe these same properties and therefore it could be argued that any such model could be used to explain the gel effect.

4.4.3. Additional Factors Related to the Gel Effect

Unfortunately, many publications in the literature addressing the gel effect in MMA polymerization cannot be compared with one another due to the difficulty in ascertaining the precise experimental conditions. In particular, due to the exothermic nature of MMA polymerization, it is questionable that many experiments said to be conducted under isothermal conditions were indeed carried out in such a manner[40,8].

Another complication related to the gel effect present in most kinetic studies prior to the 1990's was the assumption that the initiator efficiency during the free radical polymerization of MMA remains constant throughout the entire course of the reaction[41]. This is certainly not so for most polymerizing systems conducted in the bulk[8]. Experiments have shown that the changes in the efficiency of initiation at late stages of polymerization when using photo- or thermal initiators is strongly dependent upon the size of the initiator[3]. This is due to what has earlier been termed the "cage effect"[42], which in the case of polymerization via ionizing radiation would be less pronounced.

Yet another complication which received little consideration in early studies is the roll of reaction diffusion in the termination reaction[16], a mode of termination which is expected to be important at high conversion. Furthermore, an understanding about the roll of solvent on the gel effect[23] remains to be fully developed. MMA is actually a poor solvent of the polymer. This leads

to the formation of contracted polymer globules which are mutually attractive[43]. These polymer globules can aggregate leading to phase separation in which the system consists of monomer and polymer-rich regions. The extent to which such a phase separation will affect the kinetics of MMA polymerization is to this date not fully understood.

References

(1) Coote, M. L.; Zammit, M. D.; Davis, T. P. *Trends Polym. Sci.* **1996**, *4*, 189.

(2) van Herk, A. M. *Macromol. Theory Simul.* **2000**, *9*, 433.

(3) Achilias, D.; Kiparissides, C. *Macromolecules* **1992**, *25*, 3739.

(4) Dionisio, J.; O'Driscoll, K. *J. Polym. Sci., Polym. Chem. Ed.* **1980**, *18*, 241.

(5) Hoppe, S.; Renken, A. *Polym. React. Eng.* **1998**, *6*, 1.

(6) Sack, R.; Schulz, G. V.; Meyerhoff, G. *Macromolecules* **1988**, *21*, 3345.

(7) Clay, P.; Gilbert, R. *Macromolecules* **1995**, *28*, 552.

(8) O'Neil, G. A.; Torkelson, J. M. *Trends Polym. Sci.* **1997**, *5*, 349.

(9) de Kock, J. Chain-Length Dependent Bimolecular Termination in Free-Radical Polymerization, Technische Universiteit Eindhoven, 1999.

(10) Chapiro, A. *Radiation Chemistry of Polymer Systems*; Interscience Publishers: New York, 1962.

(11) van Herk, A. M. *J. Macromol. Sci. Rev. Macromol. Chem. Phys.* **1997**, *C37*, 633.

(12) Bamford, C.; Eastmon, G.; Wittle, D. *Polymer* **1969**, *10*, 771.

(13) Krongauz, V.; Bagdasaryan, K. 1st International Conference on Radioisotopes in Scientific Research, 1958.

(14) Trommsdorff, V. E.; Köhle, H.; Lagally, P. *P. Makromol. Chem.* **1947**, *1*, 169.

(15) von Schulz, G. V.; Harborth, G. *Macromol. Chemie* **1947**, *1*, 106.

(16) Anseth, K. S.; Decker, C.; Bowman, C. N. *Macromolecules* **1995**, *28*, 4040.

(17) Buback, M.; Huckestein, B.; Russell, G. *Macromol. Chem. Phys.* **1994**, *195*, 539.

(18) Olaj, O. F.; Bitai, I.; Hinkelmann, F. *Makromol. Chem.* **1987**, *188*, 1689.

(19) Norrish, R. G. W.; Brookman, E. F. *Proc. Royal Soc. A* **1939**, *171*, 147.

(20) Turner, D. T. *Macromolecules* **1977**, *10*, 221.

(21) Lachinov, M. B.; Simonian, R. A.; Beorgieva, T. G.; Zubov, V. P.; Kabanov, V. A. *J. Polymer Sci. Polymer Chem. Ed.* **1979**, *17*, 613.

(22) Tulig, T. J.; Tirrell, M. *Macromolecules* **1982**, *12*, 459.

(23) Norrish, R. G. W.; Smith, R. R. *Nature* **1942**, *150*, 336.

(24) Gee, G. *Trans. Faraday Soc.* **1939**, *35*, 1086.

(25) Benson, S. W.; North, A. M. *J. Am. Chem. Soc.* **1959**, *81*, 1339.

(26) Hayden, P.; Melville, H. *J. Appl. Polym. Sci.* **1960**, *43*, 201.

(27) North, A. M.; Reed, G. A. *Trans. Faraday Soc.* **1961**, *57*, 859.

(28) Ward, I. M.; Hadley, D. W. *An Introduction to the Mechanical Properties of Solid Polymers*; John Wiley & Sons Ltd: Chichester, 1928.

(29) Kabanov, V. A. *J. Polym. Sci. Polym. Symp.* **1975**, *50*, 71.

(30) Cardenas, J. N.; O'Driscoll, K. F. *J. Polym. Sci. Polym. Chem.* **1976**, *14*, 883.

(31) Ryabov, A. V.; Emelyanov, D. N.; Checmodeeva, J. V.; Roslyacova, V. A.; Chabalina, N. A. *Vysokomol. Soedin.* **1975**, *A17*, 1337.

(32) O'Neil, G. A.; Wisnudel, M. B.; Torkelson, J. M. *Macromolecules* **1996**, *29*, 7477.

(33) O'Shaughnessy, B. *Macromolecules* **1994**, *27*, 3875.

(34) Russell, G. T.; Gilbert, R. G.; Napper, D. H. *Macromolecules* **1993**, 3538.

(35) Balke, S. T.; Hamielec, A. E. *J. Appl. Polym. Sci.* **1973**, *17*, 905.

(36) O'Neil, G. A.; Wisnudel, M. B.; Torkelson, J. M. *Macromolecules* **1998**, *31*, 4537.

(37) Tefera, N.; Weickert, G.; Westerterp, K. R. *J. Appl. Polym. Sci.* **1997**, *63*, 1649.

(38) Achilias, D.; Kiparissides, C. *J. Appl. Polym. Sci.* **1988**, *35*, 1303.

(39) Williams, M. L.; Landel, R. F.; Ferry, J. D. *J. Am. Chem. Soc.* **1955**, *77*, 3701.

(40) Zhu, S.; Hamielec, A. E. *Polymer* **1991**, *32*, 3021.

(41) Russel, G. T.; Gilbert, R. G.; Napper, D. H. *Macromolecules* **1988**, *21*, 2141.

(42) North, A. M. *The Collision Theory of Chemical Reactions in Liquids*; Whiley: New York, 1964.

(43) Allegra, G.; Ganazzoli, F.; Raos. *Trends Polym. Sci.* **1996**, *4*, 293.

Chapter Five

Monitoring the Radiation-Induced Bulk Polymerisation of Methyl Methacrylate with *N*-(1-pyrene)maleimide

5.1. Introduction

Since the early work of Loutfy (1981, 1983 and 1986), several different classes of fluorescent probes have been developed for monitoring the progress of polymerisations; molecular rotors, excimer-forming probes, intramolecular charge transfer probes and reactive probe labels. The history of this development has been presented elsewhere (Miller *et al.*, 1994; Strehmel *et al.*, 1999).

Molecular rotor probes display dual fluorescence correlated to the initial locally excited state and the twisted (*i.e.* rotated) charge transfer state. Increasing viscosity of a polymerising matrix impedes the rotation and consequently increases the relative contribution of local fluorescence.

Molecular rotor probes are only sensitive in the very late stage of the polymerisation process. Nevertheless, molecular rotors have been frequently used for monitoring several polymerisation and copolymerisation systems (Rettig, 1986; Paczkowski and Neckers, 1991).

Excimer-forming probes make up another class. The emissive signal for these probes is dependent upon the viscosity of the matrix. Two subclasses can be distinguished among the excimer-forming probes. The difference between the two is the mechanism by which excimer fluorescence occurs, inter- or intramolecularly. Valdes-Aguilera *et al.* (1990) demonstrated how intermolecular excimer formation could be used to follow polymerisations. On the other hand, Stroeks *et al.* (1988) demonstrated the potential of intramolecular excimer formation for monitoring the course of polymerisations. The parameter of interest for this probe class is the ratio of monomer to excimer fluorescence intensities. As the viscosity of the system increases, the diffusion coefficient of the fluorophores decreases resulting in a decrease in the relative amount of excimer formation. Excimer-forming probes can be sensitive in the early stage of polymerisation as well as during vitrification.

Intramolecular charge transfer (ICT) molecules make up a class of probes which monitor changes in the dielectric properties of the medium. With these probes, the wavelength of maximum emission is monitored versus conversion (Ramesdonk *et al.*, 1987; Jager *et al.*, 1995). In the excited state ICT probes undergo partial or complete electron transfer from a donating to an accepting group of the molecule. Solvatochromism is observed due to stabilization of the charge transfer state by reorientation of molecular dipoles around the positive and negative charges of the probe. With increasing viscosity of the medium, the extent of such dipolar interactions will decrease and consequently the emission becomes blue-shifted. The response of an ICT probe in a polymerising medium is therefore mainly to changes in the dielectric relaxation or polarity of the medium.

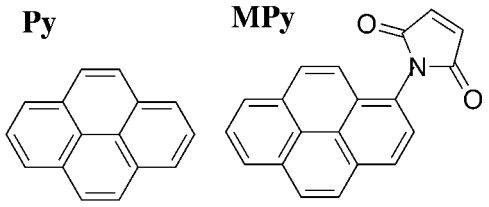

Figure 5.1. Structures of the probe molecules used in the present work; pyrene (Py) and N-(1-pyrene)maleimide (MPy).

Another class of fluorescent probes to be mentioned is the reactive probe label. These probes are incorporated into polymer chains via copolymerisation. The benefit achieved with these probes is that interpretation of the emission spectrum is not complicated by the uncertainty associated with not knowing whether the probe is preferentially concentrated in monomer- or polymer-rich regions

of the system. This technique of chemically incorporating probe molecules into polymer chains has been applied by Paczkowski and Neckers (1991) to ICT probes. A more recent development among the reactive probe labels is the use of molecules for which the fluorescence intensity increases when they are incorporated into growing chains. Miller *et al.* (1994) used intramolecular quenching in the design of ethyl (2-fluorenyl)methacrylate (FLEMA), a reactive probe label which is only partially quenched in the nonreacted state by an α,β-unsaturated ester group. Sensitivity throughout the entire course of MMA polymerisation was shown. In the early stage of polymerisation where molecular rotors are notoriously insensitive, FLEMA exhibited a sensitivity (*ca* 50% increase in the fluorescence intensity) comparable to the excimer-forming probe 1,3-*bis*(1-pyrene)propane (BPP). In the autoacceleration region, the fluorescence intensity of FLEMA increases by nearly two orders of magnitude. Warman *et al.* (1997) on the other hand demonstrated the use of fluorogenic maleimido probes for which the fluorescence is completely quenched in the nonincorporated state.

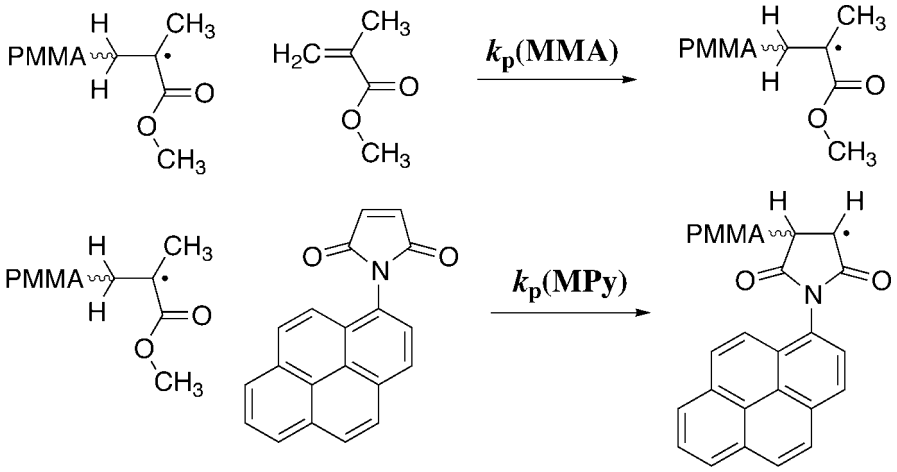

Figure 5.2. Propagation reactions: upper, homopolymerization of MMA; lower, incorporation of MPy producing the fluorescent succinimido derivative of MPy (SPy).

The work presented in this paper pertains to the reactive probe label *N*-(1-pyrene)maleimide (MPy; structure given in figure 5.1). It will be shown that the sensitivity of this fluorogenic probe is very high in the early stage of the polymerisation of MMA. As with FLEMA, the vitrification point of polymerisation is also observable with MPy. In addition, this article describes an approach by which the rate of incorporation of MPy relative to that of MMA (*i.e.* the ratio between the propagation rate constants given in figure 5.2) was determined from fluorescence and monomer conversion data.

5.2. Experimental

Synthesis grade methyl methacrylate monomer (MMA), purchased from Merck, was distilled at atmospheric pressure and 100-101 ºC immediately prior use. The fluorescent probes *N*-(1-pyrene)maleimide (MPy) and Pyrene (Py) were purchased from Molecular Probes Europe BV and Fluka Chemika respectively. They were used as obtained with no further purification.

Optical absorption spectra were measured with a Perkin Elmer Lambda 40 UV/VIS Spectrophotometer. The optical densities used at 337 nm, OD_{337}, were within the range of 0.1 to 2.0 corresponding to probe concentrations of *ca* 2 and 50 μM respectively. Fluorescence spectra and quantum yields were determined with a Photon Technology International QuantaMaster model QM-1. *In situ* fluorescence spectra were obtained with an experimental set-up described previously by Warman *et al.* (1999).

Except where mentioned otherwise, polymerisation reactions were performed inside of 1 cm square quartz fluorescence cuvettes sealed with a Teflon stopper and parafilm tape after deaeration by purging the monomer or monomer solutions with argon gas for 20 minutes. The concentrations of the fluorophores used were below those for which excimer fluorescence from pyrene could be detected. All polymerisations were carried out in the chamber of a Gammacell 200 Cobalt-60 irradiator from Atomic Energy of Canada, Ltd. The dose rate of 0.76 kGy/hr was determined using Fricke dosimetry.

Measurement of the monomer conversion upon polymerisation of MMA, Δ[MMA], was accomplished by the use of standard 20 ml scintillation vials into which was administered a known mass (*ca* 3 grams) of purified and degassed MMA. All manipulations with the monomer were carried out in a glove bag filled with nitrogen. Each sample was tightly closed and sealed with parafilm prior to extraction from the glove bag and subsequent polymerisation in the Co-60 Gammacell irradiation chamber. After an allotted time at 30 ºC, the samples were removed from the source and immediately opened to atmospheric oxygen, hence rapidly terminating the polymerisation. The mass of poly(methyl methacrylate), PMMA, formed was determined by residual monomer evaporation under reduced pressure (*ca* 10 mm Hg) at room temperature.

5.3. Results and Discussion

In order to correlate the fluorescence intensity of MPy to Δ[MMA], it is necessary to determine the relative rate of MPy copolymerisation to that of the MMA. The ideal situation is where both monomers exhibit identical reactivities to the propagating chain end. The following work will show that this condition is almost met in the MMA/MPy copolymerisation system.

In figure 5.3, the results for the monomer conversions for both MMA alone and an MMA solution of MPy are presented. MPy was introduced in order to determine if it acted as an inhibitor or retarder of the polymerisation process. The results in figure 5.3 show no evidence of such a complication. The rate of monomer conversion, R_p(MMA), in the early linear stage of the reaction

(*i.e.* below 3.5 kGy) was determined to be 1.4 x 10^{-4} M/sec (0.65 M/kGy). This corresponds to a G value for polymerisation of 6800 $(100\ eV)^{-1}$. Above 3.5 kGy the rate of polymerisation autoaccelerates reaching a maximum at *ca* 4.5 kGy; the so-called Trommsdorff effect (Trommsdorff *et al.*, 1947).

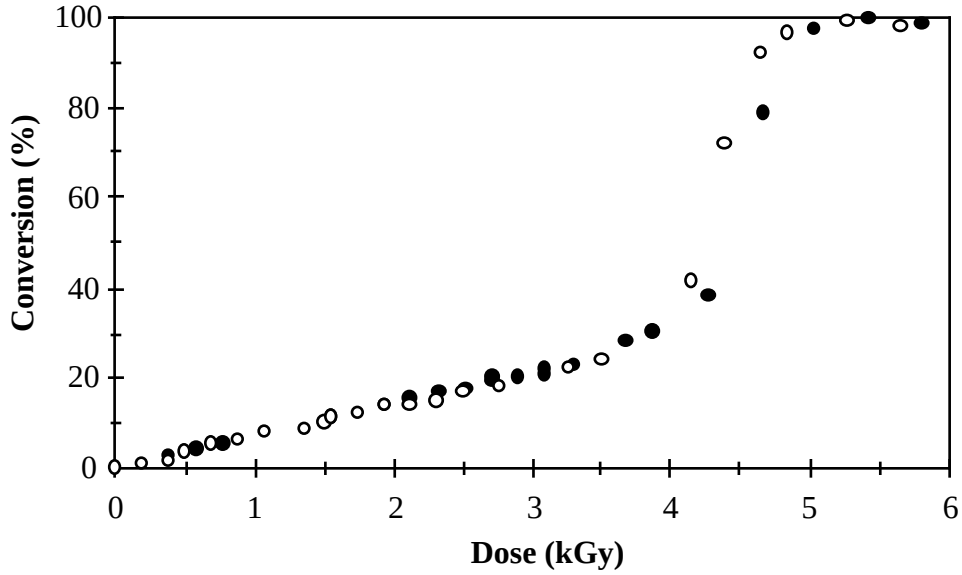

Figure 5.3. Conversion of MMA to PMMA versus dose of γ-radiation: filled circles, pure MMA; open circles, MMA + 50 mM MPy.

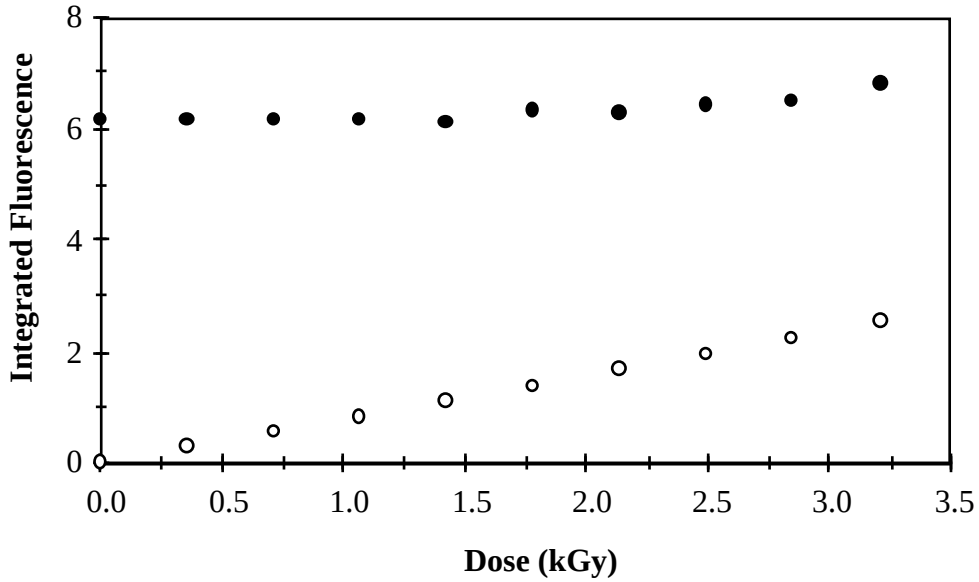

Figure 5.4. Fluorescence intensities in MMA versus dose of γ-radiation: filled circles, Py; open circles, MPy.

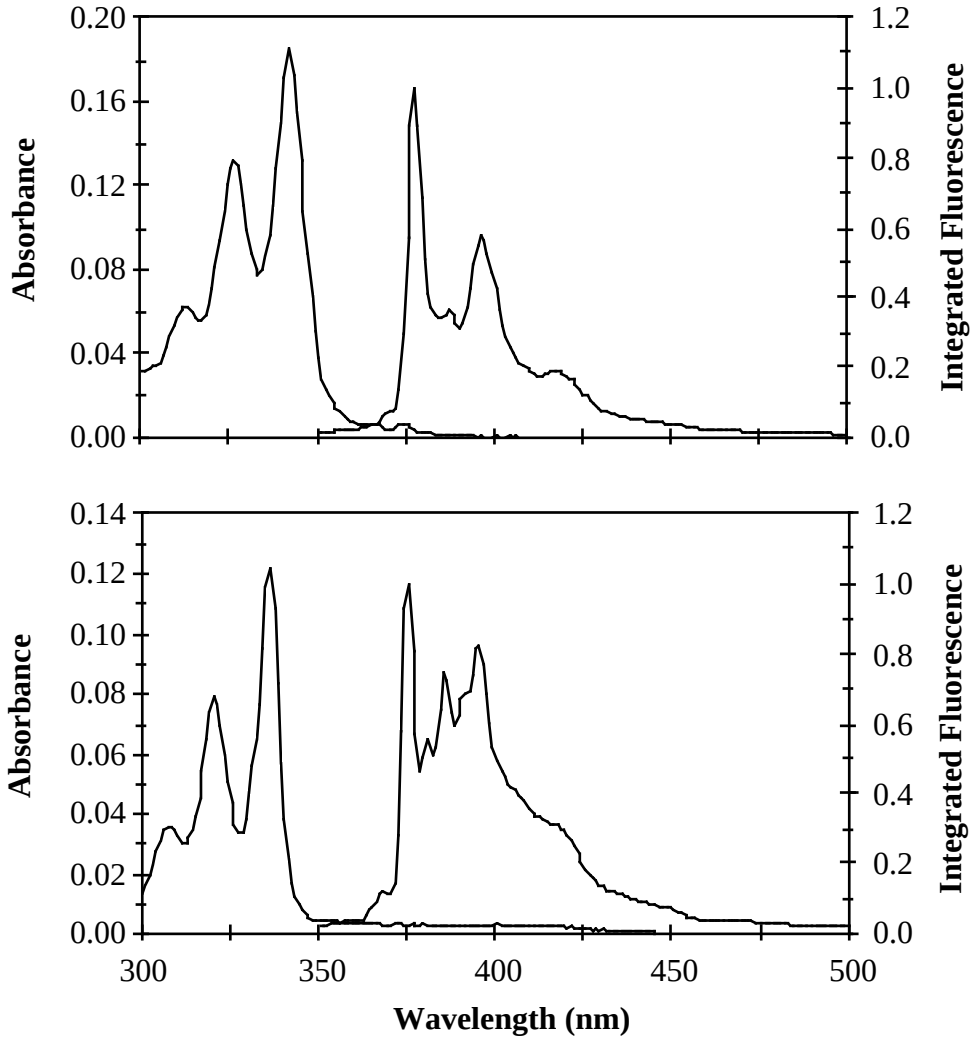

Figure 5.5. Absorption and emission spectra of sample solutions; upper, SPy-PMMA in MMA; lower, Py and PMMA in MMA.

The fluorescence measurements which follow are for samples which have been limited to irradiation doses below 3.5 kGy. At higher doses the expensive fluorescence cuvettes employed in the experiments would inevitably be lost due to vitrification of the sample. Pyrene, Py, was chosen as a reference fluorophore which has a constant fluorescence intensity throughout the entire polymerisation process (see figure 5.4). For comparative purposes, the ratio of the quantum efficiencies of fluorescence for both fluorophores is required. Since only the polymerised succinimido derivative of MPy, SPy, is fluorescent (see figure 5.2), SPy-labelled PMMA was prepared by the polymerisation of an MMA solution of MPy (OD_{337} of *ca* 2). The labelled PMMA formed after an irradiation of 3.5 kGy was isolated by precipitation with methanol. After drying under vacuum, the SPy-labelled PMMA was dissolved in MMA to yield an OD_{337} of *ca* 0.10.

Unlabelled PMMA was added to the pyrene/MMA sample in order to yield the same ratio of PMMA to MMA for both sample solutions. The optical densities of both fluorophore solutions at 337 nm were then accurately determined. Figure 5.5 provides the absorption and fluorescence spectra for both Py and SPy-PMMA sample solutions. Equation 5.1 was used in the calculation of the ratio of the fluorescence efficiencies, ϕ.

$$\frac{\phi_{SPy}}{\phi_{Py}} = \frac{(1 - 10^{-A_{Py}})I_{SPy}}{(1 - 10^{-A_{SPy}})I_{Py}} \tag{5.1}$$

Optical densities of the sample solutions are represented by A and the integrated fluorescence intensities across the entire emission band (350-550 nm) are represented by I. The refractive indices of both solutions were assumed to be identical. The average ratio and standard deviation for the fluorescence efficiencies of SPy to Py was determined from 11 measurements to be 1.37 ± 0.09. The value of ϕ_{SPy}/ϕ_{py} was found to be constant for irradiations of the solutions up to 3.5 kGy.

The next step in the experiment was to monitor the fluorescence intensity, I, of Py and MPy solutions in MMA (OD_{337} of 0.100) versus dose of gamma radiation. The I (integration 350-550 nm) versus dose data is given in figure 5.4. The conversion of MPy for a given dose, Δ[MPy], was calculated as shown in equation 5.2.

$$\Delta[MPy] = \frac{I_{SPy}\phi_{Py}}{I_{Py}\phi_{SPy}} \tag{5.2}$$

By comparison with the Δ[MMA] for an identical dose the ratio of propagation rate constants for the cross-over reaction in which an MMA radical chain-end reacts with MPy relative to the reaction with another MMA molecule could be determined by equation 5.3.

$$\frac{k_p(MPy)}{k_p(MMA)} = \frac{\Delta[MPy]}{\Delta[MMA]} F_c \tag{5.3}$$

The factor F_c in equation 5.3 is a correction factor which accounts for changes in the relative concentrations of MPy and MMA (see equation 5.4).

$$F_c = \frac{1 - \Delta[MMA]}{1 - \Delta[MPy]} \tag{5.4}$$

Table 5.1 summarises the results. The average value for the relative rate of MPy polymerisation to that of MMA is 1.38 with an estimated error of 11%. The error (± σ) was determined from the contributions from the individual errors in both the relative fluorescence efficiency of the fluorophores (± 6.6%) and the conversion of monomer (± 8.3%).

Table 5.1. Calculation of the ratio between the propagation rate constants *kp*(MPy) and *kp*(MMA).

Dose (kGy)	I_y^P	I_y^{SP}	Δ[MPy][a.]	Δ[MMA]	F_c	$\frac{kp(\text{MPy})}{kp(\text{MMA})}$[b.]
0.36	6.162	0.289	3.42	2.46	1.01	1.41
0.71	6.161	0.567	6.72	4.91	1.02	1.40
1.07	6.164	0.822	9.73	7.37	1.03	1.36
1.43	6.123	1.120	13.3	9.83	1.04	1.41
1.78	6.329	1.388	16.0	12.3	1.04	1.36
2.14	6.298	1.673	19.4	14.7	1.06	1.39
2.50	6.409	1.957	22.3	17.2	1.07	1.38
2.85	6.488	2.248	25.3	19.7	1.08	1.38
3.21	6.805	2.530	27.1	22.1	1.07	1.31

a. see equation 5.2
b. see equation 5.3

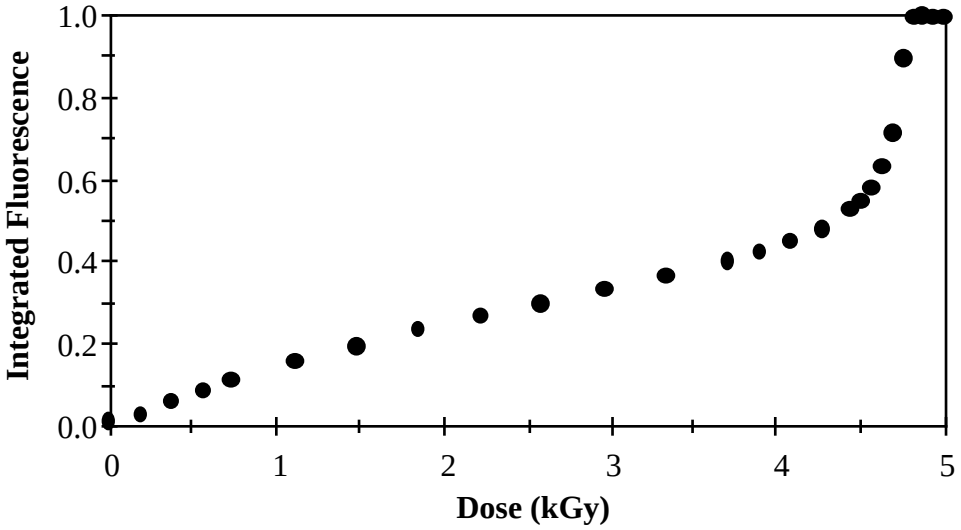

Figure 5.6. Integrated fluorescence intensity of an MPy solution in MMA versus dose of γ-radiation measured *in situ*.

As mentioned above, the present experiments were carried out in the accumulated dose region below that required for the Trommsdorff effect in order to prevent the breakage of the expensive, high quality fluorescence cells required for accurate quantum yield measurements. The dose range up to and above the occurrence of the Trommsdorff effect has been studied using lower optical quality, home-made quartz cuvettes and the *in situ* apparatus presented in a previous publication (Warman *et al.*, 1999). The results of these experiments are shown for an MPy solution

in MMA in Figure 5.6. As can be seen, an abrupt increase in the fluorescence occurs at the dose for which the MMA conversion also displays a pronounced increase (see Figure 5.3). The MPy probe is therefore capable of providing information in this extremely interesting region where autoacceleration occurs.

We are at present attempting to make a quantitative analysis of the data in the high dose region. This is complicated by the fact that the quantum yield of fluorescence is found to change by an as yet unknown amount. This will be the subject of a subsequent publication. The results however serve to illustrate how a fluorogenic probe molecule such as MPy can provide information about the degree of polymerisation from very low monomer conversions up to complete conversion.

5.4. Conclusion

It has been demonstrated that the reactive probe label MPy has a slightly larger reactivity than the monomer in the radical polymerisation of MMA. The ratio between propagation rate constants for the cross-over reaction in which an MMA radical chain-end reacts with MPy relative to the homopolymerisation reaction of MMA is found to be 1.38 ± 0.15.

The results indicate that MPy can be successfully employed to monitor the entire course of the bulk polymerisation of MMA. The sensitivity of this experimental technique is very high, especially in the early stage of the polymerisation, and can be adjusted by the choice of probe concentration or spectrofluorimeter settings. Future research will be directed towards better characterisation of probe response in the autoacceleration region of the polymerisation of MMA.

References

Jager, W. F., Volkers, A. A., Neckers, D. C., 1995. Solvatochromic Fluorescent Probes for Monitoring the Photopolymerization of Dimethacrylates. *Macromolecules* 28, 8153-8158.

Loutfy, R. O., 1981. High-Conversion Polymerization Fluorescence Probes. 1. Polymerization of Methyl Methacrylate. *Macromolecules* 14, 270-275.

Loutfy, R. O., 1983. Effect of Polystyrene Molecular Weight on the Fluorescence of Molecular Rotors. *Macromolecules* 16, 678-680.

Loutfy, R. O., 1986. Fluorescence Probes for Polymer Free-Volume. *Pure Appl. Chem.* 58, 1239-1248.

Miller, K. E., Burch, E. L., Lewis, F. D., Torkelson, J. M., 1994. In Situ Monitoring of Free-Radical Polymerization by Fluorescence Quenching of Fluorene and Reactive Derivatives. *J. Polym. Sci.: Part B: Polym. Phys.* 32,: 625-2735.

Paczkowski, J., Neckers, D. C., 1991. Twisted Intramolecular Charge-Transfer Phenomenon as a Quantitative Probe of Polymerization Kinetics. *Macromolecules* 24, 3013-3016.

Ramesdonk, H. J. van, Vos, M., Verhoeven, J. W., Möhlmann, G. R., Tissink, N. A., Meesen, A. W., 1987. Intramolecular charge-transfer fluorescence as a mobility probe in poly(methyl methacrylate). *Polymer* 28, 951-956.

Rettig, W. 1986. Charge Separation in Excited States of Decoupled Systems - TICT Compounds and Implications Regarding the Development of New Laser Dyes and Primary Processes of Vision and Photosynthesis. *Angew. Chem. Int. Ed. Engl.* 25:971-988.

Strehmel, B., Strehmel, V., Younes, M., 1999. Fluorescence Probes for Investigation of Epoxy Systems and Monitoring of Cross-linking Processes. *J. Polym. Sci.: Part B: Polym. Phys.* 37, 1367-1386.

Stroeks, A., Shmorhun, M., Jamieson, A. M., Simha, R., 1988. Cure monitoring of epoxy resins by excimer fluorescence. *Polymer* 29, 467-470.

Trommsdorff, E., Köhle, H., Lagally, P., 1947. Zur Polymerisation des Methacrylsäuremethylesters. *P. Makromol. Chem.* 1, 169-198.

Valdes-Aguilera, O., Pathak, C. P., Neckers, D. C., 1990. Pyrene as a Fluorescent Probe for Monitoring Polymerization Rates. *Macromolecules* 23, 689-692.

Warman, J. M., Abellon, R. D., Luthjens, L. H., Suykerbuyk, J. W. A., Verhey, H J., Verhoeven, J. W., 1999. In Situ Monitoring of the Radiation-Induced Polymerisation of Methyl Methacrylate using Fluorogenic Molecular Probes. *NIM B.* 151, 361-366.

Warman, J. M., Abellon, R. D., Verhey, H. J., Verhoeven, J. W., Hofstraat, J. W., 1997. Maleimido-fluoroprobe: A Dual-Purpose Fluorogenic Probe of Polymerization Dynamics. *J. Phys. Chem. B.* 101, 4913-4916.

Chapter Six

Synthesis and Characterization of a New Fluorogenic Probe Molecule *N*-(1-pyrene)methacrylamide for Monitoring Radiation-Induced Polymerization*

6.1. Introduction

Fluorogenic probes have demonstrated unprecedented sensitivity for monitoring polymerization reactions, especially at low to moderate monomer conversion[1-4]. The work of Miller *et al.*[4] demonstrated how the partial self-quenching of fluorene fluorescence in ethyl (2-fluorenyl)methacrylate (FLEMA; structure given in Fig. 6.1) ceases once the probe is incorporated into growing polymer chains. This supports the hypothesis that fluorescence quenching is caused by the enone (α,β-unsaturation to a carbonyl group) functionality. The fluorogenic behavior of

* This chapter has been published: M. S. Frahn, *et al*. *Nuc. Instr. Meth. Phys. Res. B* 185 (2001) 241-247.

completely non-fluorescent maleimido reactive probe labels such as *N*-(1-pyrene)maleimide (MPy; structure given in Fig. 6.1) was first studied by Warman *et al.*[1, 2]. In comparison to FLEMA, the enone functionality in MPy is more closely coupled to the fluorophore, *i.e.* the methylene spacer between fluorophore and quenching species is absent. This results in complete quenching of fluorescence in MPy, whereas only partial quenching is observed with FLEMA. A recent study by Frahn *et al.*[3] demonstrated that the propagation rate constant of MPy during the bulk polymerization of methyl methacrylate (MMA) is *ca.* 40% higher than that of the monomer itself.

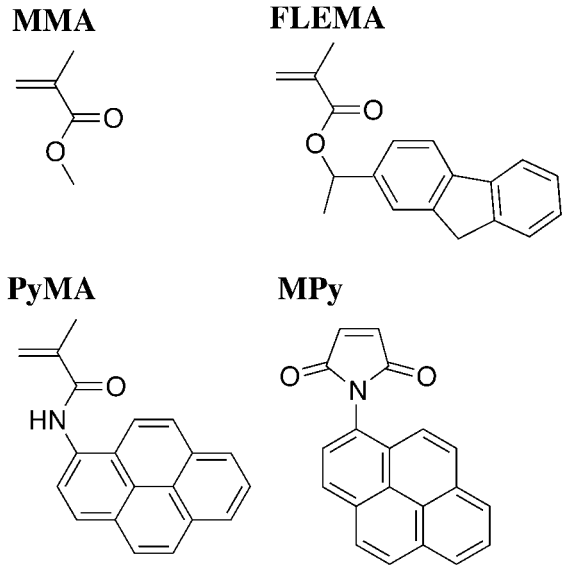

Figure 6.1. Chemical structures of the methyl methacrylate monomer (MMA) and probe molecules bearing reactive double bonds; ethyl (2-fluorenyl)methacrylate (FLEMA), *N*-(1-pyrene)methacrylamide (PyMA) and *N*-(1-pyrene)maleimide (MPy).

The successful application of fluorogenic probe molecules discussed above inspired the synthesis of the new probe *N*-(1-pyrene)methacrylamide (PyMA; structure provided in Fig. 6.1) reported in the present work. The fluorogenic character of the molecule is achieved via the α,β-unsaturated amide functionality. Once incorporated into growing polymer chains via copolymerization, the carbon-carbon double bond becomes saturated and fluorescence is observed. The probe PyMA was synthesized with the aim of achieving a closer reactivity to that of (meth)acrylate monomers in the propagation reaction combined with the fluorogenic behavior of maleimido probes. In addition to describing the synthesis of PyMA, this paper will outline the experimental procedure by which the reactivity of PyMA relative to that of MMA (*i.e.* the ratio between the propagation rate constants k_p(PyMA) and k_p(MMA) given in Fig. 6.2) was determined quantitatively at low conversion from fluorescence and monomer conversion data. Furthermore,

experiments are presented in which the *in situ* fluorescence from an MMA solution of PyMA is used to qualitatively monitor the entire course of MMA polymerization including the gel effect.

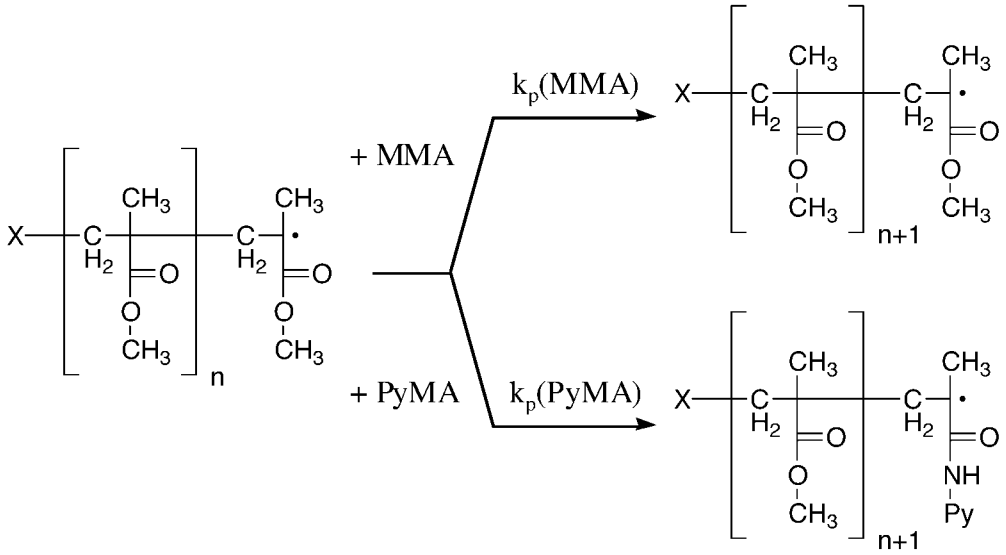

Figure 6.2. Competitive propagation reactions during the polymerization of MMA with a trace amount of the PyMA probe molecule present; homopropagation (kp(MMA)) and the crossover propagation reaction (kp(PyMA)).

6.2. Experimental

6.2.1. Reagents

The fluorogenic probe PyMA was synthesized from 1-aminopyrene and methacryloyl chloride purchased from Fluka Chemica and Aldrich respectively. All other reagents were purchased from Aldrich. Triethylamine was dried over 4 Å molecular sieve. Dichloromethane (CH_2Cl_2) was dried and purified by distillation from P_2O_5. Synthesis grade MMA, purchased from Merck, was distilled at atmospheric pressure and 100-101 ^oC immediately prior use. Pyrene (Py) was purchased from Fluka Chemika and used without any further purification.

6.2.2. Synthesis of *N*-(1-pyrene)methacrylamide

A solution of 1.00 g of 1-aminopyrene (4.60 mmol) in 20 mL of anhydrous CH_2Cl_2 was prepared, to which a second solution of 0.64 g of freshly distilled methacryloyl chloride (90% pure, 0.60 mL, 5.5 mmol) and 0.40 g triethylamine (0.42 mL, 5.5 mmol) in 5 mL CH_2Cl_2 was slowly added at ambient temperature. The yellow 1-aminopyrene solution became cloudy as

triethylammonium chloride precipitated from solution. The reaction mixture was shaken with 50 mL of 10% aq. hydrochloric acid and subsequently with an excess of distilled water. Next the mixture was filtered into a separatory funnel in order to collect the bottom CH_2Cl_2 layer. The solvent was removed by evaporation to yield 1.10 g of a pale yellow product. Recrystallization from toluene was performed twice resulting in a final yield of 0.51 g of almost colorless *N*-(1-pyrene)methacrylamide crystals with a 39% yield; m.p. = 173.5-175.5 ºC. ^{1}H NMR ($CDCl_3$, 400 MHz): 8.43 (d, *J* = 11.2 Hz, 1H), 8.18 (d, *J* = 10.3 Hz, 1H), 8.17 (d, *J* = 10.4 Hz, 1H), 8.15 (d, *J* = 10.4 Hz, 1H), 8.14_3 (d, *J* = 10.2 Hz, 1H), 8.13_9 (d, *J* = 11.2 Hz, 1H), 8.06 (d, *J* = 12.3 Hz, 1H), 8.01 (br s, 1H), 7.99 (t, *J* = 10.1 Hz, 1H), 7.97 (d, *J* = 12.3 Hz, 1H), 6.03 (s, 1H), 5.59 (s, 1H), 2.21 (s, 3H).

6.2.3. Spectroscopic Measurements

Optical absorption spectra were measured with a Perkin Elmer Lambda 40 UV/VIS Spectrophotometer. The optical densities measured at 337 nm, OD_{337}, were within the range of 0.2-2.0 corresponding to probe concentrations of *ca* 5 and 50 mM respectively. The concentrations of the fluorophores used were below those for which excimer fluorescence from pyrene could be detected. Fluorescence spectra and intensities were determined with a Photon Technology International QuantaMaster model QM-1 using an excitation wavelength of 337 nm. *In situ* fluorescence spectra were obtained with *ca* 1 second time resolution using an experimental set-up described previously by Warman *et al.* (1999)[2].

6.2.4. Polymerization Procedure

Except where mentioned otherwise, polymerization reactions were performed inside of 1 cm square quartz fluorescence cuvettes sealed with a Teflon stopper and Parafilm tape after deaeration by purging the monomer or monomer solutions with argon gas for 20 minutes. Low dose rate irradiations (*ca* 0.7 kGy/hr) were carried out with a cobalt-60 Gammacell 200 from Atomic Energy of Canada, Ltd. and high dose rate irradiations (*ca* 10 kGy/hr) were accomplished with an MDS Nordion cobalt-60 Gammacell 220 irradiator. The dose rates were accurately determined using Fricke dosimetry and corrected for natural decay.

6.2.5. Monomer Conversion Determinations

Measurement of the fractional monomer conversion, F_c(MMA), was accomplished by the use of standard 20 mL scintillation vials into which a known mass (*ca* 3 grams) of purified and degassed MMA was administered. All manipulations with the monomer were carried out in a glove

bag filled with nitrogen. Each sample was tightly closed and sealed with Parafilm tape prior to extraction from the glove bag and subsequent polymerization. After an allotted dose at 30 ºC, the samples were removed from the source and immediately opened to atmospheric oxygen, hence rapidly terminating polymerization. The conversion to polymer was determined gravimetrically after residual monomer evaporation under reduced pressure (*ca* 10 mm Hg) at room temperature.

6.3. Results and Discussion

The UV-visible absorption spectrum of PyMA is shown in Fig. 6.3. The spectrum is relatively unstructured compared with either unsubstituted pyrene or 1-aminopyrene. No fluorescence is observed from an MMA solution of PyMA. On γ-ray irradiation of the solution however fluorescence is induced and revealed by UV excitation at 337 nm, as shown in Fig. 6.3. The fluorescence spectrum of the copolymerized form of the probe molecule, denoted PPyMA, is highly structured and resembles that of unsubstituted pyrene and 1-aminopyrene.

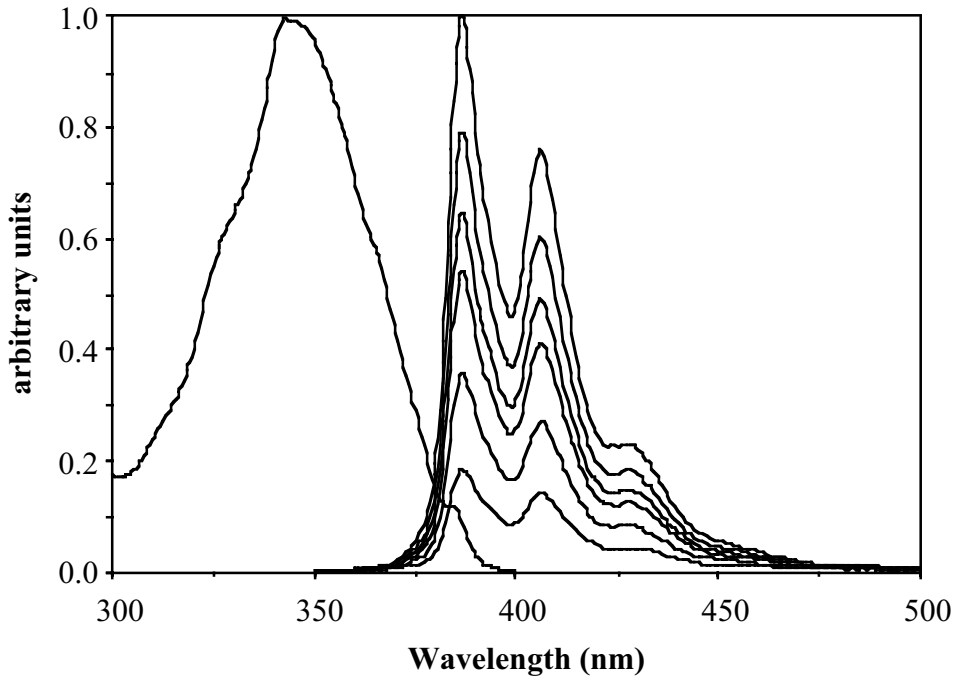

Fig. 6.3. Absorption spectrum of the fluorogenic probe molecule PyMA and the induced fluorescence spectra from PPyMA, the copolymerized derivative of PyMA, for accumulated doses of 0.34, 1.01, 1.69, 2.36, 3.03 and 3.71 kGy, at a dose rate of 0.7 kGy/hr.

In Fig. 6.4(A) the integrated fluorescence detected *in situ* is plotted as a function of the accumulated dose for two different dose rates of 0.68 and 9.8 kGy/hr. As can be seen the

fluorescence gradually increases close to linearly with increasing dose initially and then undergoes a sudden dramatic increase above approximately 4 kGy and 16 kGy for the low and high dose rate conditions respectively. This behavior resembles closely that of the dose dependence of the MMA conversion which is shown in Fig. 6.4(B). These results therefore serve to illustrate, at least qualitatively, the ability of PyMA to perform as an internal monitor of the progress of polymerization including the dramatic increase which occurs at the onset of the "gel" or "Trommsdorff" effect. The results are similar to those found previously for the probe molecule MPy[1-3, 5].

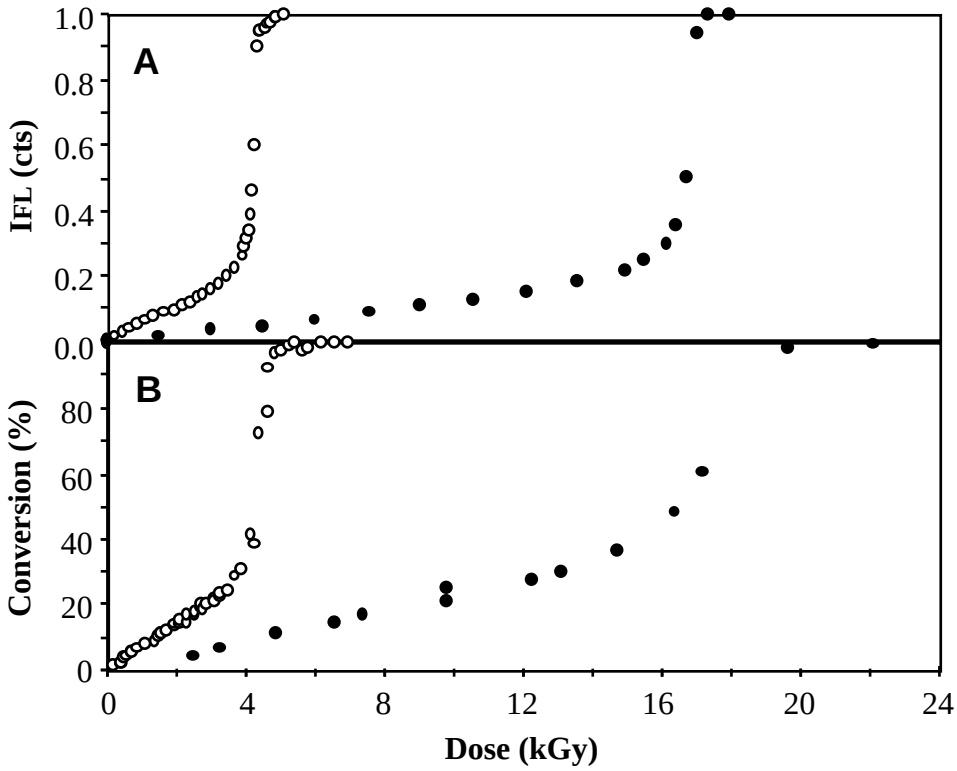

Fig. 6.4. (A) Normalized integrated fluorescence intensity versus dose of gamma radiation. (B) Monomer conversion versus dose of gamma radiation. Open circles correspond to irradiations at a dose rate of *ca* 0.7 kGy/hr and filled circles correspond to irradiations at *ca* 10 kGy/hr.

In order to quantitatively correlate the fluorescence intensity with the monomer conversion of MMA it is necessary to determine the propagation rate constant ratio for polymerization of PyMA and MMA, k_p(PyMA)/k_p(MMA). To achieve this we have carried out a procedure similar to that used previously for MPy[3].

This procedure entails obtaining a measurement of the actual PyMA conversion corresponding to a given dose. This is done by comparing the fluorescence of the irradiated PyMA solution in MMA, I_{FL}(PPyMA), with that of a solution containing unsubstituted pyrene, I_{FL}(Py),

having the same optical density at the excitation wavelength. The fractional conversion of PyMA, F_c(PyMA), can then be derived from the relationship,

$$F_c(PyMA) = \frac{I_{FL}(PPyMA) * \phi_{FL}(Py)}{I_{FL}(Py) * \phi_{FL}(PPyMA)} \tag{6.1}$$

In (6.1), ϕ_{FL}(Py) and ϕ_{FL}(PPyMA) are the fluorescence quantum efficiencies of pyrene and the polymerized form of PyMA respectively.

To determine the ratio of the quantum efficiencies, a sample of PPyMA-labeled PMMA was prepared by the polymerization of an OD_{337} 2 solution of PyMA in MMA at a dose rate of *ca* 0.7 kGy/hr. The accumulated dose was kept below that corresponding to the occurrence of the gel effect so that the medium remained fluid. The labeled polymer formed was isolated by precipitation with methanol followed by filtration and drying under vacuum. The polymer was then dissolved in MMA to yield a solution with an OD_{337} of *ca* 0.1. A solution of unsubstituted pyrene in MMA with an optical density close to 0.1 was also prepared. To this solution an amount of unlabelled PMMA prepared at the same dose rate as above was added in order to match the refractive index with that of the PPyMA-labeled PMMA sample solution. The optical densities of the solutions at 337 nm were then accurately determined and the fluorescence intensities after different irradiation doses at a dose rate of *ca* 0.7 kGy/hr were measured in the QuantaMaster fluorescence spectrophotometer. The ratio of the quantum yields was determined from the relationship,

$$\frac{\phi_{FL}(PPyMA)}{\phi_{FL}(Py)} = \frac{(1 - 10^{-OD(Py)})I_{FL}(PPyMA)}{(1 - 10^{-OD(PPyMA)})I_{FL}(Py)} \tag{6.2}$$

The average value and standard deviation from 11 measurements was determined to be 0.390 ± 0.008.

In order to accurately compare the fluorescence intensities at different total doses for irradiated solutions of Py and PyMA, high-quality, commercial fluorescence cuvettes were used rather than the disposable cuvettes used for the *in situ* measurements. The samples were removed from the cobalt source after a given accumulated dose and the fluorescence was measured using the QuantaMaster fluorimeter. To prevent breakage of the (expensive) cuvettes, these experiments were carried out only for doses below those corresponding to the gel-point. The dose dependencies of the fluorescence intensities found are presented in Fig. 6.5 and the values are listed in Table 6.1. The value of the PyMA conversion, derived from these data using relationship (6.1) and the quantum yield ratio given above, are listed in column 4 of Table 6.1. Values of the MMA conversion obtained within the same dose range are shown in Fig. 6.4(B). Interpolated values for the fractional conversion of MMA, F_c(MMA), at the same doses as used in the fluorescence measurements are listed in column 5 of Table 6.1.

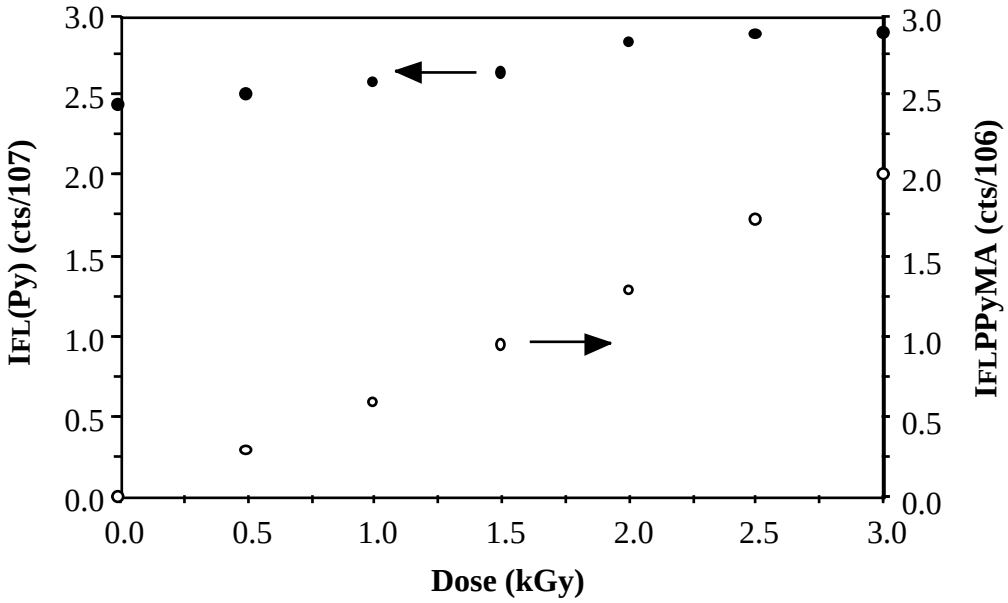

Fig. 6.5. Experimental dose dependencies of the fluorescence intensities found for Py and PyMA sample solutions for MMA polymerization at a dose rate of 0.7 kGy/hr.

Table 6.1. Experimental and calculated results for irradiation at a dose rate of 0.7 kGy/hr used to determine the ratio between the competitive propagation rate constants kp(PyMA) and kp(MMA).

Dose (kGy)	I_{FL} (Py)	I_{FL} (PPyMA)	F_c (PyMA)*	F_c (MMA)	$\frac{kp(PyMA)}{kp(MMA)}$
0.50	25.01	0.28	0.029	0.035	0.83
1.00	25.71	0.58	0.058	0.069	0.84
1.50	26.41	0.95	0.092	0.104	0.88
2.00	28.26	1.29	0.117	0.138	0.84
2.50	28.75	1.72	0.154	0.173	0.88
3.00	28.82	2.00	0.178	0.208	0.84

* Calculated result derived from equation 6.1.

We can now proceed to the derivation of the propagation rate constant ratio $k_p(PyMA)/k_p(MMA)$. The fact that the rate coefficients may differ depending on whether the propagating chain-end is an MMA- or a PyMA-derived free-radical is of no importance for the overall monomer consumption in the system of our study. Since the concentration of PyMA monomer units is orders of magnitude lower than MMA units, it is reasonable to assume that the propagating step involves exclusively an MMA derived chain-end radical, MMA·. The rate

equations describing the incorporation of MMA and PyMA into growing polymer chains are in this case given as,

$$R_p(MMA) = -\frac{d[MMA]}{dt} = k_p(MMA)[MMA\cdot][MMA] \tag{6.3}$$

$$R_p(PyMA) = -\frac{d[PyMA]}{dt} = k_p(PyMA)[MMA\cdot][PyMA] \tag{6.4}$$

Taking as a first approximation the radical concentration to be constant in the low conversion region as evidenced by the close-to-linear increase in conversion with time (dose), the following expressions can be derived for the conversion of MMA and PyMA at a given time of irradiation from (6.3) and (6.4).

$$\ln(1 - F_c(MMA)) = -k_p(MMA)[MMA\cdot]t \tag{6.5}$$

$$\ln(1 - F_c(PyMA)) = -k_p(PyMA)[MMA\cdot]t \tag{6.6}$$

The propagation rate coefficient ratio will then be given by

$$\frac{k_p(PyMA)}{k_p(MMA)} = \frac{\ln(1 - F_c(PyMA))}{\ln(1 - F_c(MMA))} \tag{6.7}$$

At very low conversions (6.7) reduces to

$$\frac{k_p(PyMA)}{k_p(MMA)} = \frac{F_c(PyMA)}{F_c(MMA)} \tag{6.8}$$

The ratios determined using (6.7) and the measured conversions given in Table 6.1 are listed in the last column of the Table. As can be seen the value is independent of conversion (total dose) and has an average value of 0.85 with an estimated error of 8.5% (± 0.07). The error (± σ) was determined from the contributions from the individual errors in both the relative fluorescence efficiency (± 2.1%) and the monomer conversion (± 8.3%). This is to be compared with a value of 1.38 ± 0.15 found previously for MPy[3]. The initial hope, that the methacrylate group of PyMA would result in a copolymerization ratio closer to unity than found for the maleimido functionality of MPy has therefore been realized.

A quantitative interpretation of the fluorescence yield data in the region of the gel effect is complicated by the fact that the quantum yield of fluorescence may change on vitrification of the solution due to the much greater rigidity of the matrix. We are at present carrying out experiments in an attempt to take such effects into account and this will be the subject of a future report.

6.4. Conclusion

We have found that the reactive probe label PyMA has a slightly lower reactivity than the monomer in the radical polymerization of MMA. The ratio between propagation rate constants for the cross-over reaction in which an MMA radical chain-end reacts with PyMA relative to the homopolymerization reaction of MMA is found to be 0.85 ± 0.07. The result may be explained by a smaller diffusion coefficient for the large PyMA molecule relative to that for MMA, assuming that the reactivity of an acrylamide functionality approximates that of the MMA methacrylate group.

Results indicate that the fluorogenic probe label PyMA can be successfully employed to qualitatively monitor the entire course of the bulk polymerization of MMA. The sensitivity of this experimental technique is very high, especially in the early stage of the polymerization where quantification of monomer conversion by comparison to probe fluorescence intensity is possible, and can be adjusted by the choice of probe concentration or spectrofluorimeter settings. Future research will be directed towards better characterization of probe response in the autoacceleration region of the polymerization of MMA.

References

[1] Warman, J. M., R. D. Abellon, H. J. Verhey, J. W. Verhoeven and J. W. Hofstraat, J. Phys. Chem. B. **101** (1997) 4913.

[2] Warman, J. M., R. D. Abellon, L. H. Luthjens, J. W. A. Suykerbuyk, H. J. Verhey and J. W. Verhoeven, Nuc. Instrum. and Methods in Phys. Research. **B 151** (1999) 361.

[3] Frahn, M. S., J. M. Warman, R. D. Abellon and L. H. Luthjens, Radiation Physics and Chemistry. **60** (2001) 433.

[4] Miller, K. E., E. L. Burch, F. D Lewis and J. M. Torkelson, J. Polymer Sci.: Part B: Polymer Phys. **32** (1994) 2625.

[5] Frahn, M. S., R. D. Abellon, L. H. Luthjens and J. M. Warman, Radiation Research; Proceedings of the 11th ICRR, Dublin 1999. **2** (2000) 86.

Chapter Seven

N-(2-anthracene)methacrylamide: A New Fluorogenic Probe Molecule for Monitoring *In Situ* the Radiation-Induced Polymerization of Methyl Methacrylate In Bulk and In Solution*

7.1. Introduction

Since the early investigations of Loutfy [1-3] into the use of fluorescent molecules for *in situ* monitoring of polymerization, continued research in this field has led to the development of several different types of fluorescent probes. Common to most of these probe types is sensitivity to the mobility and/or (micro-)viscosity of the molecular environment in which the probe molecules are located. This sensitivity can be achieved via a number of physical interactions; intramolecular reorientation (*e.g.* molecular rotors [1,4,5] and intramolecular excimer-forming probes [6,7]),

* This chapter has been submitted to *Polymer* in 2003 for publication.

diffusion-controlled interactions (*e.g.* intermolecular excimer-forming probes [8]), or solvent dipole stabilization of the probe's excited state (*e.g.* charge-transfer (CT) probes [9,10]). It is important to note that the physical origin of the sensitivity to the molecular environment for a given probe molecule is not necessarily determined by only one of the above mentioned interactions.

A new class of probe molecules which have been studied recently are the fluorogenic molecular probes [11-15]. Such molecules are completely non-fluorescent until they are incorporated, *i.e.* copolymerized, into growing polymer chains. This aspect, unique to the fluorogenic probes, provides unprecedented sensitivity for monitoring polymerization at the early stage of reaction. Furthermore, as is demonstrated in this paper, fluorogenic probe molecules can also be employed for monitoring solution polymerizations.

Our research group has devoted considerable effort to studying fluorogenic molecular probes. The molecular structures of some examples are provided in figure 7.1. The fluorogenic character of these molecules is achieved by the α,β-unsaturation relative to the carbonyl groups in the free radical-reactive moieties of the probes. For MPy the reactive moiety is a maleimide group, whereas for PyMA and AnMA it is a methacrylamide group. When copolymerized into growing polymer chains, the double bonds become saturated and consequently the molecule becomes fluorescent. With increasing conversion of monomer to polymer more probe molecules are converted into the fluorescent derivative resulting in a steadily increasing intensity of fluorescence. Furthermore, since the primary probe response is based upon a chemical change and not a change in the physical properties of the polymerizing medium, fluorogenic molecules can be used for sensitive monitoring of solution polymerizations which to the best of our knowledge is not possible with traditional fluorescent probes.

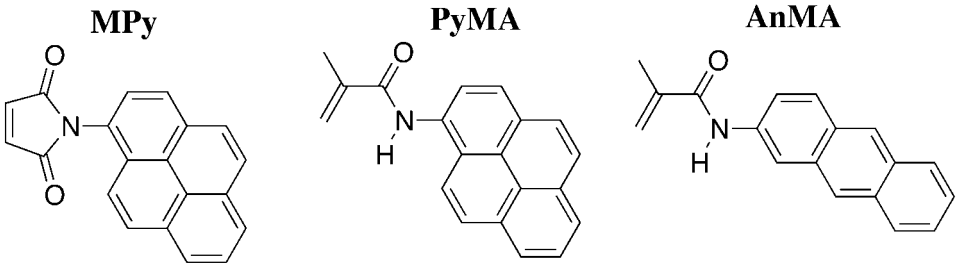

Figure 7.1 Molecular structures of the fluorogenic probes *N*-(1-pyrene)maleimide (MPy), *N*-(1-pyrene)methacrylamide (PyMA) and *N*-(2-anthracene)methacrylamide (AnMA).

An important parameter required for the quantitative monitoring of polymerization via fluorogenic probes is the relative rate at which such molecules are incorporated, *i.e.* copolymerized, in relation to the polymerizing monomer. Because the amount of probe used is considerably less

than that for typical copolymerization reactions, conventional techniques by which monomer reactivity ratios can be determined are impractical. We have previously reported a sensitive technique by which the reactivity of a probe molecule in relation to that of the monomer, *i.e.* the ratio between the propagation rate constants given in figure 7.2, could be determined from fluorescence experiments [15,14]. This technique has been repeated for the AnMA probe molecule and is discussed in the results section of this paper. Using this result in combination with considerations given to density changes and changes occurring in the probe molecule's fluorescence quantum efficiency during the course of MMA polymerization, quantitative monitoring of the entire course of MMA polymerization using AnMA is possible.

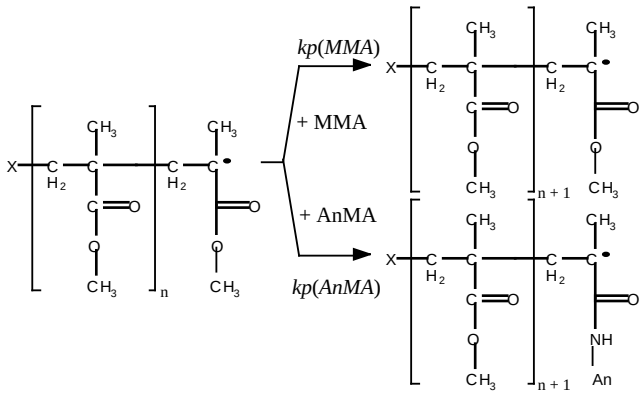

Figure 7.2 Competitive propagation reactions during the free radical polymerization of MMA with a trace amount of the AnMA probe molecule present.

We emphasize that the concentration of the probe molecules in the present experiments is only a few millimolar corresponding to less than one probe molecule per 1000 MMA molecules. The probability of propagation involving an AnMA radical end group with another AnMA molecule is therefore extremely small and can be neglected. The rate constant for the reaction of a radical AnMA end group with MMA would have to be very much smaller than that for a radical MMA end group with MMA in order to have an appreciable influence on the overall polymerization process. Evidence for the lack of a significant effect of the probe on overall MMA polymerization is the fact that the dose at which the gel effect occurs is identical to that found from measurements of the monomer conversion in the absence of the probe.

One of the main advantages in using the anthracene derivative instead of the previously used pyrene derivatives is the considerably shorter lifetime of the excited state of the anthracene moiety; *ca* 10 ns compared with *ca* 200 ns. Because of this, quenching of fluorescence by trace impurities such as oxygen is less of a problem.

7.2. Experimental Section

7.2.1. Materials

Methyl methacrylate (Merck Synthesis grade) was trap-to-trap distilled on a greaseless vacuum line at 100^0C to remove the hydroquinone stabilizer immediately prior to use. The synthesis of the fluorogenic probe AnMA was analogous to that fully described for the pyrene methacrylate derivative [15]. The freshly prepared AnMA was purified by re-crystallization from a 4:1 methylene chloride/hexane solvent mixture prior to use. Anthracene (Fluka HPLC >99%) and 9,10-diphenylanthracene (Molecular Probes HPLC >99%) were used as received. The benzene solvent, used in the MMA solution experiments, was obtained from Merck (UV spectroscopic grade) and was purified by distillation on a Fischer "Spaltrohr HMS500" spinning-band column.

7.2.2. Methods

Except when mentioned otherwise, sample cells were constructed in-house from Heraeus Suprasil quartz tubing. Deaeration of the samples was carried out by three consecutive freeze-pump-thaw cycles on a vacuum line or via purging with argon gas for 15 minutes prior sealing with a Teflon stopper and Parafilm tape.

Optical absorption spectra were measured using a Perkin Elmer Lambda 40 UV/VIS Spectrophotometer. Optical densities of the probe solutions were determined at 337 nm, the excitation wavelength used in fluorescence measurements.

Fluorescence spectra and quantum yields were obtained with a Photon Technology International QuantaMaster model QM-1 spectrometer. *In situ* fluorescence spectra were obtained using an experimental set-up described previously [12]. *In situ* fluorescence lifetime measurements were also obtained using an experimental flash-photolysis set-up described in a separate publication [16].

Low dose rate irradiations at *ca* 0.6 kGy/hr were carried out with a cobalt-60 Gammacell 200 irradiator from Atomic Energy of Canada, Ltd. High dose rate irradiations at *ca* 7 kGy/hr were accomplished with an MDS Nordion cobalt-60 Gammacell 220 irradiator. Dose rates were accurately determined by Fricke dosimetry [17] and corrected for the natural decay of the source.

Direct measurement of monomer conversion was accomplished by the use of standard 20 mL scintillation vials into which a known mass (*ca* 3 grams) of purified and degassed MMA was administered. All manipulations with the monomer were carried out in a glove bag filled with nitrogen. Each sample was tightly closed and sealed with Parafilm tape prior to extraction from the glove bag and subsequent polymerization. After an allotted dose, the samples were removed from the source and immediately opened to atmospheric oxygen, hence rapidly terminating

polymerization. The conversion to polymer was determined gravimetrically after residual monomer evaporation under reduced pressure (*ca* 10 mm Hg) at room temperature.

7.3. Results and Discussion

7.3.1. Anthracene Methacrylamide (*AnMA*)

The absorption spectrum of AnMA in MMA is shown in figure 7.3 along with the fluorescence spectrum of the copolymerized derivative of the probe. The AnMA probe molecule is non-fluorescent until the double bond of the methacrylamide group becomes saturated due to copolymerization into growing polymer chains. The vibrational structure in the absorption spectrum resembles that of anthracene with an additional long wavelength absorption peak due to the electronic coupling with the methacrylamide group. The fluorescence spectrum of the copolymerized derivative is similar to that of the anthracene chromophore alone but with less sharp vibrational structure.

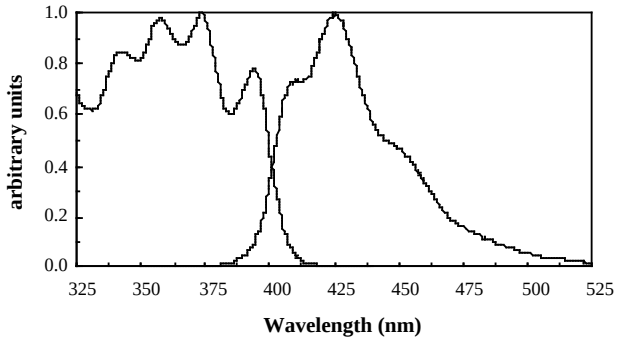

Figure 7.3 The absorption spectrum of AnMA in MMA and the fluorescence spectrum of the copolymerized derivative.

7.3.2. The Relative Reactivity of AnMA During MMA Polymerization

In order to be able to correlate the MMA monomer conversion to the fluorescence intensity observed from a polymerizing sample containing the AnMA probe molecule it is necessary to determine the relative reactivity of AnMA to that of MMA, *i.e.* $k_p(AnMA)/k_p(MMA)$ as shown in figure 7.2. The ideal situation is that in which the probe molecule and the MMA monomer both exhibit an identical reactivity to propagating free radicals. We have previously reported on a method for determining this relative reactivity parameter [14,15]. Essential to this method is the use of a reference fluorescent molecule for which the photophysical properties do not change during

the low conversion region of polymerization. The reference molecule initially chosen for this purpose was unsubstituted anthracene, A.

Figure 7.4 shows the integrated fluorescence intensities, $I_{FL}(A)$ and $I_{FL}(PAnMA)$, as a function of dose from A and AnMA sample solutions respectively, both having an optical density at 337 nm of 0.10. As is evident in the figure, the fluorescence intensity from the A sample does not change during the initial period of polymerization whereas that for the AnMA sample steadily increases with increasing dose.

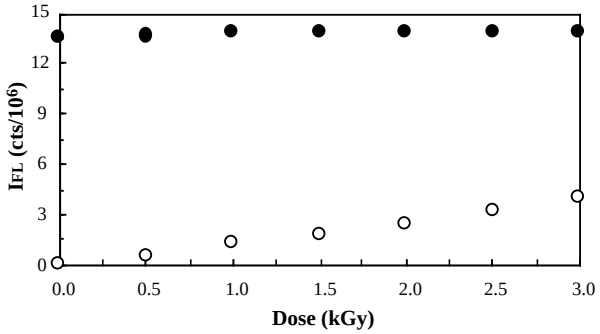

Figure 7.4 Fluorescence intensities versus dose of γ-radiation on photoexcitation at 337 nm of OD_{337} = 0.10 solutions of anthracene (filled circles) and AnMA (open circles) in MMA.

The fractional conversion of AnMA, $F_C(AnMA)$, can be derived from the data in the figure 7.4 (see equation 7.1) if the ratio between the fluorescence efficiencies of A, $\phi_{FL}(A)$, and the polymerized derivative of AnMA, $\phi_{FL}(PAnMA)$, is known.

$$F_c(AnMA) = \frac{I_{FL}(PAnMA) * \phi_{FL}(A)}{I_{FL}(A) * \phi_{FL}(PAnMA)} \tag{7.1}$$

A value of 1.33 ± 0.05 for $\phi_{FL}(A)/\phi_{FL}(PAnMA)$ has been determined from separate spectrofluorimeter measurements on solutions of A and PAnMA as described previously [15,14] using equation (7.2).

$$\frac{\phi_{FL}(PAnMA)}{\phi_{FL}(A)} = \frac{(1-10^{-OD(A)})I_{FL}(PAnMA)}{(1-10^{-OD(PAnMA)})I_{FL}(A)} \tag{7.2}$$

In (7.2), $OD(A)$ and $OD(PAnMA)$ are the optical densities of the solutions.

As discussed previously [15], for copolymerization with only a trace amount of probe molecules (*i.e.* comonomer) present, the ratio between the relevant propagation rate coefficients at low conversions is given by equation 7.3.

$$\frac{k_p(AnMA)}{k_p(MMA)} = \frac{F_c(AnMA)}{F_c(MMA)} \tag{7.3}$$

Table 7.1 gives the experimental results obtained from the data in figure 7.4 and the corresponding values of MMA conversion. The average value of the results given in the final column of table 7.1 is 0.93.

Table 7.1. Calculated ratios between the propagation rate constants $k_p(AnMA)$ and $k_p(MMA)$.

Dose (kGy)	$I_{FL}(A)$ (cts/10^6)	$I_{FL}(AnMA)$ (cts/10^6)	F_c $(AnMA)$[a.]	F_c (MMA)[b.]	$\frac{k_p(AnMA)}{k_p(MMA)}$[c.]
0.5	13.65	0.515	0.028	0.035	0.82
1.0	13.90	1.168	0.063	0.069	0.91
1.5	13.89	1.768	0.096	0.104	0.92
2.0	13.88	2.409	0.131	0.138	0.94
2.5	13.92	3.131	0.169	0.173	0.98
3.0	13.91	3.945	0.213	0.208	1.03

a. calculated using equation 7.1
b. determined by monomer evaporation
c. calculated using equation 7.3

A repeat of the experiment conducted under identical conditions with however the choice of DPA as the reference fluorophore [$\phi_{FL}(PAnMA)/\phi_{FL}(DPA) = 0.34 \pm 0.01$] gave an average value of 1.00 for the ratio between the above mentioned propagation rate constants. The average value from the two data sets is 0.96. It is therefore evident that the ideal condition in which the reactivity of the probe molecule is equal to that of the monomer is closely met.

7.3.3. Monitoring the Gel Effect in MMA Using AnMA

In addition to being able to monitor the progress of polymerization in the low conversion regime, fluorogenic probes are also capable of sensitively monitoring the occurrence of the gel effect; the autoacceleration of polymerization which occurs above a certain monomer conversion. This is illustrated in figure 7.5 by the dramatic increase in fluorescence from a solution of AnMA in MMA above a total dose of *ca* 3.5 kGy using the Gammacell 200 irradiator. Within the shaded area

of the figure the fluorescence intensity increases by a factor of 5.5. Over the same dose range the monomer conversion is found to increase by a factor of 4.3, from 0.23 to 0.98. The fact that the increase in the fluorescence intensity is significantly larger than the increase in MMA conversion would appear to be in conflict with the close to equality of the propagation rate constants for AnMA and MMA. It is known however that the quantum yield of fluorescence can be influenced by changes in the rigidity of the medium, an effect that accompanies the gel effect.

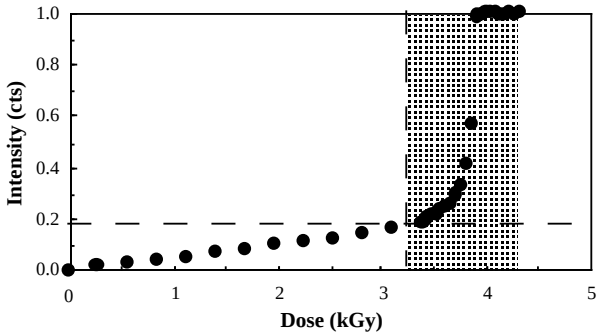

Figure 7.5 Normalized fluorescent light intensity from the AnMA probe in MMA (OD_{337nm} = 0.20) versus dose in the Gammacell 200 irradiator (dose rate of 0.58 kGy/h). The shaded region of the graph corresponds to an increase in MMA conversion from 0.23 to 0.98.

The quantum yield of fluorescence, ϕ_{FL}, is related to the rates of radiative decay, k_r, non-radiative internal conversion, k_{nr}, and intersystem crossing, k_{isc}, by

$$\phi_{FL} = k_r / \left(k_r + k_{nr} + k_{isc}\right) \tag{7.4}$$

It has been argued that an increase in ϕ_{FL}, which is often observed when the environment of a fluorescent chromophore changes from a low viscosity fluid to a rigid glass, can be attributed to a decrease in the rate constant for internal conversion [18]. This argument is based on the fact that coupling between the molecule and the surrounding medium can be a determining factor in the rate of radiationless processes [19] since the medium provides an additional sink for the dissipation of the excitation energy. Since both k_r and k_{isc} are expected to be insensitive to the rigidity of the medium, a decrease in k_{nr} should result in an increase in the fluorescence lifetime, τ, according to

$$\tau = \left(k_r + k_{nr} + k_{isc}\right)^{-1} \tag{7.5}$$

We have measured *in situ* the fluorescence decay of PAnMA throughout the course of MMA polymerization using flash-photolysis equipment described elsewhere [16]. The decay was

monoexponential both prior to and after the autoacceleration region and the lifetimes obtained, using the Gammacell 220 irradiator, are shown in figure 7.6. As can be seen the lifetime increases from an average value of 9.6 ns to 11.2 ns on vitrification.

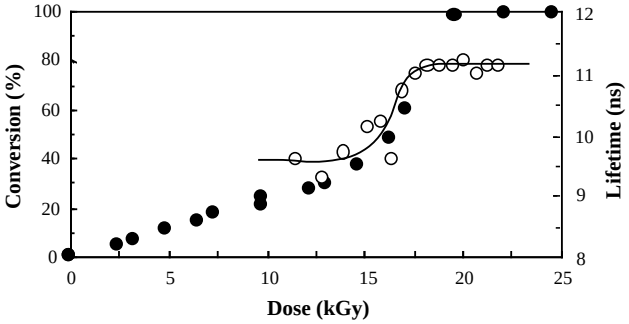

Figure 7.6 MMA conversion (filled circles) and fluorescence lifetime (open circles) of the AnMA probe molecule versus γ-ray dose in the Gammacell 220 irradiator. The drawn line is a spline fit through the lifetime data points.

From equations 7.4 and 7.5, the fluorescence quantum yield is related to the fluorescence lifetime by equation 7.6.

$$\phi_{FL} = k_r \tau \tag{7.6}$$

Taking k_r to be unaffected by changes in the rigidity of the matrix, the increase in ϕ_{FL} on vitrification will be equal to the ratio of the lifetimes found, *i.e.* 11.2/9.6 = 1.17. When this is taken into account, the increase in fluorescence on vitrification due to causes other than incorporation of the AnMA probe is reduced from 5.5 to 4.7 which is closer to the factor of 4.3 found for the increase in MMA conversion.

A second factor which could contribute to a change in the measured fluorescence intensity is the increase in density of the matrix which accompanies vitrification. This will result in an increase in the concentration of the incorporated probe molecules and an increase in the refractive index of the medium. These effects will at least partially compensate each other as shown by equation 7.7 for the ratio of the measured intensity for a fluorophore with a given fluorescence quantum yield in a solid of refractive index n_S to that in a liquid of refractive index n_L.

$$\frac{I_S}{I_L} = \frac{(1-10^{-OD_S})n_L^2}{(1-10^{-OD_L})n_S^2} \tag{7.7}$$

On vitrification the density of MMA increases by a factor of 1.25 and the refractive index increases from 1.41 to 1.49. Using equation 7.7, it can be estimated that these changes should cause an

increase in the measured fluorescence intensity by 6% for an initial optical density of 0.2 in the liquid phase. When this is taken into account, in addition to the increase expected on the basis of the increased quantum yield of fluorescence, the increase in fluorescence on vitrification due to the increased incorporation alone is found to be a factor of 4.4. This is in good agreement with the increase in MMA conversion observed indicating that the fluorogenic probe used is equally capable of providing a measure of the degree of polymerization even in the high conversion, gel effect regime.

7.3.4. Monitoring of MMA Solution Polymerization with AnMA

As mentioned in the introduction, the majority of previously proposed fluorescent probe molecules rely for their application on the sensitivity of one or more of their photophysical properties to changes in the viscosity and/or dielectric properties of the polymerizing medium. This limits their use to bulk or only slightly diluted polymerizing systems. More highly diluted monomer solutions, which undergo relatively small changes in physical properties on complete polymerization of the monomer, cannot be studied using these compounds. The action of fluorogenic probes on the other hand does not rely solely on changes occurring in the physical properties of the medium and therefore should be equally applicable for monitoring solution polymerization, as they have been shown to be for bulk polymerization. We demonstrate this unique capability for the first time in figure 7.7 with results on the radiation-induced polymerization of MMA in MMA/benzene mixtures with MMA volume fractions varying from 80% to as low as 20%. The results bear a strong resemblance to those found many years ago for the dependence on time of the monomer conversion for similar mixtures undergoing thermal polymerization [20].

The results serve to illustrate the strong dependence of the form of the monomer conversion versus dose on dilution. Thus, while evidence can still be seen for the occurrence of the gel effect for the 60% MMA mixture, the dose required to reach this onset is approximately a factor of 3 higher than for the bulk monomer. The results also clearly show the disappearance of the gel effect when the MMA fraction is decreased from 60% to 40%.

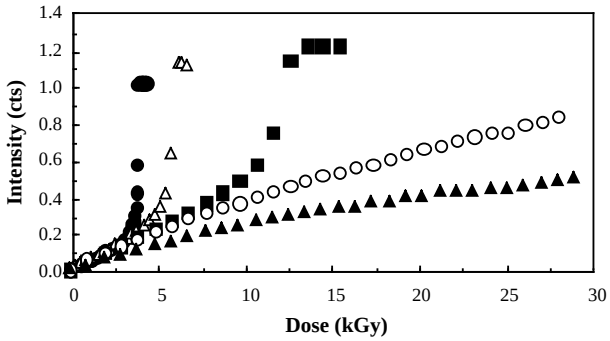

Figure 7.7 The dose dependence of the fluorescence intensity from irradiated MMA/benzene mixtures containing AnMA (OD_{337nm} = 0.20) for MMA volume fractions of 1.0 (●), 0.8 (△), 0.6 (■), 0.4 (○) and 0.2 (▲).

7.4. Conclusions

It was experimentally determined that the AnMA probe has a close to identical reactivity with that of the monomer during the free radical polymerization of MMA. The ratio between the propagation rate constants for the cross-over reaction in which an MMA radical chain-end reacts with AnMA relative to the homopolymerization reaction of MMA is found to be 0.96. By taking into account the change in the fluorescence quantum efficiency observed during the autoacceleration region of polymerization, in addition to the associated density change and change in the refractive index, it was possible to determine the increase in probe conversion during the gel effect of MMA. Very good agreement was found between the experimental MMA conversion and that predicted by monitoring the complete reaction with the fluorogenic probe AnMA. We have therefore demonstrated that the fluorogenic probe AnMA can be applied for sensitive, *in situ* monitoring of MMA polymerization throughout the entire course of the reaction.

In addition, MMA solution polymerization experiments conducted *in situ* involving the AnMA probe molecule demonstrate that fluorogenic probes can also be used for quantitative monitoring of solution polymerizations. This ability to monitor solution polymerization by fluorescent probe techniques with high sensitivity is to the best of our knowledge unprecedented.

References

1. Loutfy, R. Macromolecules 1981, **14**, 270.
2. Loutfy, R. Macromolecules 1983, **16**, 678.
3. Loutfy, RO; Teegarden, DM. Macromolecules 1983, **16**, 452.
4. Loutfy, R. Pure & Appl. Chem. 1986, **58**, 1239.
5. Paczkowski, J; Neckers, D. Macromolecules 1991, **24**, 3013.

6. Stroeks, A; Shmorhun, M; Jamieson, AM; Simha, R. Polymer 1988, **29**, 467.
7. Jing, D. Polymer 1990, **31**, 110.
8. Valdes-Aguilera, O; Pathak, CP; Neckers, DC. Macromolecules 1990, **23**, 689.
9. Rettig, W. Angew. Chem. Int. Ed. 1986, **25**, 971.
10. van Ramesdonk, H; Vos, M; Verhoeven, J; Möhlmann, G; Tissink, N; Meesen, A. Polymer 1987, **28**, 951.
11. Warman, JM; Abellon, RD; Verhey, HJ; Verhoeven, JW; Hofstraat, JW. J. Phys. Chem. B 1997, **101**, 4913.
12. Warman, J; Abellon, R; Luthjens, L; Suykerbuyk, J; Verhey, H; Verhoeven, J. Nucl. Instr. Meth. Phys. Res. B 1999, **151**, 361.
13. Frahn, MS; Abellon, RD; Luthjens, LH; Warman, JM. Radiat. Res. Proc. 1999, **2**, 86.
14. Frahn, MS; Warman, JM; Abellon, RD; Luthjens, LH. Radiat. Phys. Chem. 2001, **60**, 433.
15. Frahn, MS; Abellon, RD; Jager, WF; Luthjens, LH; Warman, JM. Nucl. Instr. Meth. Phys. Res. B 2001, **185**, 241.
16. Frahn, MS; Abellon, RD; Luthjens, LH; Vermeulen, MJW; Warman, JM. Nucl. Instr. Meth. Phys. Res. B in print 2003.
17. Fricke, H; Hart, EJ *Radiation Dosimetry*; Academic Press: New York, 1966; Vol. 2.
18. Kropp, JL; Dawson, WR; Windsor, MW. J. Phys. Chem. 1969, **73**, 1747.
19. Robinson, GW; Frosch, RP. J. Chem. Phys. 1962, **37**, 1962.
20. von Schulz, GV; Harborth, G. Macromol. Chemie 1947, **1**, 106.

Chapter Eight

Radiation-Induced Polymerization Monitored *In Situ* by Time-Resolved Fluorescence of Probe Molecules in Methyl Methacrylate*

8.1. Introduction

There are a number of competing processes which determine the lifetime of the S_1, excited state of a fluorophore following photo-excitation. These are (radiative) fluorescence or (non-radiative) internal conversion from S_1 to S_0, intersystem crossing to T_1 and intermolecular energy transfer or quenching. In the absence of intermolecular quenching the rate at which the concentration of excited fluorophores decreases following an infinitely short excitation pulse is given by

* This chapter has been published in *Nuc. Instr. Meth. Phys. Res. B* 208 (2003) 405-410.

$$\frac{dN}{dt} = -(k_r + k_{nr} + k_{isc})N \tag{8.1}$$

in which k_r, k_{nr} and k_{isc} are the rate constants of fluorescence, internal conversion and intersystem crossing respectively. At a given time following the excitation pulse the concentration of excited fluorophores present is therefore given by

$$N(t) = N(0)e^{-(k_r + k_{nr} + k_{isc})t} \tag{8.2}$$

and since the fluorescence intensity, *I(t)*, is proportional to the concentration of excited fluorophores,

$$I(t) = I(0)e^{-(k_r + k_{nr} + k_{isc})t} \tag{8.3}$$

From equation 8.3, the mean lifetime of the excited singlet state of the fluorophore τ is given by

$$\tau = \left(k_r + k_{nr} + k_{isc}\right)^{-1} \tag{8.4}$$

The quantum yield of fluorescence ϕ_f is related to τ and k_r as given below.

$$\phi_f = k_r / \left(k_r + k_{nr} + k_{isc}\right) = k_r \tau \tag{8.5}$$

The rate constants of the decay processes may be influenced by properties of the environment, such as (micro-)viscosity, polarity and temperature. Consequently, any such change in the molecular environment of a probe molecule which accompanies polymerization could result in a change in its excited state lifetime. For typical aromatic fluorophores, *e.g.* anthracene (the fluorescent chromophore in the probe molecule *N*-(2-anthracene)methacrylamide, AnMA, molecular structure given in figure 8.1), the radiative decay constant is not expected to be sensitive to temperature, (micro-)viscosity or polarity. This is not the case however for the non-radiative internal conversion decay rate constant [1, 2]. For this reason one might expect that the excited state lifetime of a probe molecule may change as a polymerizing system changes from a fluid monomer to a rigid polymeric glass.

The excited state properties of charge-transfer (CT) fluorophores typically exhibit strong sensitivity to environmental parameters [3, 4]. This is a direct consequence of the highly polar character of their excited states and the significant amount of stabilization that mobile, dipolar solvent molecules can provide. The fluorescent derivative of maleimido fluoroprobe (MFP,

molecular structure given in figure 8.1) [5] formed by incorporation (*i.e.* copolymerization) into growing PMMA chains undergoes very rapid and efficient intramolecular electron transfer from a donor to an acceptor group in the molecule. The reduction in the energy of the thus formed CT state by orientation of solvent dipoles is evident as a bathochromic (red) shift in the fluorescence with increasing solvent polarity. If the viscosity of the medium increases (as occurs during polymerization), complete solvation of the CT state may not occur within the lifetime of the excited fluorophore. This will result in a blue shift in the fluorescence as has been observed previously on lowering the temperature of dilute solutions of CT compounds [6, 7] and on vitrification of polymerizing media [8]. In the present work we show that the lifetime of the excited state also undergoes a substantial change on vitrification accompanied by a change from mono-exponential to multi-exponential decay kinetics.

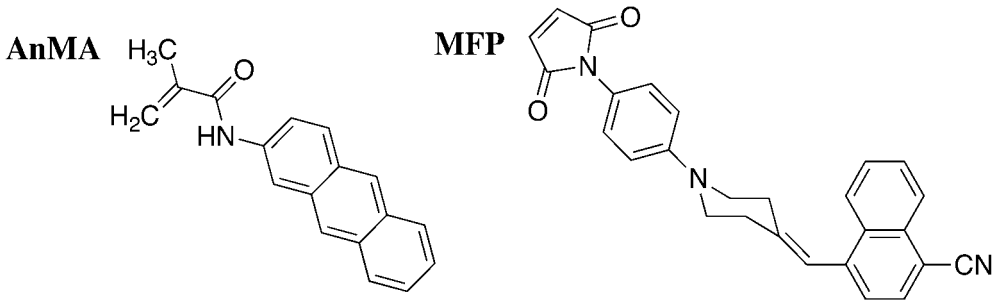

Fig. 8.1. Molecular structures of the fluorogenic probe molecules *N*-(2-anthracene)methacrylamide, AnMA, and maleimido fluoroprobe, MFP.

It should be noted that the molecular probes AnMA and MFP are fluorogenic molecules which become fluorescent only after (co-)polymerization into growing polymer chains [9-12]. This leads to the observation of fluorescence only from probe molecules which are covalently bound to polymer chains.

8.2. Experimental

8.2.1. Materials and Radiation Procedure

Synthesis grade MMA, purchased from Merck, was distilled at atmospheric pressure and 100-101 ºC immediately prior to use. The synthesis of the fluorogenic probe AnMA was analogous to that described previously for the pyrene derivative PyMA [11]. The fluorogenic probe MFP was synthesized in the group of Prof. J.W. Verhoeven of the Department of Organic Chemistry at the University of Amsterdam [5].

All probe solutions were prepared in MMA at an optical density of 2 at 337 nm in a 1 cm cuvette. Sample cells were constructed in-house from Heraeus Suprasil quartz tubing. Deaeration of the samples was carried out on a vacuum line using three freeze-pump-thaw cycles.

Irradiation of the samples was accomplished using an MDS Nordion cobalt-60 Gammacell 220 irradiator. The dose rate of *ca* 8 kGy/h was accurately determined by Fricke dosimetry and corrected for the natural decay of the source. The ambient temperature within the source chamber was 33ºC.

8.2.2. *In Situ* Fluorescence Measurements

The experimental set-up for in situ time-resolved fluorescence lifetime measurements (see figure 8.2) consisted of a pulsed nitrogen laser (LTB Lasertechnik Berlin MSG 800) which provides a 337 nm excitation light pulse with a full width at half maximum of 0.5 ns. The excitation light is transmitted to the sample via the inner optical fiber of a multi-fiber optical light guide (Top Sensor Systems UV/VIS: FC-UV 200-2). The probe tip makes contact with the sample cell at a 70º angle to the surface to reduce back reflection of excitation light. The emitted light is transmitted via the six outer fibers of the multi-fiber optical cable and exits the fiber bundle via a 350 nm UV cut-off filter prior to detection by a silicon semiconductor photodiode (EG&G FWD-100Q) with 1 ns rise and fall times. The photodiode therefore detects emitted light of wavelengths 350 nm and above. The output of the photodiode is recorded, averaged and stored using a 1 GHz digital oscilloscope (Tektronix TDS 680B). Data analysis was accomplished using a PC.

In situ fluorescence spectra were obtained by replacing the photodiode and cut-off filter shown in figure 8.2 with a diode array spectrophotometer described previously [10, 13]. Fluorescence spectra and time-resolved fluorescence decay measurements could be made on the same sample within a time duration of one minute.

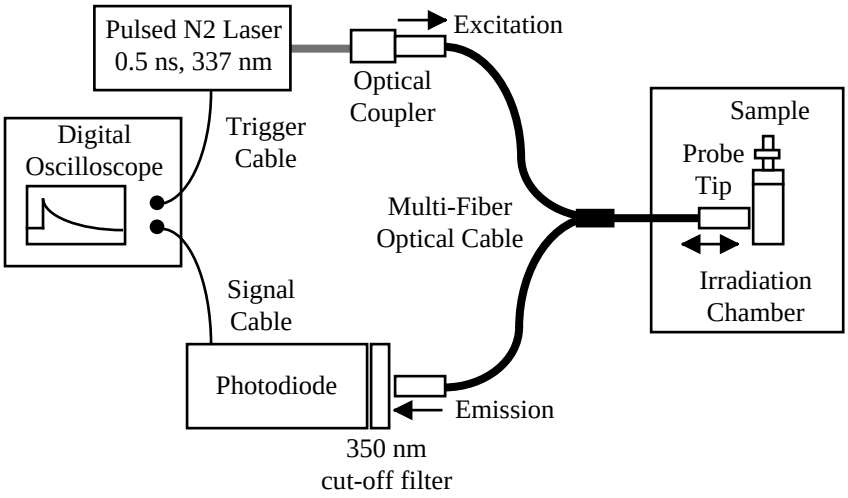

Fig. 8.2. Schematic representation of the set-up used for *in situ* determination of fluorescence lifetimes.

8.3. Results and Discussion

As the MMA monomer with trace amounts of dissolved AnMA or MFP polymerizes, the fluorogenic probe molecules are incorporated (*i.e.* copolymerized) into the growing polymer chains and consequently become fluorescent. This leads to an increase in fluorescence intensity from the samples with increasing monomer conversion. The fluorescence intensity is therefore an indication of the extent of monomer conversion [11-13].

During the autoacceleration stage of bulk MMA polymerization, characteristic of the gel or Trommsdorff effect, the fluorescence intensity increases not only due to additional incorporation of the fluorogenic probes but also due to a change in the fluorescence quantum efficiency of incorporated probe molecules. Normalized *in situ* fluorescence spectra measured both immediately before and after the gel effect for both AnMA and MFP samples are shown in figure 8.3. As can be seen, the AnMA sample shows an increase in fluorescence intensity but no change in the spectral shape or position. For the MFP sample however, in addition to an increase in intensity there is also a marked blue-shift in the maximum wavelength of fluorescence. This can be ascribed to reduced energetic stabilization of the CT state of the probe molecule in the more rigid environment.

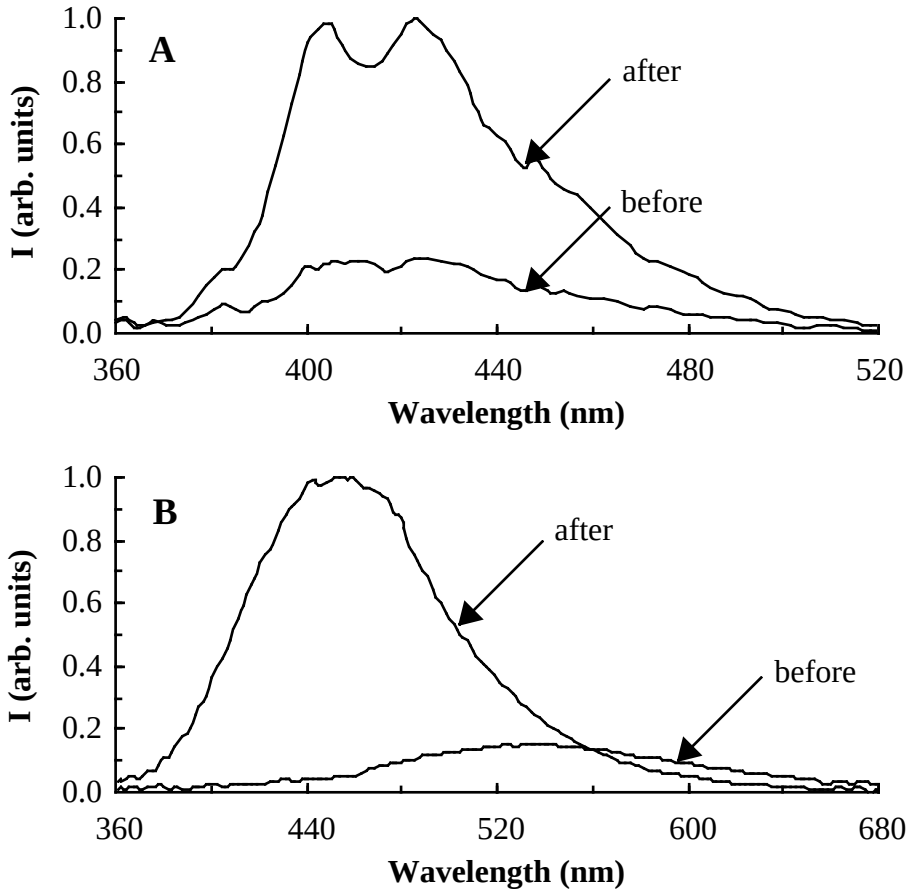

Fig. 8.3. *In situ* fluorescence spectra of AnMA, **A**, and MFP, **B**, in polymerizing MMA; before and after the gel effect.

In an attempt to gain more insight into the changes occurring in the environment of the probe molecules during this late stage of polymerization we have monitored fluorescence lifetimes *in situ* from just prior to the autoacceleration of polymerization until the end of the reaction. Example fluorescence decays are shown in figure 8.4 for AnMA. It is apparent that the decay remains mono-exponential when going from the viscous solution to the rigid polymeric glass. Figure 8.5A gives the fluorescence lifetime as a function of γ-ray dose during the investigated region of polymerization. At lower doses the fluorescence intensity was too low for accurate determination of the lifetime. Prior to the onset of the gel effect the lifetime is close to constant with a value of 9.6 ns, whereas on vitrification it suddenly increases to 11.2 ns. A similar percentage increase in the lifetime from 5.5 to 6.3 ns has been found for unsubstituted anthracene which does not copolymerize. As is evident in figure 8.5A, the technique of measuring the fluorescence lifetime is only useful in the late stage of MMA polymerization as opposed to the fluorescence intensity which provides information also in the earlier stage of polymerization.

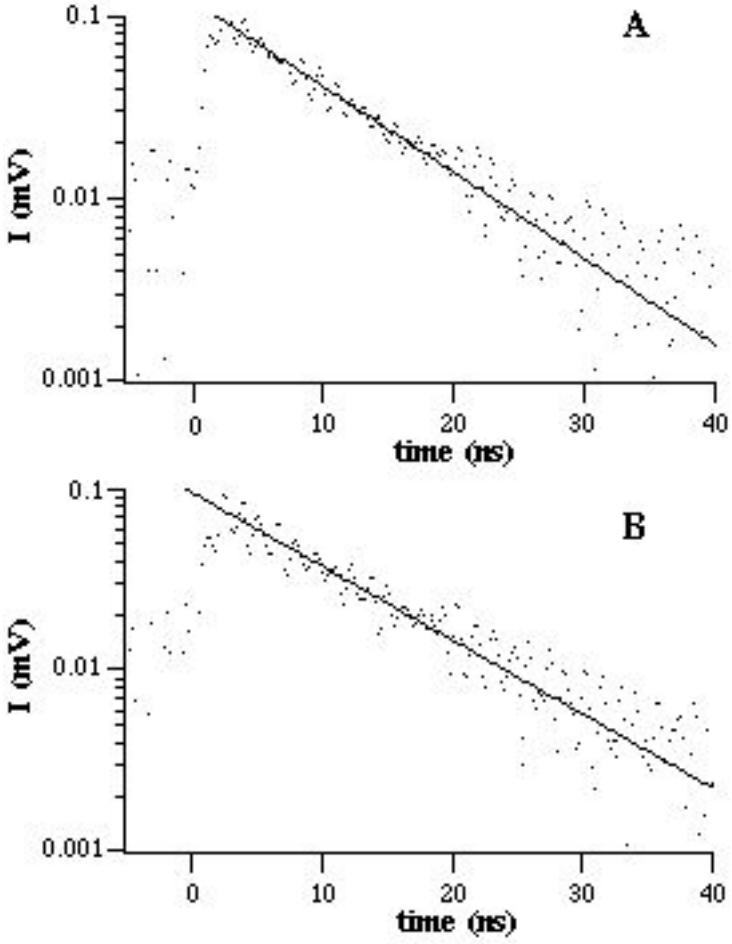

Fig. 8.4. Time-resolved integrated fluorescence (> 350 nm) from AnMA in polymerizing MMA; prior to, **A**, and after, **B**, the gel effect.

Theories about radiationless transitions are based upon the assumption that coupling between the molecule and medium in which it resides is important for the occurrence of radiationless processes [14]. The medium essentially provides a sink for the dissipation of molecular excitation energy. The extent of this coupling is expected to decrease with increasing rigidity of the medium. For these reasons, the increase in the excited state lifetime of the incorporated AnMA probe when the polymerizing system changes from a viscous sample to a polymeric glass is attributed to a decrease in the rate constant for non-radiative decay k_{nr}. This being the case, the increase in lifetime on vitrification will result in a corresponding increase by a factor of 1.17 in the quantum efficiency of fluorescence according to equation 8.5. This factor can be used to correct the change in intensity of emission from AnMA at the gel transition in order to obtain the contribution due to increased AnMA copolymerization alone.

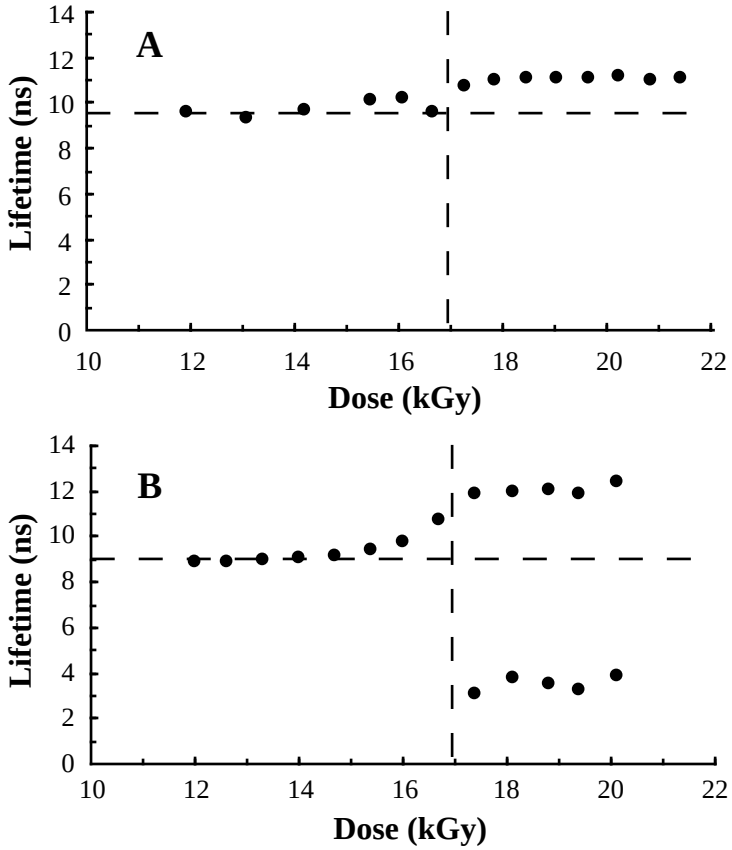

Fig. 8.5. *In situ* fluorescence lifetime measurements of AnMA, **A**, and MFP, **B**, in MMA versus gamma-ray dose. The vertical dashed line shows the dose at which the maximum rate of polymerization during the gel effect occurs as determined from monomer conversion measurements [Luthjens, *et. al.*, Res. Chem. Intermed. (2001) **27** (7,8) 765-773].

Fluorescence decays for MFP before and after the gel effect are shown in figure 8.6. Unlike the results for AnMA, the fluorescence decay changes from mono-exponential in the viscous monomer with a lifetime of 8.8 ns to multi-exponential in the rigid PMMA matrix. Reasonably good fits to the latter fluorescence decays could be obtained by using a double-exponential model as illustrated in figure 8.6B. The measured lifetimes are shown as a function of γ-ray dose in figure 8.5B. There is an indication of an increase in the (mono-exponential) lifetime just prior to the gel effect but subsequently the two lifetime components of 3.5 and 12.2 ns remain constant with further increase of dose.

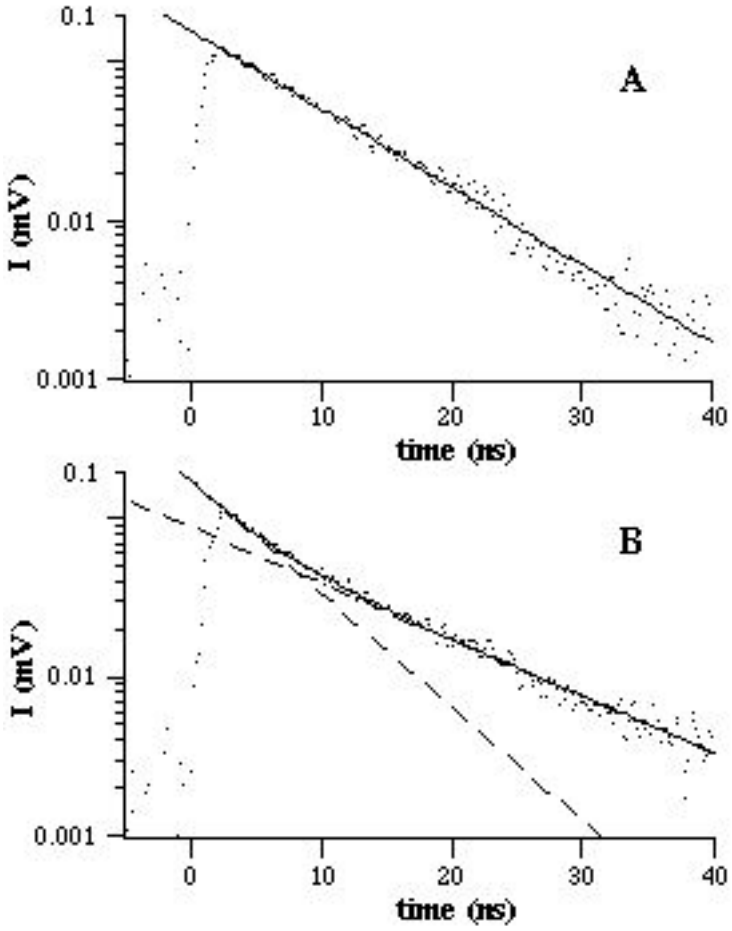

Fig. 8.6. Time-resolved integrated fluorescence (> 350 nm) from MFP in polymerizing MMA; prior to, **A**, and after, **B**, the gel effect.

The excited state lifetime of 8.8 ns prior to autoacceleration may be expected to increase in the fully cured system for the same reasons given above for the AnMA probe molecule. In fact, the fluorescing chromophore of MFP is strongly sensitive to solvent polarity exhibiting a maximum in τ at intermediate polarities [15]. Furthermore, due to the rigid environment of the PMMA chains, the stabilization of the CT state by solvent dipoles is significantly hindered. This results in the dramatic blue shift in the steady-state emission spectrum from the MFP sample shown in figure 8.3B. The effect that this reduced stabilization will have on the excited state lifetime of the fluorescent MFP derivative is difficult to predict.

One explanation for the multi-exponential character of the fluorescence decay is that fluorescing probe molecules are reporting on different molecular environments and therefore reflect a heterogeneity on the molecular scale in the PMMA. This could be rationalized as regions of relatively high and low micro-viscosity. Another explanation is that the PMMA chains could be

reorienting and therefore providing stabilization of the CT state on the time-scale of the excited state lifetime of the probe molecule. This would lead to a gradual increase in both the emission wavelength and excited state lifetime with increasing time following excitation [16]. Measurements of the fluorescence decay rate at various wavelengths of the emission spectrum are required in order to differentiate between these two models. This will be the subject of a future publication in which we will address the influence of PMMA micro-heterogeneity and/or PMMA molecular relaxation on the fluorescence signal of the MFP sample and its non-fluorogenic analog fluoroprobe [15].

8.4. Conclusions

An experimental set-up has been designed and constructed for the *in situ* measurement of time-resolved fluorescence within a cobalt-60 γ-ray irradiator. Experimental results are presented for dilute solutions of two fluorogenic probe molecules in polymerizing MMA. It was found that the fluorescence lifetimes of the probe molecules were sensitive only to the vitrification stage of MMA polymerization. The excited state lifetime of the copolymerized derivative of AnMA increased from its nearly constant value of 9.6 ns to 11.2 ns on vitrification. This is attributed to a decrease in the rate constant of non-radiative internal conversion of the probe molecule. Results have also been presented for the fluorogenic, CT probe molecule MFP. The fluorescence decay rate from the copolymerized derivative changes from mono-exponential to multi-exponential on vitrification. The molecular origin of this multi-exponential decay will be the subject of a future communication.

References

1. J.L. Kropp, W.R. Dawson, and M.W. Windsor, J. Phys. Chem. 73(6) (1969) 1747-1752.
2. G. Greiner, J. Photochem. Photobiol. A: Chem. 137 (2000) 1-7.
3. C. Reichardt, Chem. Rev. 94 (1994) 2319-2358.
4. W. Rettig, Ang. Chem., Int. Ed. Eng. 25 (1986) 971-988.
5. H.V. Verhey, *et al.*, New J. Chem. 20 (1996) 809-814.
6. M. Goes, *et al.*, J. Phys. Chem. A 106 (2002) 2129-2134.
7. E. Görlach, *et al.*, Chem. Phys. 194 (1995) 185-193.
8. T.C. Schaeken and J.M. Warman, J. Phys. Chem. 99 (1995) 6145-6151.
9. J.M. Warman, *et al.*, J. Phys. Chem. B, 101 (1997) 4913-4916.
10. J. Warman, *et al.*, Nuc. Instr. and Meth. B 151 (1999) 361-366.
11. M.S. Frahn, *et al.*, Nuc. Instr. and Meth. B 185 (2001) 241-247.
12. M.S. Frahn, *et al.*, Rad. Phys. and Chem. 60 (2001) 433-437.

13. M.S. Frahn, *et al.*, in: Proc. 11th Int. Conf. of Radiation Research, Dublin, Ireland 1999, Rad. Res. 2 (1999) 86-88.
14. G.W. Robinson and R.P. Frosch, J. Chem. Phys. 37(9) (1962) 1962-1973.
15. G.F. Mes, *et al.*, J. Am. Chem. Soc., 106 (1984) 6524-6528.
16. J.R. Lakowicz, Principles of Fluorescence Spectroscopy (2nd ed.) Kluwer Academic/Plenum Press, New York, 1999, ch. 7.

Chapter Nine

Time-Resolved Emission Spectra of Fluoroprobe and Maleimido-Fluoroprobe Before, During and After Sudden Vitrification of Radiation-Polymerized Methyl Methacrylate*

9.1. Introduction

In the present study we have monitored the fluorescence of the probe molecules 1-phenyl-4-[(4-cyano-1-naphthyl)methylene]piperidine, hereafter named Fluoroprobe (FP), and the fluorogenic derivative 1-*p*-maleimido-phenyl-4-[(4-cyano-1-naphthyl)methylene]piperidine, hereafter named Maleimido-Fluoroprobe (MFP) during the course of radiation-induced polymerization of bulk MMA. The chemical structures of both probe molecules are given in Figure 9.1. Of interest was a comparison between the behaviour of the free fluorophore (FP) with that of a derivative which only

* This chapter has been submitted to *J. Phys. Chem. B* in 2003 for publication.

fluoresces when copolymerized (MFP). Previous studies have shown how the latter, fluorogenic probe molecule can be used to monitor the progress of polymerization even in the early stages of polymerization where the viscoelastic properties of the medium differ little from those of the starting material[1-3]. MFP has also the unique fluorogenic property which makes it possible to monitor polymerization in dilute solution as well as in the bulk monomer[4]. In this paper we focus more on the changes occurring in the region of the "gel" or Trommsdorff effect where sudden vitrification occurs. Particular attention is paid to the information that can be gained concerning the microscopic nature of the ultimate, glassy PMMA matrix.

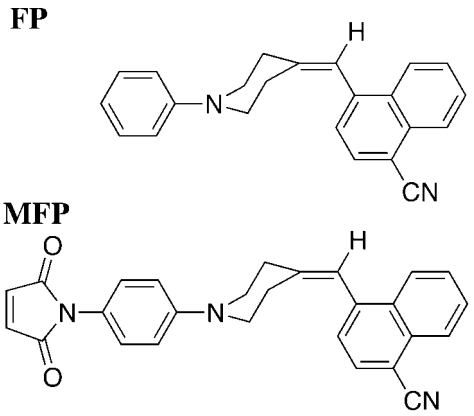

Figure 9.1. Molecular structures of the fluorescent (FP) and fluorogenic (MFP) probe molecules used in the present work.

When the carbon-carbon double bond of the maleimido group in MFP becomes saturated, this non-fluorescent molecule exhibits strong charge-transfer (CT) fluorescence similar to that of FP. Because of the exceptional sensitivity of their fluorescence to specific material properties such as polarity, polarizability and viscosity, both of these probes have been extensively investigated[2,5-8,3,9-13]. This sensitivity is attributed to the formation of a large dipole moment in the excited state following photoexcitation[7]. This large dipole moment is a consequence of electron transfer from the donor, dialkylanilino group to the cyano-naphthylmethylene acceptor.

Figure 9.2 illustrates the consequences of solvent relaxation on the CT fluorescence. After electron transfer occurs, dipolar solvent molecules reorient around the molecule, predominately by rotation, thus stabilizing the excited state. Femtosecond time-resolved fluorescence measurements and molecular dynamics calculations on FP have established that this stabilization occurs in low viscosity solvents within a time-scale of a few picoseconds[11-13]. The extent of stabilization is strongly dependent on the polarity of the solvent. For this reason, increasingly red-shifted fluorescence is observed in solvents of increasing polarity.

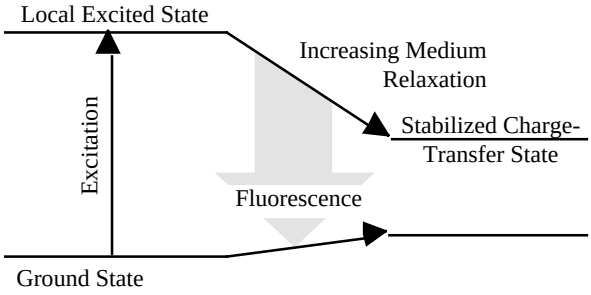

Figure 9.2. A schematic representation of the photoexcitation of a donor-spacer-acceptor molecule such as Fluoroprobe illustrating the decrease in energy of the emission from the highly-dipolar, charge separated state which results from reorganization of the dipoles in the surrounding medium.

The solvatochromic power of the present probe molecules can be demonstrated by constructing Lippert-Mataga plots in which the wavenumber of the fluorescence maximum, ν_{CT}, is plotted against the solvent polarity parameter Δf. This parameter is related to the static dielectric constant ε_s and the optical refractive index n, as shown in Equation 9.1.

$$\Delta f = (\varepsilon_s - 1)/(2\varepsilon_s + 1) - (n^2 - 1)/(2n^2 + 1) \tag{9.1}$$

The Lippert-Mataga equation[14,15], derived by assuming the ground state dipole moment to be negligible in comparison to that in the emissive CT state, is given below.

$$\nu_{CT} = \nu_{CT}(0) - 1.007 \times 10^4 \, [(\mu_{CT})^2/\rho^3] \, \Delta f \tag{9.2}$$

In Equation 9.2, $\nu_{CT}(0)$ (cm^{-1}) is the wavenumber corresponding to the (hypothetical) gas-phase fluorescence maximum, μ_{CT} is the dipole moment of the CT state in Debye, and ρ is the effective radius in Å of a spherical cavity containing the molecule (frequently taken to be 40% of the long axis for elongated molecules such as FP[7]). A plot of ν_{CT} versus Δf for FP has the exceptionally large slope of –34,000 cm^{-1} from which a dipole moment of the CT state of *ca* 25 D, corresponding to complete charge separation, is determined. This large dipole moment has been confirmed by time-resolved microwave conductivity measurements[7].

Additional photophysical characteristics of FP are presented in Table 9.1 together with the frequently used solvent polarity parameter $E_T(30)$[16]. The dependencies of the photon energy at the maximum of the emission, E_{max}, and the fluorescence lifetime, τ_{FL}, on the solvent polarity parameter are shown in Figure 9.3. As expected from the previous discussion, E_{max} decreases continuously with increasing solvent polarity. The dependence of τ_{FL} on polarity is however seen to be more

complex, passing through a maximum at intermediate polarities. The decrease in lifetime on the high polarity side of the maximum is attributed to the decrease in energy between the CT state and the ground state which results in an increased rate of charge recombination according to the Marcus expression for the inverted region[17]. The decrease in lifetime on the low polarity side is attributed to mixing between the CT state and the locally excited state of the acceptor which results in an additional pathway to the ground state[10,18].

Table 9.1. Photophysical properties of Fluoroprobe in various solvents.

Solvent[a.]	$E_T(30)$[b.]	λ_{max}(nm)	E_{max}(eV)	τ_{FL} (ns)
cyclohexane	31.2	412	3.01	1.2
di-n-butyl ether	33.4	468	2.65	12
benzene	34.5	478	2.59	15
diethyl ether	34.6	506	2.45	14
1,4-dioxane	36.0	516	2.40	15
tetrahydrofuran	37.4	574	2.16	7.0
ethyl acetate	38.1	573	2.16	6.0
1,2-dimethoxyethane	38.2	595	2.08	4.0
pyridine	40.2	627	1.98	1.0
MMA		550	2.25	9.0
PMMA		450	2.75	11[c.]

a. Data from: G. F. Mes, *et a.l*, J. Am. Chem. Soc. (1984) 106, 6524-6528.
b. C. Reichardt, *Solvent Effects in Organic Chemistry*, text reference number 16.
c. Long-time decay component (when fit using a bi-exponential decay model).

As mentioned previously, relaxation of solvent molecules around the excited state dipole of FP will occur within a few picoseconds in fluid media, *i.e.* on a time-scale much shorter than the nanosecond lifetime of the excited state. The emission can therefore be taken to be from the fully matrix-equilibrated CT state. However, when imbedded in a highly viscous medium, the time-scale on which reorientation of dipoles occurs can approach, or even exceed, that of the fluorescence lifetime. Such an occurrence is experimentally detectable as a bathochromic shift of the fluorescence with time. This effect has previously been demonstrated for FP in glass-forming solvents by thermochromic studies involving streak camera measurements[9]. A method of analysing such time-resolved emission spectra (TRES) has been presented by Lakowicz[19]. This treatment will be discussed in more detail and applied to the present measurements in the Results and Discussion section.

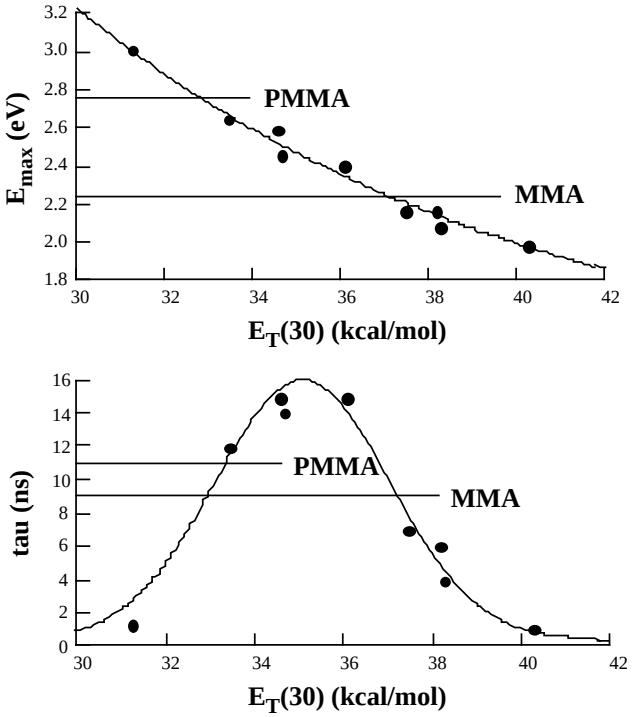

Figure 9.3. The dependence of the maximum energy (upper figure) and the decay time (lower figure) of Fluoroprobe emission on the polarity parameter $E_T(30)$ for the solvents listed in Tabel 9.1. The horizontal lines correspond to the values of Emax and tau found for MMA and PMMA.

9.2. Experimental

9.2.1. Materials

Methyl methacrylate (Merck, Synthesis grade) was deaerated and distilled on a vacuum line at atmospheric pressure and 100-101 ºC immediately prior to use. The probe molecules FP[7,20] and MFP[21] were synthesized in the group of Prof. J.W. Verhoeven of the Department of Organic Chemistry at the University of Amsterdam (for molecular structures see Figure 9.1). Dilute solutions in MMA of *ca* 10^{-4} molar were prepared and pipetted into sample cells constructed (in-house) of Heraeus Suprasil, 1 cm square, quartz tubing with an attachment which allowed the solutions to be dearated by three freeze-pump-thaw cycles on a vacuum line.

9.2.2. Methods

Optical absorption spectra of the solutions were measured using a Perkin Elmer Lambda 40 UV/VIS spectrophotometer. The optical densities at the excitation wavelength of 337 nm used in fluorescence measurements were 0.5 or 2 for the 1 cm pathlength of the cells used. Steady-state fluorescence spectra of irradiated samples could be measured outside of the radiation chamber using a Photon technology International "Quantamaster 1" spectrofluorimeter.

In situ measurements of the fluorescence spectra, carried out within the irradiation chamber during the course of polymerization, were achieved using an experimental set-up which has been described in detail previously[1]. The excitation wavelength was *ca* 340 nm and emission spectra were recorded using a diode array spectrophotometer (Ocean Optics Europe S2000). Spectra could be obtained at time intervals as short as 2 seconds.

In situ fluorescence decay measurements were obtained using an experimental flash-photolysis set-up described in detail in a separate publication[22]. The samples were photoexcited with a *ca* 500 ps duration pulse of 337 nm light from a Lasertechnik Berlin MSG 800 laser. The integrated emission above 350 nm was detected using a silicon semiconductor photodiode with rise and fall times of *ca* 1 ns (EG&G FWD-100Q). The output of the detector was monitored and stored using a 1 GHz digital oscilloscope (Tektronix TDS 680B).

Wavelength dependent, time-resolved fluorescence decay measurements on fully-polymerized samples were made outside the gamma irradiator using a nitrogen laser (Laser Photonics MegaPlus LN 1000) which produces pulses of 337 nm radiation with a pulse width at half height of ca 800 ps. The excitation light is incident on the sample at an angle of 90º to the detection system. Emitted light is focused onto a monochromator (American ISA Incorporated H-20 SA) with variable entrance and exit slits. In this way the bandwidth could be varied from 2 to 8 nm. The emitted light is detected using a single channel-plate photomultiplier (Photek PMT 113/UHF Ultrafast MCP Photomultiplier) with *ca* 100 ps rise and fall times. The output of the detector is monitored by a real-time, 1 GHz digital oscilloscope (Tektronix TDS 680B). Data acquisition and handling was accomplished with the LabVIEW Package (version 5.1) from National Instruments Corporation.

Gamma-ray irradiations at *ca* 8 kGy/hr were accomplished with an MDS Nordion cobalt-60 Gammacell 220 irradiator. Dose rates were accurately determined by Fricke dosimetry and corrected for the natural decay of the source. The ambient temperature within the source chamber was 33ºC.

9.3. Results and Discussion

In this section we present results on the changes which occur in the spectrum and decay kinetics of the fluorescence from dilute solutions of FP and MFP in MMA during the course of radiation-induced polymerization. We focus particularly on the range of radiation dose within

which the gel effect occurs. The application of MFP and other fluorogenic probe molecules to quantitatively monitor the degree of monomer conversion at lower doses and in dilute solution has been demonstrated in previous publications[1,2,23,3,24,22,4].

An aspect of interest in the present study was whether or not different fluorescent behaviour would be observed in the gel region between that from "free" FP molecules and that from the FP chromophoric units of copolymerized MFP, "pMFP", which are pendantly bound to polymer chains[2]. It was thought that if phase separation occurred during vitrification, then FP might be preferentially concentrated in low molecular weight, *monomer-rich* regions whereas pMFP would emit mainly from *polymer-rich* regions. By comparing the two probe molecules therefore, we hoped to be able to obtain more detailed information on the morphological changes occurring on a microscopic scale during the course of autoacceleration and vitrification.

9.3.1. Fluorescence Spectra; In Situ Measurements

Fluorescence spectra of MMA solutions of FP and MFP measured *in situ* for radiation doses in the vicinity of the gel effect are shown in Figure 9.4. For both solutes an abrupt blue-shift in the emission maximum, from *ca* 550 nm (2.25 eV) to *ca* 450 nm (2.75 eV) occurs within the dose range between 15 and 17 kGy. The wavelength shift is very similar to that found on thermal curing of MMA containing FP[5]. Also, as expected, it agrees with that found previously in this laboratory in an experimental procedure which required the samples to be removed from the radiation source and measured using an external spectrofluorimeter[1]. The present, *in situ* measurement capability was designed in order to make it possible to take spectra at more frequent time intervals during the gel effect and to eliminate post-irradiation effects during sample transport between the source and the spectrofluorimeter. The spectra shown in Figure 9.4 were taken at 5 minute intervals subsequent to a prior irradiation for a period of *ca* 2 hours.

The energy maxima of the spectra in Figure 9.4 are plotted as a function of radiation dose in Figure 9.5. Also shown in the figure is the MMA monomer conversion measured under the same dose-rate conditions. The response of the two probe molecules during the course of vitrification is seen to be very similar. MFP does however display evidence of a gradual blue shift prior to vitrification which is absent for FP. In fact, for FP only one of the spectra within a 5 minute time span differs significantly from that of the two extremes. This is thought to reflect the different tendencies of the pMFP and FP fluorophores to be concentrated mainly in polymer-rich or monomer-rich regions of the medium respectively. The close to discontinuous change found for FP indicates therefore that polymerization within the monomer-rich regions must eventually occur *extremely* rapidly.

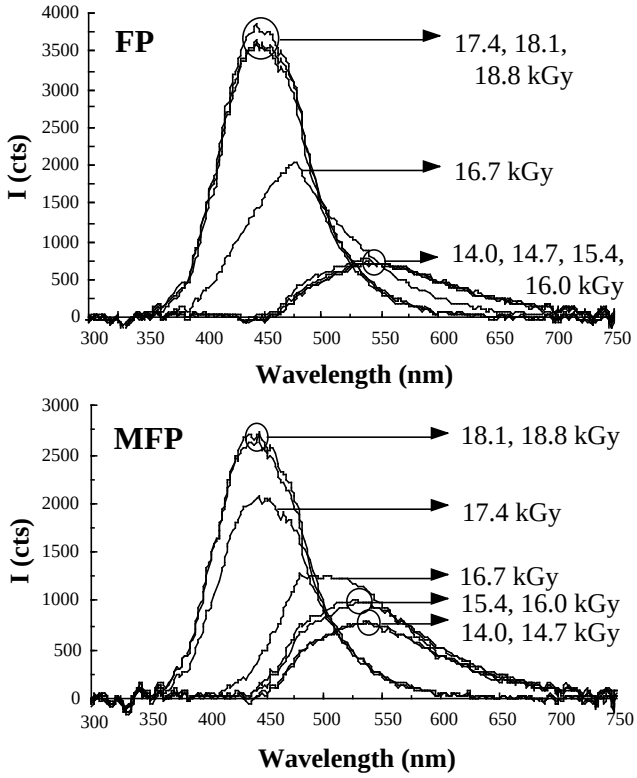

Figure 9.4. Fluorescence spectra measured *in situ* during radiation-induced polymerization of MMA containing Fluoroprobe (upper) and Maleimido-Fluoroprobe (lower). The data are show for radiation doses just prior to, during, and just after the occurrence of the gel effect and the sudden virtrification of the medium.

Comparison of the E_{max} values prior to and after the gel effect with the data in Figure 9.3 for the emission from solvents of different polarity, indicates that the effective polarity parameter, $E_T(30)$, changes from 37 to 33. The latter value, for the fully polymerized PMMA matrix, is still higher than the value of *ca* 31 found for a completely nonpolar (hydrocarbon) medium. It is, in fact, close to the value found for the weakly polar solvent di-*n*-butyl ether which has a dielectric constant of 3.08. Since the room temperature dielectric constant of PMMA is 3.45, it would appear that a large fraction of the dipolar relaxation potential of the PMMA matrix is involved in reducing the energy level of the CT state of FP and pMFP, even within the excited state lifetime of a few nanoseconds. This will be discussed in more detail after first considering the time-resolved measurements of the fluorescence decay kinetics.

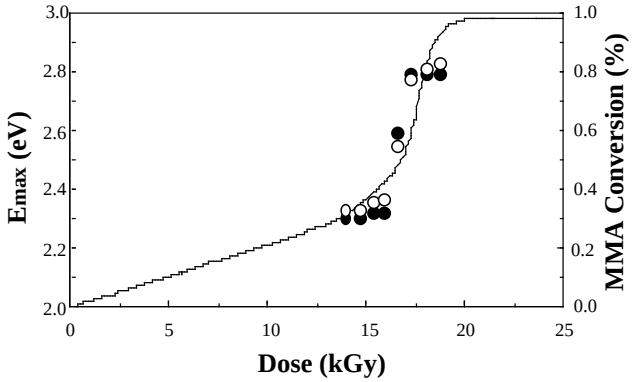

Figure 9.5. The dependence of the maximum energy of the emission, Emax, on radiation dose in the region of the occurrence of the gel effect for MMA containing FP (open circles) and MFP (open squares). Also shown is the monomer conversion under the same radiolysis conditions.

9.3.2. Fluorescence Decay; In Situ Measurements

In addition to the sudden hypsochromic shift in the emission maximum on vitrification, there is also an abrupt change in the decay kinetics of the fluorescence for both probe molecules. The decay of the integrated fluorescence for FP, measured *in situ*, is shown in Figures 9.6A and 9.6B. For radiation doses just prior to the gel effect the decay is monoexponential with a mean decay time of 9.0 ns. On vitrification however the decay deviates considerably from monoexponential at early times. A best bi-exponential fit to the data, given by the full line in Figure 9.6B, was found for lifetime components $\tau_1 \approx 3.0$ and $\tau_2 \approx 11$ ns. The values of τ_1 and τ_2 determined from best fits for both FP and MFP are plotted against dose in Figure 9.7. As with the spectral shifts, the change in decay kinetics is also seen to occur over an extremely narrow range of dose and no substantial difference is found between the two probe molecules.

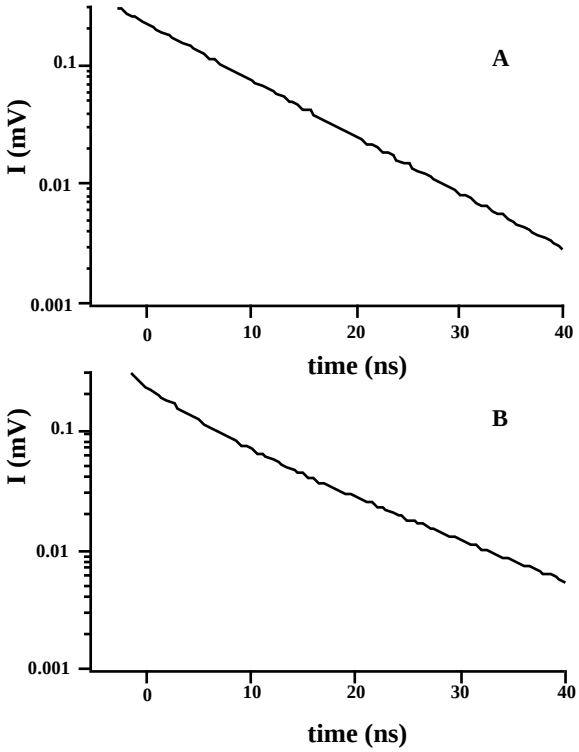

Figure 9.6. Integrated fluorescence transients measured *in situ* on laser flash-photolysis (500 ps, 337 nm pulse) of MMA containing Fluoroprobe; (A) just prior to the gel effect: dose = 14.0 kGy and (B) just after the gel effect: dose = 18.8 kGy. The full lines are fits to the after-pulse decay of fluorescence using in (A) a single exponential with a mean lifetime of 9.0 ns, and in (B) a bi-exponential with lifetime components of 3.0 and 11 ns.

Comparison of the major, long-lifetime component of 11 ns for the fully polymerized medium with the lifetimes found for solvents of different polarities indicates that the effective $E_T(30)$ value is close to 33 for PMMA, in agreement with the conclusion reached on the basis of the emission maximum. The spectral and kinetic data are therefore consistent. To investigate further the underlying cause of the non-exponential decay of the integrated fluorescence in the polymerized medium found in the *in situ* measurements, more detailed experiments have been carried out on fully polymerized samples which were removed from the radiation source and investigated using time-resolved fluorescence equipment capable of monitoring fluorescence transients at specific wavelengths. These measurements are reported in the next subsection.

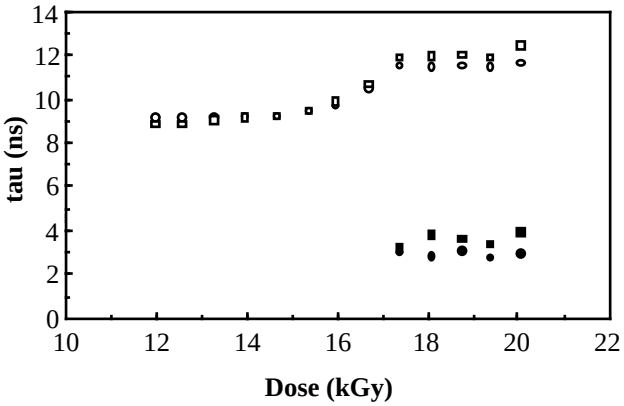

Figure 9.7. The short (filled symbols) and long (open symbols) lifetime components determined from bi-exponential fits to the fluorescence decay for radiation doses in the region of the occurrence of the gel effect, for MMA containing FP (circles) and MFP (squares).

9.3.3. Fluorescence Decay Kinetics in PMMA; Wavelength Dependence

The two most common underlying causes of the non-exponential decay of the integrated fluorescence in solid matrices can be separated into "static" and "dynamic" effects. In the static case, the fluorescent molecules are considered to be entrapped within a variety of local dielectric or structural environments, each resulting in a different spectrum and/or decay time of the fluorophore emission. In the dynamic case, changes in the emissive properties are brought about by relaxation of the local environment or the structure of the fluorophore itself on a time-scale similar to that of the mean lifetime of the fluorescent state. Molecules with highly dipolar excited states, as in the present work, are expected to be particularly susceptible to both static and dynamic effects.

In the case of static effects, the fluorescence may display different decay times at different wavelengths hence resulting in an overall non-exponential decay of the integrated fluorescence. However, the decay at all individual wavelengths will be continuous and monoexponential. In the case of dynamic effects, which are invariably expected to result in a gradual decrease in the energy of the emission, a decay in the short wavelength region is expected to be accompanied by a *growth* at long wavelengths.

In Figure 9.8 fluorescence transients are shown which were taken at the blue and red extremes of the fluorescence spectrum found in the *in situ* experiments, at 380 nm and 580 nm respectively. The decay at 380 nm is seen to be much faster than at 580 nm with a lifetime close to the value of 3 ns found for the short component in the *in situ* measurements. More importantly, the fluorescence at 580 nm is seen to grow in over the first few nanoseconds after the pulse. This growth, over a post-pulse period of approximately 5 ns is much slower than would be expected on

the basis of the *ca* 200 ps response time of the equipment. This presents therefore clear-cut evidence that dynamic changes in the local environment or structure of the fluorophores are the underlying cause of the non-exponential decay of the integrated fluorescence.

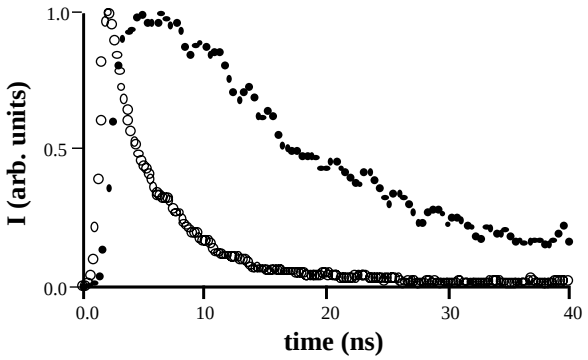

Figure 9.8. Fluorescence transients monitored at 380 nm and 580 nm on laser flash-photolysis of a fully-polymerised PMMA sample containing Fluoroprobe illustrating the rapid decay at the short wavelength extreme of the emission and the after-pulse growth at the long wavelength extreme.

To more fully investigate the relaxation process involved requires constructing time-resolved emission spectra which will be discussed in the following subsection.

9.3.4. Time-Resolved Emission Spectra (TRES)

TRES can be measured directly, *e.g.* by pulse-sampling with time-gated detection, or can be constructed from the wavelength-dependent decays together with the steady-state emission spectrum. The latter procedure involves fitting the decays $I(\lambda,t)$ with the following multi-exponential relationship[19].

$$I(\lambda,t) = \sum_i \alpha_i(\lambda)\exp[-t/\tau_i(\lambda)] \qquad (9.3)$$

In Equation 9.3, $\tau_i(\lambda)$ and $\alpha_i(\lambda)$ are wavelength-dependent decay times and pre-exponential factors (with $\sum\alpha_i = 1$). Because of parameter correlation and limited resolution, no molecular significance can be assigned to these parameters. A set of parameters $H(\lambda)$ is then determined in which the intensity decays are normalized to the steady-state emission spectrum $F(\lambda)$

$$H(\lambda) = F(\lambda) / \int I(\lambda,t)dt \tag{9.4}$$

which for multi-exponential analysis becomes

$$H(\lambda) = F(\lambda) / \sum_i \alpha_i(\lambda)\tau_i(\lambda) \tag{9.5}$$

The normalized intensity decay functions $I'(\lambda,t)$ are then given by

$$I'(\lambda,t) = H(\lambda)I(\lambda,t) = \sum_i \alpha_i'(\lambda)\exp[-t/\tau_i(\lambda)] \tag{9.6}$$

in which $\alpha_i'(\lambda) = H(\lambda)\alpha_i(\lambda)$. These appropriately normalized decays are then used to construct the TRES.

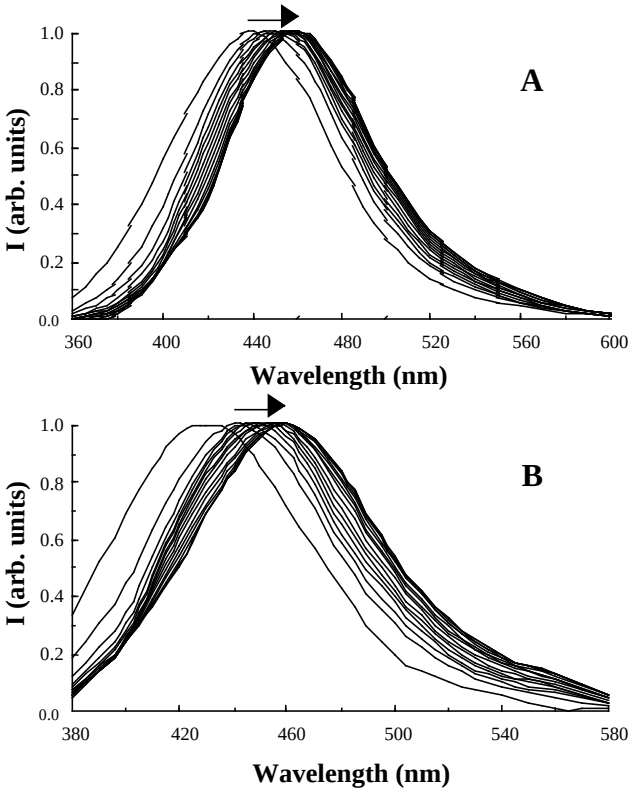

Figure 9.9. Peak-normalised, time-resolved emission spectra (TRES) for PMMA samples containing Fluoroprobe (A) and Maleimido-Fluoroprobe (B). The spectra, which are for time intervals of 2.5 ns within a total elapsed time of 40 ns after the pulse, show a gradual spectral shift to longer wavelengths with time.

Using this procedure TRES were calculated for both FP and MFP in PMMA. For this purpose, external measurements of both the decay profiles and steady-state emission spectra were made. Figure 9.9 shows the peak-normalized TRES for both FP and MFP. The spectra given in the figure were calculated at time intervals of 2.5 ns. The left-most TRES corresponds to a time of 2.5 ns following the excitation pulse and the right-most TRES corresponds to a time of 40 ns. The data are similar for both solutes, apart from what would appear to be a larger spectral shift at early times for MFP.

In Figure 9.10 the values of E_{max} are plotted as a function of time. Apart from the initial rapid decrease for MFP mentioned above, the decrease in energy is seen to display a closely similar temporal behaviour for both solutes. The full lines in the figure were calculated on the basis of an exponential relaxation to a long-time limiting value of E_{max} = 2.68 eV, with a relaxation time of 16 ns.

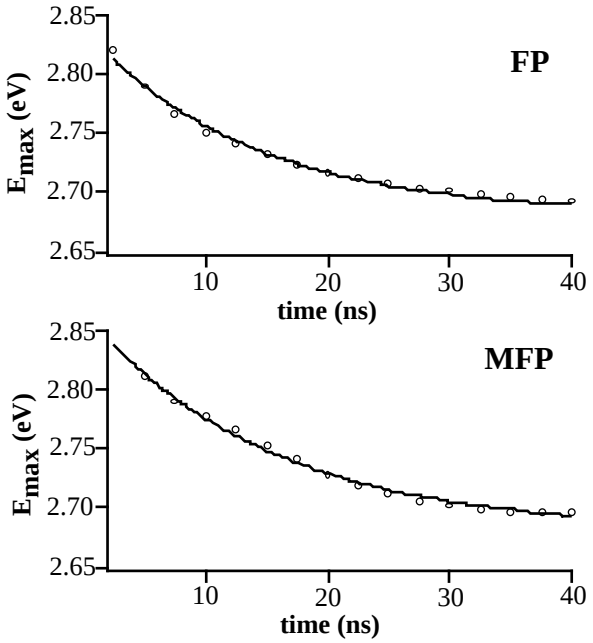

Figure 9.10. The time dependence of the maximum of the time-resolved emission spectra shown in Fig. 9.9 (circles). The full lines correspond to a mono-exponential relaxation of Emax to an eventual constant value of 2.68 eV with a relaxation time of 16 ns.

The overall shift in E_{max} from 2.83 eV (438 nm) to 2.68 eV (462 nm) is very close to the 20 nm shift over a time-span of 100 ns reported by van Ramesdonk *et al.* for FP in thermally polymerized MMA[5]. Ramesdonk *et al.* argued that the source of the spectral relaxation on a

nanosecond time-scale must be due to conformational rearrangement of the fluorophore rather than relaxation of the PMMA matrix. This was based on the fact that dielectric relaxation of PMMA has been found to occur on a time-scale orders of magnitude longer than that for relaxation of the FP emission[25-27]. The intramolecular conformational change was ascribed to "rehybridization of the amino nitrogen into a planar trigonal situation". We consider that the identical values for the fluorescence relaxation time found for FP and MFP argues against this interpretation. In the case of pMFP the anilino group is coupled, via the copolymerized maleimido moiety, to the polymer chains. This added restriction to the motional freedom would be expected to have a considerable retarding effect on the kinetics of planarization about the anilino nitrogen and hence result in a slower relaxation time than for the free FP molecules. The lack of a difference in relaxation kinetics leads us to conclude that the underlying cause of relaxation must, indeed be reorganization of the PMMA matrix, probably involving side-chain motions of neighboring ester groups. As mentioned above, the time-scale of fluorescence relaxation is orders of magnitude shorter than the dielectric relaxation time attributed to such motions. We conclude that the coulombic interaction between the fully charged donor and acceptor moieties in the excited state of the present fluorophores and neighboring dipolar ester groups is sufficiently strong to overcome the barrier to structural reorganization.

Because all experiments were conducted at a temperature above the β-relaxation transition of PMMA[28], the molecular origin of the stabilization interaction is tentatively attributed to side-chain motions of the PMMA ester groups. This is perhaps counterintuitive when one considers the time-scale attributed to such relaxations in PMMA[25,29,27,26,5]. Nevertheless, the large dipole moment of *ca* 25 +/- 2 D produced upon charge-separation in the excited state is highly probable to exert a significant Coulombic force on nearby ester groups in the matrix thus providing a pathway for matrix reorganization within the nanosecond time-scale.

9.4. Conclusions

In situ measurements have been made of the spectra and decay kinetics of the charge-transfer fluorescence of the fluorescent and fluorogenic probe molecules Fluoroprobe (FP) and Maleimido-Fluoroprobe (MFP) during the course of radiation-induced polymerization of methyl methacrylate (MMA) in a cobalt gamma-ray source. Particular attention has been paid to the range of radiation dose in which the gel effect, resulting in sudden vitrification, occurs. This effect results in an abrupt blue-shift in the fluorescence maximum from *ca* 550 nm to *ca* 450 nm for both compounds with a slight indication of a pre-vitrification shift for MFP but not for FP. This difference in behaviour is attributed to the preferential concentration in polymer-rich and monomer-rich regions of the sample respectively. The spectral change is accompanied by a change in the decay kinetics from monoexponential with a decay time of 9.0 ns to non-monoexponential, with a

bi-exponential fit yielding lifetime components of *ca* 3 ns and *ca* 11 ns. Both the spectral shift and the change in the (long) lifetime correspond to a change in the $E_T(30)$ polarity parameter of the medium from 37 prior to, to 33 after the gel effect. The latter value, for the fully-polymerized matrix, corresponds to that found for the weakly polar solvent di-n-butylether which has a dielectric constant of 3.08; close to the static dielectric constant of PMMA. A wavelength-dependent study of the fluorescence decay in fully-polymerized samples, conducted outside of the source, has been used to construct time-resolved emission spectra (TRES). The TRES display a gradual red-shift in the emission maximum which occurs with an exponential relaxation time of 16 ns. This is attributed to reorganization of the dipolar side-chain ester groups of the polymer induced by the highly-dipolar, fully charge-separated state of the probe molecules, on a time-scale orders of magnitude shorter than the dielectric relaxation time of PMMA. No evidence is found for (micro)heterogeneity in the PMMA matrix.

Acknowledgement

The authors thank professor J.W. Verhoeven (University of Amsterdam) for providing the Fluoroprobe and Maleimido-Fluoroprobe compounds used in this work.

References

(1) Warman, J.; Abellon, R.; Luthjens, L.; Suykerbuyk, J.; Verhey, H.; Verhoeven, J. *Nucl. Instr. Meth. Phys. Res. B* **1999**, *151*, 361.
(2) Warman, J. M.; Abellon, R. D.; Verhey, H. J.; Verhoeven, J. W.; Hofstraat, J. W. *J. Phys. Chem. B* **1997**, *101*, 4913.
(3) Frahn, M. S.; Abellon, R. D.; Luthjens, L. H.; Warman, J. M. *Radiat. Res. Proc.* **1999**, *2*, 86.
(4) Frahn, M. S.; Luthjens, L. H.; Warman, J. M. *Polymer* **accepted 2003**.
(5) van Ramesdonk, H.; Vos, M.; Verhoeven, J.; Möhlmann, G.; Tissink, N.; Meesen, A. *Polymer* **1987**, *28*, 951.
(6) Jenneskens, L.; Verhey, H.; van Ramesdonk, H.; Witteveen, A.; Verhoeven, J. *Macromolecules* **1991**, *24*, 4038.
(7) Mes, G. F.; Jong, B. d.; van Ramesdonk, H. J.; Verhoeven, J. W.; Warman, J. M.; Haas, M. P. d.; Horsman-van den Dool, L. E. W. *J. Am. Chem. Soc.* **1984**, *106*, 6524.
(8) Hofstraat, J.; Verhey, H.; Verhoeven, J.; Kumke, M.; Li, G.; Hemmingsen, S.; McGrown, L. *Polymer* **1997**, *38*, 2899.
(9) Goes, M.; Groot, M. d.; Koeberg, M.; Verhoeven, J. W.; Lokan, N. R.; Shephard, M. J.; Paddon-Row, M. N. *J. Phys. Chem. A* **2002**, *106*, 2129.
(10) Pasman, P.; Rob, F.; Verhoeven, J. W. *J. Am. Chem. Soc.* **1982**, *104*, 5127.

(11) Middelhoek, E. R.; Vermeulen, P.; Verhoeven, J. W.; Glasbeek, M. *Chem. Phys. Lett.* **1995**, *198*, 373.
(12) Middelhoek, E. R.; Zhang, H.; Verhoeven, J. W.; Glasbeek, M. *Chem. Phys.* **1996**, *211*, 489.
(13) Brown, R.; Middelhoek, R.; Glasbeek, M. *J. Phys. Chem.* **1999**, *111*, 3616.
(14) Lippert, E. Z. *Naturforsch* **1955**, *10a*, 541.
(15) Mataga, N. *Bull. Chem. Soc. Japan* **1955**, *28*, 690.
(16) Reichardt, C. *Solvent Effects in Organic Chemistry*; Weinheim: New York, 1979; Vol. 3.
(17) Marcus, R. A. *Annu. Rev. Phys. Chem.* **1964**, *15*, 155.
(18) Depaemelaere, S.; Viaene, L.; Auweraer, M. v. d.; Schryver, F. C. D.; Hermant, R. M.; Verhoeven, J. W. *Chem. Phys. Lett.* **1993**, 215.
(19) Lakowicz, J. R. *Principles of Fluorescence Spectroscopy*, 2nd ed.; Kluwer Academic/Plenum Press: New York, 1999.
(20) Hermant, R. M., Ph.D. Thesis - University of Amsterdam, **1990**.
(21) Verhey, H. V.; Bekker, C. H. W.; Verhoeven, J. W.; Hofstraat, J. W. *New J. Chem.* **1996**, *20*, 809.
(22) Frahn, M. S.; Abellon, R. D.; Luthjens, L. H.; Vermeulen, M. J. W.; Warman, J. M. *Nucl. Instr. Meth. Phys. Res. B* **in print 2003**.
(23) Frahn, M. S.; Abellon, R. D.; Jager, W. F.; Luthjens, L. H.; Warman, J. M. *Nucl. Instr. Meth. Phys. Res. B* **2001**, *185*, 241.
(24) Frahn, M. S.; Warman, J. M.; Abellon, R. D.; Luthjens, L. H. *Radiat. Phys. Chem.* **2001**, *60*, 433.
(25) Deutsch, K.; Hoff, E. A.; Reddish, W. *J. Polym. Sci.* **1954**, *13*, 565.
(26) McCrum, N. G.; Read, B. E.; Williams, G. *Anelastic and Dielectric Effects in Polymeric Solids*; John Wiley & Sons Ltd.: London, 1967.
(27) Smyth, C. P. *Physics and Chemistry of the Organic Solid State*; Interscience: New York, 1963; Vol. 1.
(28) Ward, I. M.; Hadley, D. W. *An Introduction to the Mechanical Properties of Solid Polymers*; John Wiley & Sons Ltd: Chichester, 1928.
(29) Sinnot, K. M. *J. Polym. Sci.* **1960**, *42*, 3.

Summary

Each year over one billion pounds of acrylic-based polymeric products are produced world wide. Such products include windows in aircraft, lenses in eyeglasses and CD players, coatings on parquet flooring and various architectural structures such as skylights and domes. Often these products are made by injecting monomer or monomer solutions into molds in which it is polymerized, *i.e.* cured, by the application of heat. Alternatively, acrylic-based products are produced as coatings by exposing the polymerizable medium to UV light or high-energy radiation. Obviously, it is of importance to such processes that the curing stage is optimized. Insufficient curing will lead to the production of materials with inferior properties. Alternatively, excessive heating or exposure can lead to both slow rates and high costs of production.

In this thesis a novel method is introduced by which the polymerization process may be monitored. This non-invasive manner of monitoring the polymerization process involves the use of trace concentrations of molecular probes in the polymerizing media. Unique to the molecular probes discussed in this thesis is their fluorogenic character. These probe molecules which are initially non-fluorescent chemically react with growing polymer chains and thereby become fluorescent. The fluorescence from the polymerizing system is therefore a direct measure of the overall extent of polymerization. Because of the associated chemical change to the probe molecule, this is a highly sensitive technique for monitoring the polymerization process. This is especially true for the early stage of polymerization, a stage in which the physical properties (viscosity, dielectric constant) of the polymerizing media do not change significantly (see chapter seven). Furthermore, because of the high sensitivity of fluorescence techniques, only a very small (millimolar or less) probe concentration is required.

The polymerization of methyl methacrylate, MMA, was chosen as the system to study for two reasons; the ready availability of scientific data on this system and the associated Trommsdorff effect observed as a rapid autoacceleration of polymerization when the monomer conversion reaches a certain extent. Obviously, the bulk of scientific data present in the literature enabled rapid comparisons between the experimental results obtained with those from research institutes throughout the world. Chapter four is an in-depth discussion related to the polymerization of MMA. The Trommsdorff effect is a dramatic deviation from classical (steady-state) polymerization kinetics. Despite over 60 years of scientific investigation into this phenomenon, a comprehensive and scientifically verifiable description to the Trommsdorff effect remains elusive. By applying a new technique by which the Trommsdorff effect could be monitored, it was hoped that new insights into this phenomenon would be obtained. As it turned out, many questions remain unanswered.

Chapter one serves as a general introduction to radiation-induced polymerization. The investigations described in this thesis all involved the utilization of high-energy ionizing radiation for the initiation of polymerization. Chapter two provides more details relating to the steady-state

(Co-60 γ-rays) and pulsed (3 MeV electrons) ionizing radiation sources employed. Furthermore, this chapter gives complete descriptions of the experimental set-ups used for conducting both external and *in situ* measurements for the investigations described in later chapters. The materials studied, in particular the probe molecules, are described in chapter three. These include commercially available molecules in addition to probes synthesized either by the author at the Technical University of Delft or at the University of Amsterdam in the group of Prof. J. W. Verhoeven.

In chapter five the fluorescence response from *N*-(1-pyrene)maleimide (MPy) in polymerizing MMA is quantified in order to determine the relative rate of incorporation of the probe during polymerization. By using the reference fluorophore pyrene (Py) and determining the relative quantum efficiencies of fluorescence of the fluorescent, *i.e.* copolymerized, MPy derivative to that of Py, it was possible to determine the relative rate of MPy incorporation in relation to that of the MMA monomer. It was found that the MPy probe is *ca* 40% more reactive than the MMA monomer. Consequently, as polymerization proceeds the probe will be consumed at (relatively) a faster rate than the monomer itself. The ideal situation is that in which both probe and monomer exhibit identical reactivities. Although this ideal situation was not observed, this chapter does illustrate however the possibility to monitor the entire course of bulk MMA polymerization using the fluorogenic molecular probe MPy.

With the intention of matching reactivities of both probe and monomer during MMA polymerization, a new probe N-(1-pyrene)methacrylamide (PyMA) was synthesized. The new probe is a derivative of the MPy probe in which the reactive (copolymerizable) maleimido group is replaced by a methacrylamide group. As the methacrylamide group more closely resembles the methacrylate group of the monomer, it was hoped that the new probe would exhibit a similar chemical reactivity. Furthermore, it was predicted that α,β–unsaturation to the carbonyl group in the methacrylamide functionality of the probe would successfully quench pyrene fluorescence. This proved to be the case. Using the experimental procedure described in chapter five, it was observed that the PyMA probe exhibits a slightly lower reactivity (85%) than the monomer itself. This lower reactivity was attributed to a smaller diffusion coefficient for the large PyMA molecule relative to that for MMA. Again, the success in using fluorogenic molecular probes for monitoring the entire course of bulk MMA polymerization is presented.

The characteristically long lifetime of pyrene fluorescence makes this fluorophore particularly susceptible to quenching interactions, *e.g.* by trace amounts of oxygen. This makes those experimental results that rely on quantitative measurements of fluorescence likewise susceptible to systematic errors. This complication was eliminated by synthesizing the new probe molecule *N*-(2-anthracene)methacrylamide (AnMA) which incorporates the short-lived fluorophore anthracene. Again, the α,β–unsaturation to the carbonyl group in the methacrylamide functionality of the probe was presumed to be an effective quencher of fluorescence. This was indeed found to be the case. Repetition of the experimental procedure described in chapter five, using anthracene as the reference fluorophore, indicated that the AnMA probe exhibits a close to identical reactivity (96%) with that of the monomer. It was further demonstrated that the fluorogenic AnMA probe could be used to sensitively monitor the entire course of MMA polymerization quantitatively, even in the region beyond the Trommsdorff effect. Experimental results are also presented in this chapter which demonstrate that fluorogenic probes such as AnMA can be employed for the sensitive monitoring of solution polymerization. This ability to monitor solution polymerization by fluorescent probe techniques with high sensitivity is to the best of our knowledge unprecedented.

Chapter eight introduces the application of time-resolved fluorescence techniques for monitoring polymerization. Accepting that the rate of non-radiative relaxation of fluorophores is sensitive to the physical properties of the medium, it was reasonable to assume that measurement of probe molecule fluorescence lifetimes in a polymerizing medium could be used for monitoring the polymerization process itself. The experimental results showed that both the AnMA probe and the fluorogenic, charge-transfer molecule maleimido fluoroprobe (MFP) exhibit sensitivity only at the vitrification stage of bulk MMA polymerization. The experiment involving MFP indicated however that in addition to a decrease in the rate of non-radiative relaxation, the fluorescence decay rate of the copolymerized derivative changes from mono-exponential to multi-exponential on vitrification. The origin of this multi-exponential decay rate is the subject of the final chapter of this thesis.

In chapter nine both steady-state and time-resolved fluorescence measurements of two charge-transfer probes (fluoroprobe and MFP) were used to investigate the Trommsdorff effect of MMA polymerization. It was of interest to compare the behavior of the free probe FP to that of the fluorogenic probe MFP. In the Trommsdorff region an abrupt blue-shift in the fluorescence maximum (from *ca* 550 nm to *ca* 450 nm) is observed. The onset of this blue-shift occurs at a slightly earlier stage with the MFP probe and this difference is attributed to the preferential concentration of the MFP probe in polymer-rich regions of the sample (recall that the MFP probe only fluoresces once copolymerized into growing polymer chains). In addition to the spectral change, a change from mono-exponential to multi-exponential decay kinetics is observed with both probes. By construction of the time-resolved emission spectra (TRES) of the probes in the PMMA matrix it is possible to show that a gradual red-shift in fluorescence occurs for both probes with an exponential relaxation time of 16 ns. This is attributed to reorganization of the dipolar side-chain ester groups of the polymer induced by the highly-polar, fully charge-separated state of the probe molecules on a time-scale orders of magnitude shorter than the dielectric relaxation time of PMMA. No evidence was found for (micro)heterogeneity in the PMMA matrix.

Samenvatting

Ieder jaar worden wereldwijd meer dan een half miljoen ton polymeerproducten gemaakt gebaseerd op acrylaten. Het betreft vensters in vliegtuigen, lenzen in brillen en CD-spelers, beschermlagen op parketvloeren, en verschillende onderdelen voor de bouw zoals daklichten en koepels. Vaak worden deze producten gemaakt door het spuitgieten van monomeren of monomeer-oplossingen in mallen, waarin ze uitharden onder invloed van warmte. Ook worden acrylhoudende polymeriseerbare producten gebruikt als beschermlaag uitgehard door blootstelling aan UV-licht of hoog-energetische straling. Het is duidelijk van belang voor deze processen dat de uitharding geoptimaliseerd wordt. Onvoldoende uitharding leidt tot producten van slechte kwaliteit. Te sterke verhitting of bestraling kan echter leiden tot langzame uitharding en hoge productiekosten.

In dit proefschrift wordt een nieuwe methode geïntroduceerd waardoor het polymerisatie-proces kan worden gevolgd. Deze niet-ingrijpende manier om het polymerisatie-proces te volgen maakt gebruik van zeer lage concentraties van moleculaire probes in de polymeriserende media. Uniek voor de moleculaire probes besproken in dit proefschrift is hun fluorogene karakter. Deze probe moleculen die aanvankelijk niet fluoresceren reageren chemisch met groeiende polymeer-ketens en worden daardoor fluorescerend. De fluorescentie van het polymeriserend systeem is daardoor een directe maat voor de totale polymerisatiegraad. Vanwege de gerelateerde chemische verandering van het probe molecuul is dit een zeer gevoelige techniek om het polymerisatie proces te volgen. Dit is vooral zo voor het vroege stadium van polymerisatie waarin de fysische eigenschappen (viscositeit, diëlectrische constante) van de polymeriserende media niet in belangrijke mate veranderen (zie Hoofdstuk 7). Vanwege de grote gevoeligheid van fluorescentie-technieken is slechts een zeer lage (millimolair of minder) probe-concentratie nodig.

De polymerisatie van methylmethacrylaat, MMA, werd gekozen als systeem voor studie om twee redenen: de overvloedige beschikbaarheid van wetenschappelijke gegevens over dit systeem, en het bekende Trommsdorff effect, waargenomen als een plotselinge zelfversnelling van de polymerisatie zodra de monomeerconversie een bepaald punt heeft bereikt. De massa aan wetenschappelijke gegevens in de literatuur maakte een snelle vergelijking mogelijk tussen de zelf-verkregen experimentele resultaten en die van research instituten over de hele wereld. Hoofdstuk 4 bevat een diepgaande discussie over de polymerisatie van MMA. Het Trommsdorff effect is een dramatische afwijking van klassieke (evenwichts) polymerisatiekinetiek. Ondanks meer dan 60 jaar van wetenschappelijk onderzoek van dit verschijnsel blijft een begrijpelijke en wetenschappelijk verantwoorde beschrijving van het Trommsdorff effect een wensdroom. Door toepassing van een nieuwe techniek waardoor het Trommsdorff effect kon worden gevolgd hoopten wij dat nieuwe inzichten in dit verschijnsel konden worden verkregen. Het bleek echter dat veel vragen onbeantwoord blijven.

Hoofdstuk 1 is een algemene inleiding in stralingsgeïnduceerde polymerisatie. Het onderzoek beschreven in dit proefschrift heeft geheel betrekking op het gebruik van hoog-energetische ioniserende straling voor het initieren van polymerisatie. Hoofdstuk 2 geeft meer details over de gebruikte continue (Co-60 γ-stralen) en gepulseerde (3 MeV electronen) bronnen voor ioniserende straling. Verder geeft dit hoofdstuk volledige beschrijvingen van de experimentele opstellingen gebruikt voor de uitvoering van zowel externe als *in situ* metingen voor het onderzoek beschreven in de volgende hoofdstukken. De bestudeerde materialen, in het bijzonder de probe moleculen, worden beschreven in Hoofdstuk 3. Deze omvatten commercieel verkrijgbare moleculen en ook de moleculen gesynthetiseerd door de auteur op de Technische Universiteit Delft, of op de Universiteit van Amsterdam in de groep van Prof. J. W. Verhoeven.

In Hoofdstuk 5 wordt de fluorescentie response van *N*-(1-pyreen)maleimide (MPy) in polymeriserend MMA gequantificeerd om de relatieve inbouwsnelheid van de probe gedurende de polymerisatie te bepalen. Door de fluorofoor pyreen (Py) als referentie te gebruiken en de relatieve quantumefficiënties voor fluorescentie van het fluorescerende, dus gecopolymeriseerde, MPy derivaat ten opzichte van Py, was het mogelijk om de relatieve snelheid van MPy inbouw in relatie tot die van MMA monomeer te bepalen. Gevonden werd dat de MPy probe *ca* 40% meer reactief is dan het MMA monomeer. Dientengevolge zal de probe bij voortschrijdende polymerisatie opgebruikt worden met een (relatief) grotere snelheid dan het monomeer zelf. De ideale situatie is die waarin probe en monomeer beide dezelfde reactivititeit vertonen. Hoewel deze ideale situatie niet werd waargenomen illustreert dit hoofdstuk toch de mogelijkheid om het gehele verloop van de bulk MMA polymerisatie te volgen met gebruik van de fluorogene moleculaire probe MPy.

Met de bedoeling om de reactiviteiten van probe and monomeer gedurende MMA polymerisatie aan elkaar gelijk te maken, werd een nieuwe probe N-(1-pyreen)methacrylamide (PyMA) gesynthetiseerd. De nieuwe probe is een afgeleide van de MPy probe waarin de reactieve (copolymeriseerbare) maleimide groep is vervangen door een methacrylamide groep. Omdat de methacrylamide groep meer lijkt op de methacrylaat groep van het monomeer, bestond de hoop dat de nieuwe probe een vergelijkbare chemische reactiviteit zou vertonen. Verder werd de aanwezigheid van een dubbele binding naast de carbonyl-groep in the methacrylamide-functionaliteit van de probe vooronderstelde een effectieve fluorescentiedover te zijn. Dit bleek het geval. Met behulp van de experimentele procedure beschreven in Hoofdstuk 5 werd vastgesteld dat de PyMA probe een enigszins lagere reactiviteit (85%) heeft dan het monomeer zelf. Deze lagere reactiviteit werd toegeschreven aan een lagere diffusiecoëfficient voor het grote PyMA molecuul relatief ten opzichte van MMA. Opnieuw wordt het succes van het gebruik van fluorogene moleculaire probes voor het volgen van het gehele verloop van bulk MMA polymerisatie gedemonstreerd.

De karakteristieke lange levensduur van de pyreen fluorescentie maakt dat deze fluorofoor bijzonder gevoelig is voor quenching, bijvoorbeeld door sporen van zuurstof. Dit heeft als gevolg dat deze experimentele resultaten, die berusten op quantitatieve metingen van fluorescentie, evenzeer gevoelig zijn voor systematische fouten. Deze complicatie werd geëlimineerd door synthese van een nieuw probe molecuul, *N*-(2-anthraceen)methacrylamide (AnMA), dat de kortlevende fluorofoor anthraceen bevat. Opnieuw werd de aanwezigheid van een dubbele binding naast de carbonyl-groep in the methacrylamide-functionaliteit van de probe vooronderstelde een effectieve fluorescentiedover te zijn. Dat bleek inderdaad weer het geval. Een herhaling van de experimentele procedure beschreven in Hoofdstuk 5, met anthraceen als de referentie-fluorofoor, gaf aan dat de AnMA probe een bijna identieke reactiviteit (96%) met die van het monomeer

vertoont. Verder werd gedemonstreerd dat de fluorogene AnMA probe gebruikt kan worden om gevoelig het gehele verloop van MMA polymerisatie quantitatief te volgen, zelfs in het gebied voorbij het Trommsdorff effect. In dit hoofdstuk worden ook experimentele resultaten gepresenteerd die aantonen dat fluorogene probes zoals AnMA kunnen worden gebruikt voor het met grote gevoeligheid volgen van polymerisatie in oplossingen. Deze mogelijkheid om polymerisatie in oplossingen te volgen met fluorescerende probe technieken met een grote gevoeligheid is naar ons beste weten nooit eerder aangetoond.

Hoofdstuk 8 introduceert de toepassing van tijdsopgeloste fluorescentietechnieken om polymerisatie te volgen. Wanner we aannemen dat de snelheid van stralingsloze relaxatie van fluoroforen gevoelig is voor de fysische eigenschappen van het medium, dan is het redelijk om te veronderstellen dat meting van de fluorescentielevensduren van een probe molecuul in een polymeriserend medium gebruikt kan worden voor het volgen van het polymerisatie-proces zelf. De experimentele resultaten lieten zien dat de AnMA probe en het fluorogene, charge-transfer molecuul maleimido fluoroprobe (MFP) alleen gevoelig zijn tijdens de verglazing bij bulk MMA polymerisatie. Het experiment met MFP toonde echter aan dat, behalve een afname in de snelheid van stralingsloze relaxatie, de fluorescentie-vervalsnelheid van de gecopolymeriseerde vorm verandert van mono-exponentieel naar multi-exponentieel bij verglazing. De oorsprong van dit multi-exponentiele verval is het onderwerp van het laatste hoofdstuk van dit proefschrift.

In Hoofdstuk 9 worden continue en tijdopgeloste fluorescentie metingen van twee charge-transfer probes (fluoroprobe en MFP) gebruikt om het Trommsdorff effect van MMA polymerisatie te onderzoeken. Het is interessant om het gedrag van de vrije probe FP te vergelijken met dat van de fluorogene probe MFP. In het Trommsdorff-gebied wordt een plotselinge blauw-verschuiving van het fluorescentie-maximum (van *ca* 550 nm naar *ca* 450 nm) waargenomen. De aanzet van deze blauw-verschuiving heeft plaats op een enigszins vroeger tijdstip voor de MFP probe, hetgeen wordt toegeschreven aan de voorkeur van de MFP probe voor concentratie in polymeer-rijke gebieden van het monster (bedenk dat de MFP probe alleen fluoresceert wanneer deze gecopolymeriseerd is in de groeiende polymeerketens). Naast de spectrale verandering wordt een verandering van mono-exponentiële naar multi-exponentiële vervalkinetiek waargenomen voor beide probes. Door middel van constructie van “time-resolved emission spectra (TRES)” van de probes in de PMMA-matrix is het mogelijk om aan te tonen dat een graduele rood-verschuiving in de fluorescentie optreedt voor beide probes met een exponentiële relaxatie-tijd van 16 ns. Dit wordt toegeschreven aan reorganisatie van de dipolaire estergroepen van de zijketen van het polymeer, geïnduceerd door de sterk polaire, volledig ladingsgescheiden toestand van de probe moleculen op een tijdschaal die ordes van grootte korter is dan de diëlectrische relaxatie-tijd van PMMA. Er werd geen aanwijzing gevonden voor (micro)heterogeniteit in de PMMA-matrix.

Acknowledgements

I would like to express my gratitude to a number of individuals who have helped me tremendously in getting to where I am today. First and foremost, I wish to express my thanks to both Meg and Pam for assisting me during a time which in all certainty was the most difficult period of my life. Naturally both of my grandparents receive my utmost appreciation. Without their financial support, my hopes in receiving an education at the university level would likely have amounted to nothing more than a pipe dream for a forklift operator working in the orange groves of Florida.

Also, I would also like to express my gratitude to those rare and inspirational teachers and supervisors I've had the good fortune to meet throughout the passing years. For the most part, it was your enthusiasm that encouraged me to apply myself to accademics. In particular, I would like to thank Dr. Ken Wagener and Dr. Doetze Sikkema for their highly valued assistance in giving my academic career a jump-start.

Last on the list would be my more recent colleagues at the IRI of the TU Delft. Beginning with my supervisors John and Lee, I would have to say that words could never sufficiently express the thoughts that come to my mind. The countless hours that we have spent together, at times collaborating and at other times trying one another's patience, could best be described as "bitter-sweet". Although the damage I have ensued may be permanent, I feel that I have learned much from the both of you, and for that I am very much indebted. My thanks also are extended to my strongest sympathizers, the promovendi of both past and present. It was your support that made this trying time not only bearable, but also *gezellig*!

Curriculum Vitae

Mark Stephen Frahn was born in Dunedin, Florida of the United States of America on the 20th of February 1973. He obtained his Bachelor of Science degree in chemistry in 1992 at the University of Florida. During his studies at the University of Florida he participated in undergraduate research projects focusing on polymer and organometallic synthesis in the group of Dr. Ken B. Wagener. Following two internships involving polymer chemistry research, one at Dow Corning and the other at Akzo Nobel, he started post-graduate studies in polymer science and plastics engineering at the University of Massachusetts in Lowell. From September 1998 to November 2003 he was a PhD student in the department of Radiation Chemistry of the Interfaculty Reactor Institute at Delft University of Technology. In this group his studies focused on monitoring radiation-induced polymerization using fluorogenic molecular probes. This work was carried out under the supervision of Dr. J. M. Warman and Dr. L. H. Luthjens.